Cours/Lecture Series

1994– 1995 ACADEMIC TRAINING PROGRAMME

LECTURE SERIES

SPEAKER	:	Alberto DEL GUERRA / University of Ferrara, Italy
TITLE	:	Detector applications in medecine and biology
TIME	:	9, 10, 11, 12 & 13 January from 11.00 to 12.00 hrs
PLACE	:	Auditorium

ABSTRACT

In recent years new diagnostic and therapeutic methods have been attracting more and more dedicated attention by the scientific community. The goal is a better understanding of the anatomy, physiology and pathology of the human being in an effort to find more appropriate medical prevention, diagnosis and therapy. Many of the achievements obtained so far derive from the use and the optimisation of detectors and techniques, which originated in the other fields of physics. The spin-off of High Energy Physics to Medical Physics has been particularly relevant in the field of detectors for medical imaging and especially for medical imaging with ionizing radiation. In this series of lectures, starting from the requests of each technique and/or application I will attempt to present a survey of the detectors for medecine and biology. Various fields of medical imaging will be touched : radiology, digital radiography, mammography, Single Photon Emission Computed Tomography, Positron Emission Tomography and radiotherapy. The capabilities of the major types of detectors (1-D and 2-D position sensitive, and pixel type) will be correspondingly analyzed : scintillation, gaseous and solid state detectors. Finally some specific applications as in synchrotron radiation and in the biological field will be addressed.

Div. DG/CP
Distr. int. & ext.

Detectors for Medicine and Biology

Alberto Del Guerra

Department of Physics, University of Ferrara and INFN, Sezione di Ferrara
Via Paradiso 12 , I-44100 FERRARA (Italy)
Ph:+39-532-781822; fax: +39-532-781810
e_mail:delguerra@ferrara.infn.it; vaxfe::delguerra

(CERN - Academic training - 9,10,11,12 &13 January 1995)

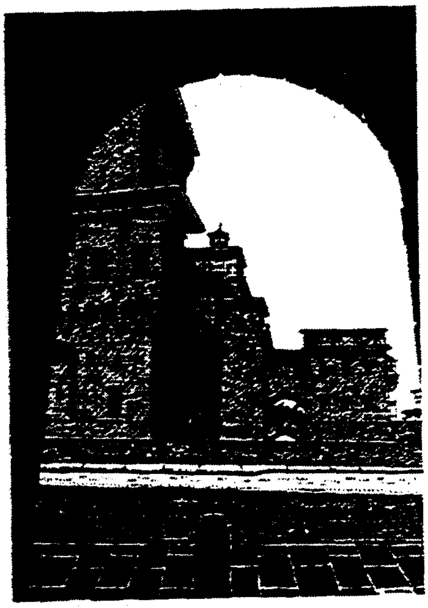

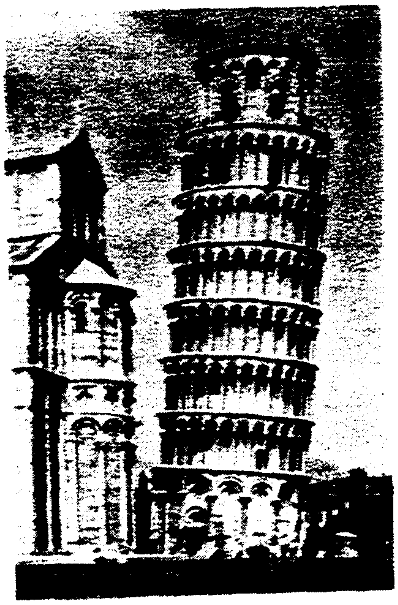

Contents

Many thanks are due to:

Georges *Charpak*	CERN
Ugo *Amaldi*	CERN (for the TERA group)
Ronaldo *Bellazzini*	Pisa (Italy)
Roberto *Pani*	Roma (Italy) (for the HIRESPET collaboration) Roma I - Ferrara- Bologna
Victor *Perez-Mendez*	LBL(US)
Fabio *Sauli*	CERN
Yuri *Zaneski*	Dubna (Russia)

RADIN and MEDIM collaborations (INFN group V)
Cagliari-Pisa-Ferrara- Napoli

Figure 4A
The first medical radiograph This radiograph of Mrs. Roentgen's hand was made by Roentgen before he announced his discovery of x rays. On January 1, 1896, Roentgen sent a copy of a separate printing of his first paper on x rays and examples of his x-ray photographs to several colleagues. Photographic positive prints made from the x-ray plate of his wife's hand and eight other plates formed the collection from which he selected the examples forwarded to his colleagues with his paper.

LARGE HADRON COLLIDER: ONE CROSSING (MINIMUM BIAS BACKGROUND)

CMS SIMULATION
$L = 1.8 \times 10^{34}\ cm^{-2}\ s^{-1}$

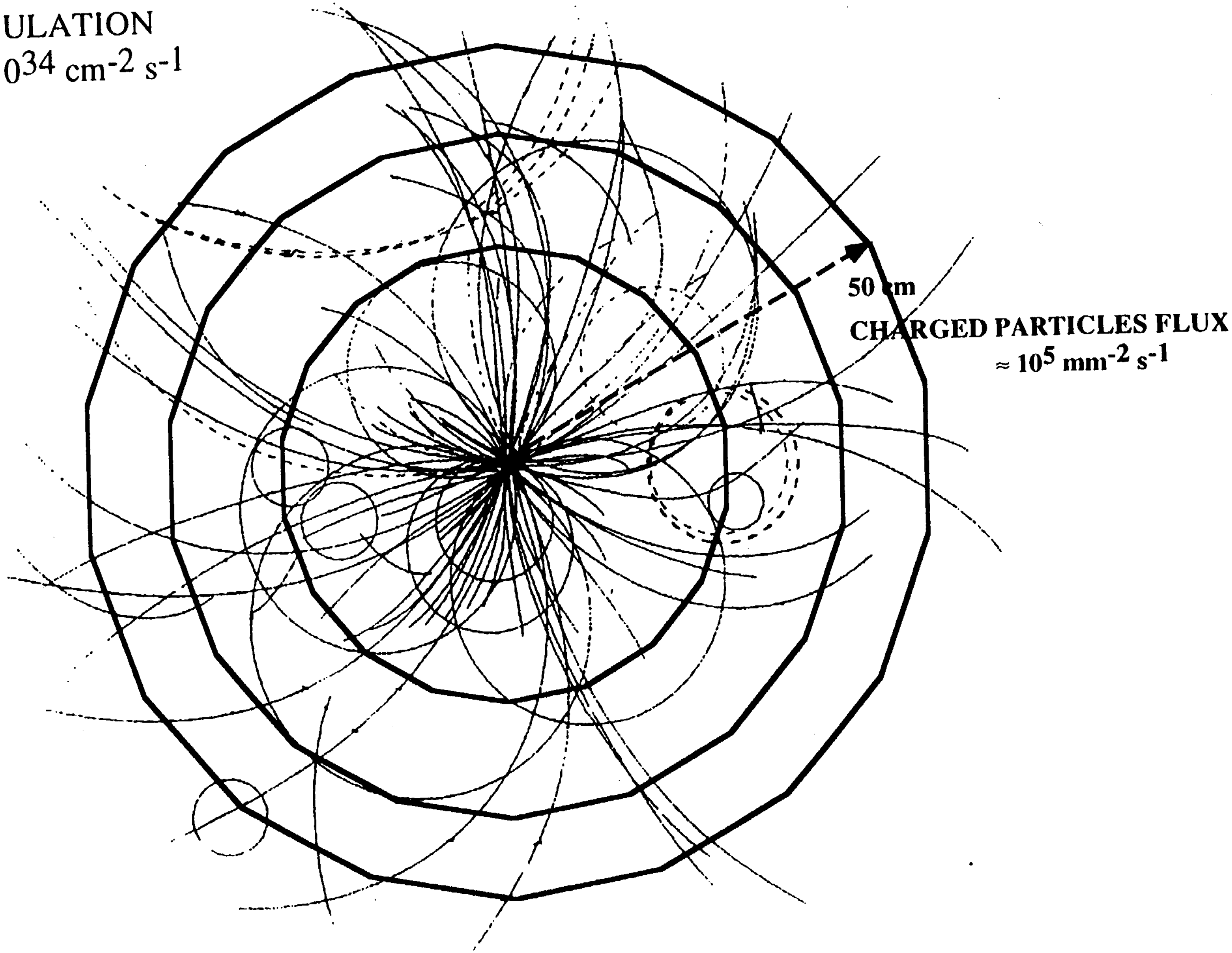

Example:

Problems solved for HEP experiments:

1. μ-strip silicon detector for charged particle tracking

2. Dimension: 4x (5x5 cm^2) ; thickness $\leq$ 500 μm

3. Electronics for m.i.p. (in 300 $\mu m \approx$ 70 keV energy loss)
   low noise : 200 e^-
   reasonably fast : 50 -100 ns
   integration on VLSI (see Viking)

4. Trigger

5. DAQ for collider
   low multiplicity
   sparse readout via multiplexer (in between two pulses)

6. n. of channels: 10^6-10^7

7. event size: 10^6 bytes (level 1 trigger)

8. n. of sellable apparatus: 1 (may be two!!)
   But the apparatus is made of thousands of modules!

Problems *to be tackled for Imaging with X-rays (10-100 keV):DR*

1. μ-strip silicon detector for *X-rays*

2. Dimension: *20x20 cm^2* ; thickness *(300 μm - 3 mm)*

3. Electronics for *X-rays (down to 10 keV)*
   low noise : 200 e^-
   fast *: 10 ns*
   integration on VLSI

4. *Self -Triggering*

5. DAQ for *DR*
   $5x10^4$ Hz/mm^2 (on a 20x20 cm^2 $2x10^9$ Hz)
   1 s acquisition time (duty cycle 100%)

6. n. of channels: *10^3-10^4*

7. event size: *1 bit - 10 bytes*

8. n. of sellable apparatus: *10^3-10^6*

	Experiment in HEP	Exp in Medical Physics
Group size:	10^2 - 10^3 people	1 or 2
Preparation:	5 - 10 years	5' - 10'
Data collection:	1 - 5 years	1' - 5'
Data analysis:	1 - 5 years	1' - 5'
Run by:	physicists	technician
Analyzed by:	physicists w/ hardware & software	physician "mostly by experience"

However in both cases the right approach is the same:

- *I have the best detector for .. what??*

- *I have this experiment to do w/ these requirements. Which is the best detector?*

A century-old example of physics applied to medicine. Hughes apparatus was developed in the early 1880's to locate metal fragments in wounds by means of electro-magnetic induction.

Detectors for Bio-Medical Imaging w/ ionising (mostly X and γ) radiations

1. DIAGNOSIS

(Discipline)	*(Parameters measured)*	*(Medical application)*

- **X-RAY RADIOLOGY**

2-D Film	X-ray absorption	Anatomy; mineral content
X-ray TCT	Density and average Z	movement of contrast
DSA	Contrast distribution	material

ULTRASOUND

	Acoustic impedance mismatch; sound velocity and attenuation	Anatomy; tissue structural characteristics; blood velocity

- **NUCLEAR MEDICINE**

Planar scintigraphy ECT	Concentration of radionuclides	Metabolism; receptor site concentration and flow

NUCLEAR MAGNETIC RESONANCE

MRI	Concentration of nuclides (^{1}H,..); relaxation parameters T1 and T2	Anatomy of tissues; free water content; flow concentration of
MRS	Frequency shifts due to chemical forms	some molecular species and contrast agents

OTHER Techniques
Biomagnetism, BioImpedance, ...

- **SOME BIOLOGICAL APPLICATIONS**
  Autoradiography
  Cristallography

2. THERAPY

- **only RADIOTHERAPY**

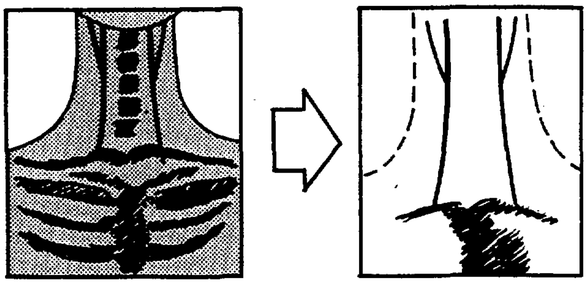

Figure 1. Contrast filled vessels are extracted from the background using DSA.

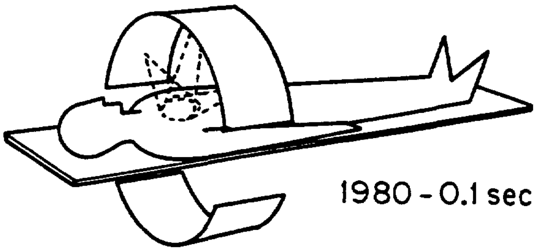

Figure 2. X-ray computed tomography measures photon attenuation coefficients.

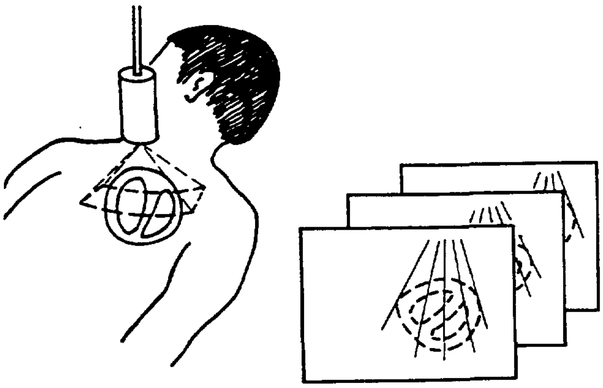

Figure 3. Ultrasound measures surface movement and blood velocity.

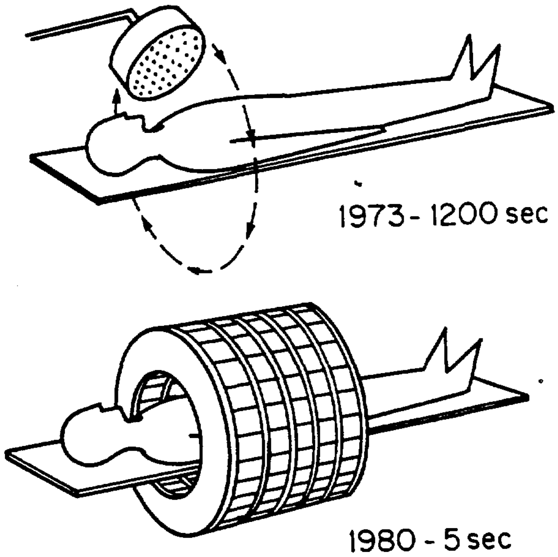

Figure 5. Emission tomography has evolved from the Anger camera to multilayer positron tomographs.

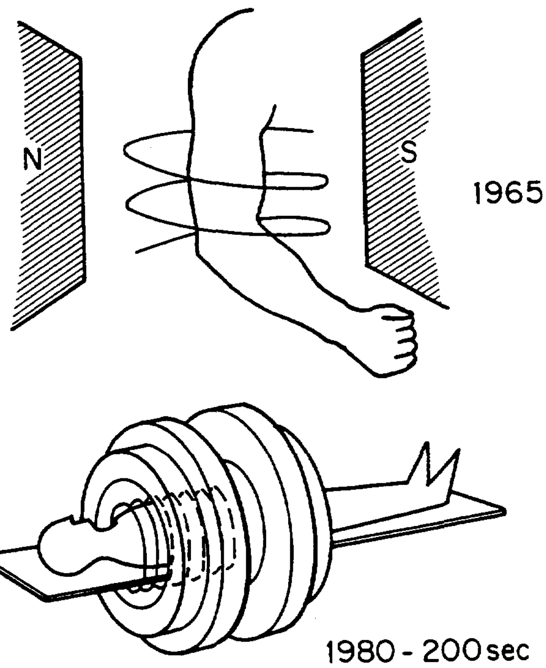

Figure 6. Nuclear magnetic resonance measures the chemical state and abundance of some nuclei (e.g., ^{1}H, ^{23}Na, ^{32}P).

Name Theodore Roosevelt. Attending Physician and Surgeon Moravitz.
Race ... Age 53. Nativity ... Occupation Ex President U.S.
Where and by whom employed
Diagnosis
Admitted Oct 14. 1912 Hour 10 P.M. Discharged ... Results ...
Color Odor Reaction Sp. Gr. Sugar Albumen Remarks:
Urinalysis:

Examination made by X Ray shows location of bullet about 1 in below nipple on right side and about 4½ in to right of mid line lodged against 4th rib.

J. B. Jansen

Treatment.
Shaved the area around the wound. Washed the area around the wound with 50% of Alcohol. Painted inside and outside of the wound with 10% tincture iodine Applied dry steril gauze dressing

from: Nancy Knight "75 years of the RSNA. Approaching a century of Radiology. Museum & Information Resources. In: RADIOGRAPHICS Stephen Balter, Guest Ed., November 1989, vol 9(6) – p. 1109

Radiological Imaging

fluence exposure

$N\,[ph/mm^2] \propto X \left(= \frac{\Delta Q}{\Delta m}\right)$

N_T transmitted fluence

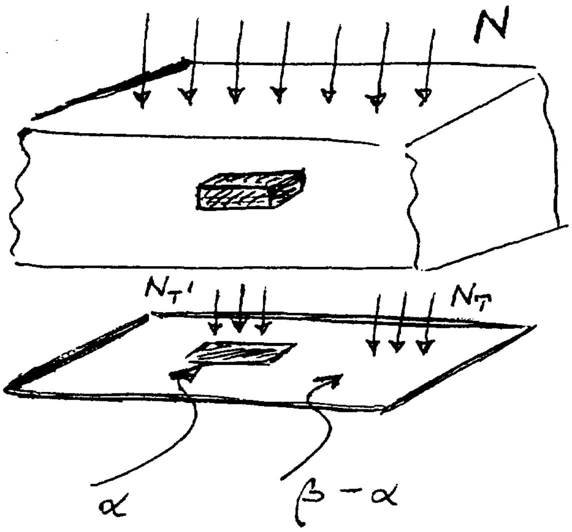

Signal $= |n - n'|$ $\qquad n = N_T\,(\beta - \alpha)$

$n' = N_T'\,\alpha$

Noise $= \sqrt{n + n'}$ **(from Poisson statistic)**

$$SNR = \frac{|n - n'|}{\sqrt{n + n'}}$$

Signal to Noise Ratio

$$SCR = \frac{|n - n'|}{(n + n')/2} = \frac{2 * SNR}{\sqrt{n + n'}}$$

Signal to Contrast ratio

for $n \gg n'$ $\qquad SNR = \frac{|n-n'|}{\sqrt{n}} \qquad SCR = \frac{2 * SNR}{\sqrt{n}}$

for $n \approx n'$ $\qquad SNR = \frac{|n-n'|}{\sqrt{2}\,\sqrt{n}} \qquad SCR = \frac{2 * SNR}{\sqrt{2}\,\sqrt{n}}$

For $\beta = 2\,\alpha$, $\sqrt{\alpha} = d$ **and** $N_T \approx N_T'$

$$SCR = \frac{2 * SNR}{d\,\sqrt{N_T}\sqrt{2}} = \frac{\sqrt{2} * SNR}{d\,\sqrt{N_T}}$$

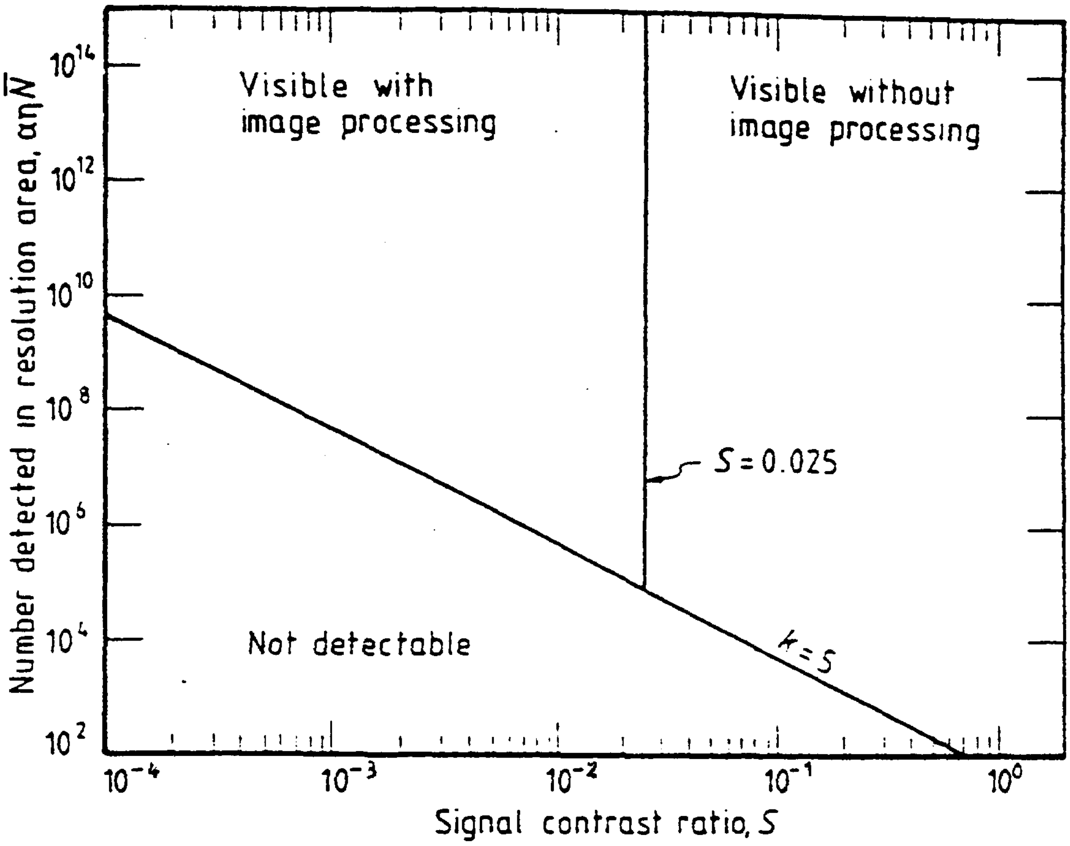

Fig. 2. Number of photons detected in a given resolution area as a function of signal contrast ratio. Threshold signal-to-noise ratio is taken as 5 in this example, with the visibility threshold of 2.5% (η is the area of the spatial resolution element, α is the X-ray detection efficiency of the imaging system and $\bar{N}$ is the average transmitted X-ray fluence. [Courtesy Dr. J.W. Motz and Med. Phys. 5 (1978) 8.]

$$SCR = \frac{\sqrt{2} * SNR}{\sqrt{n}} \quad \text{(for equal area)}$$

$$SNR \geq k = 5$$

$k = 5$

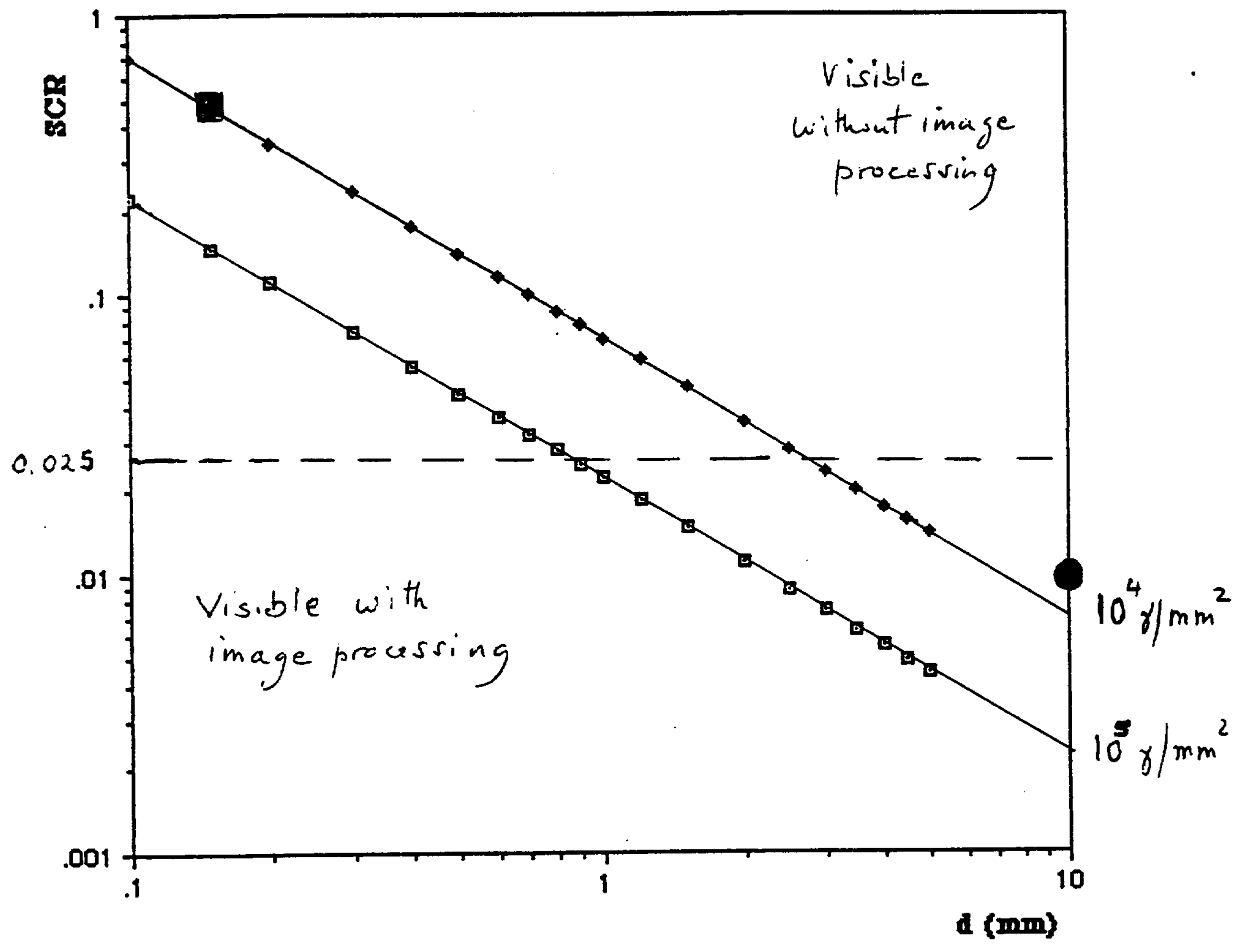

● → nodule (1 cm φ, 1% SCR)

▨ → μ-calcification (150 μm φ, 50% SCR)
(100–200 μm)

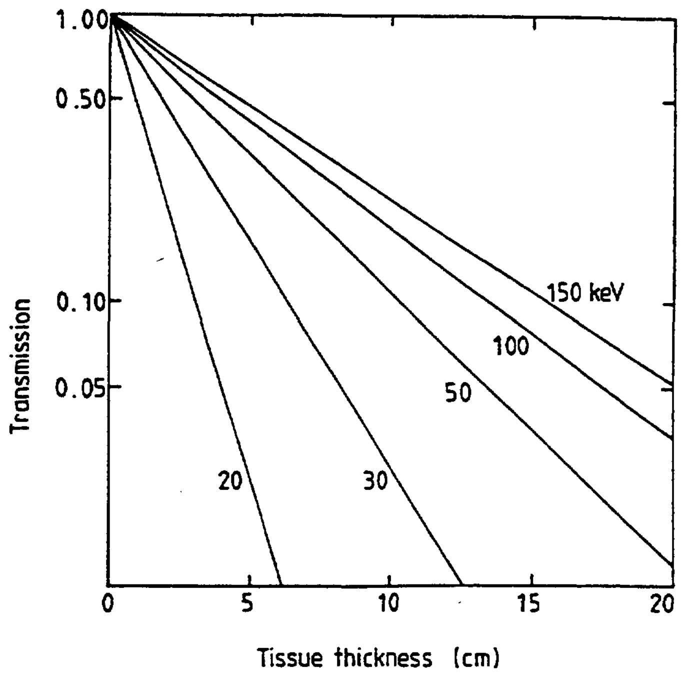

Figure 2.3 Transmission of monoenergetic photons through soft tissue. Curves are shown for photon beams with energies 20, 30, 50, 100 and 150 keV.

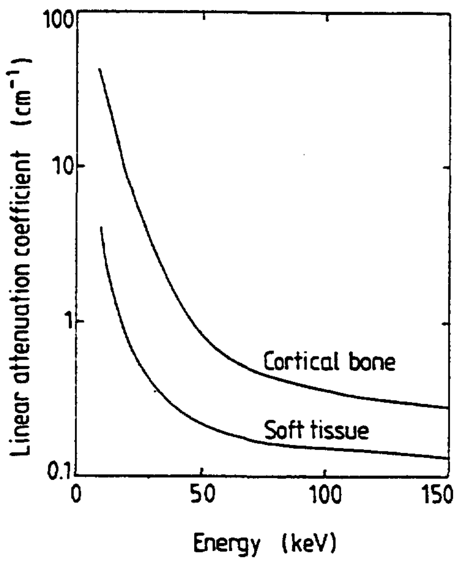

Figure 2.5 Variation with energy of the linear attenuation coefficients for soft tissue and cortical bone.

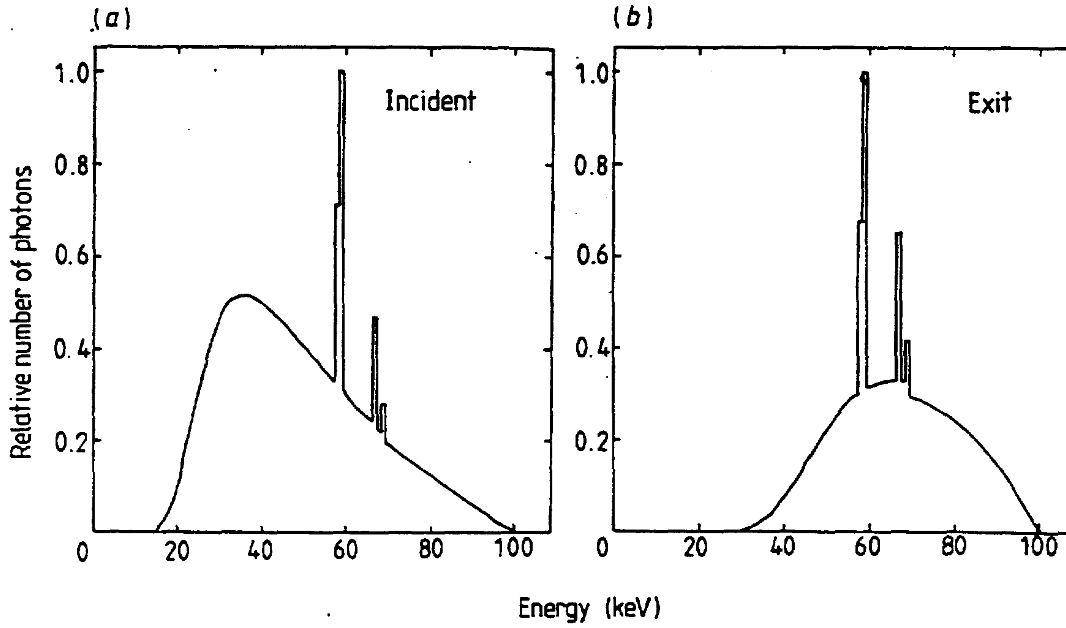

Figure 2.11 X-ray spectra for an x-ray tube with a tungsten target; 100 kV constant potential with 2.5 mm aluminium added. The spectra are shown both before and after attenuation by 18.5 cm soft tissue plus 1.5 cm bone. (The spectra are based on the work of Birch *et al* (1979).)

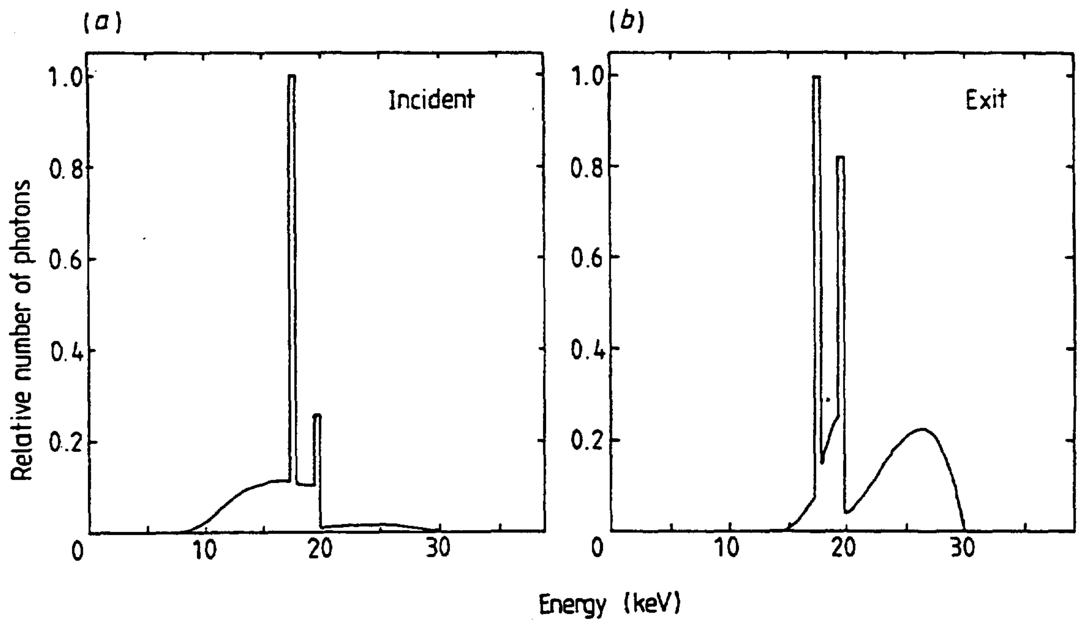

Figure 2.12 X-ray spectra for an x-ray tube with a molybdenum target; 30 kV constant potential with 0.03 mm molybdenum filter. The spectra are shown both before and after attenuation by 5 cm tissue. (The spectra are based on the work of Birch *et al* (1979).)

from: D. Dance "Diagnostic radiology with x-rays", In: "The Physics of Medical Imaging". S. Webb (Ed)

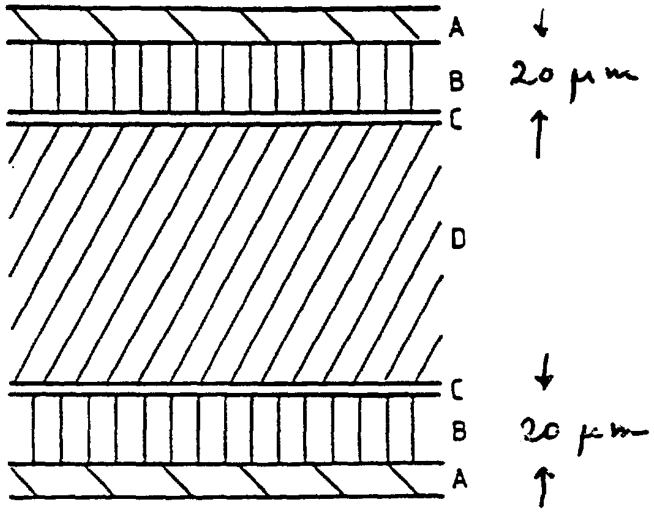

Figure 2.16 Construction of direct-exposure x-ray film: A, protective coating; B, film emulsion (20 μm) of silver halide grains in gelatin; C, subbing layer; D, film base (200 μm). (After Barrett and Swindell (1981) p196.)

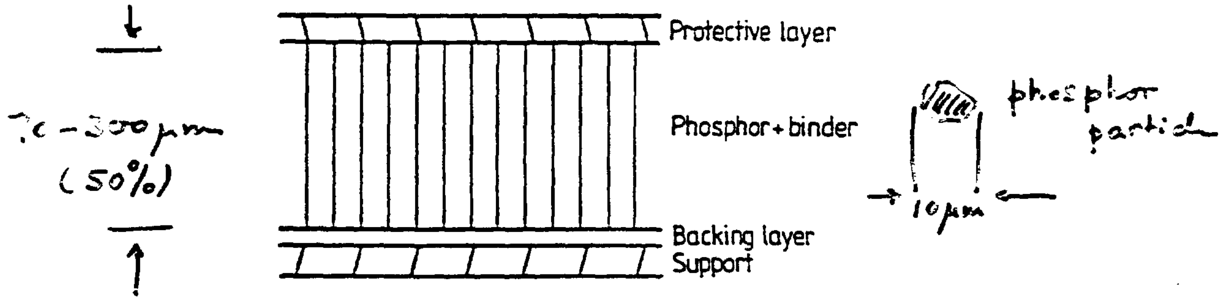

Figure 2.19 Construction of a fluorescent screen.

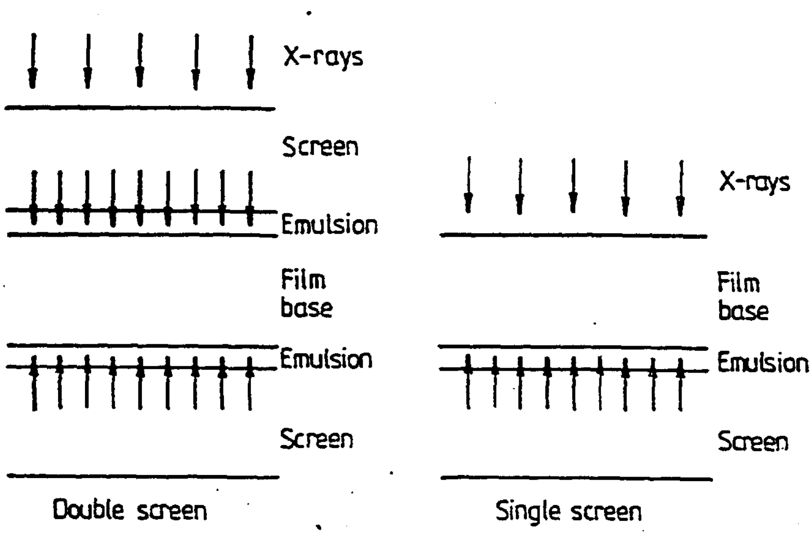

Figure 2.20 The use of double and single screens. The arrows at the top of each figure represent the incident x-rays, which interact in the screens, and the arrows originating in the screens represent the light fluorescent photons, which expose the film emulsion.

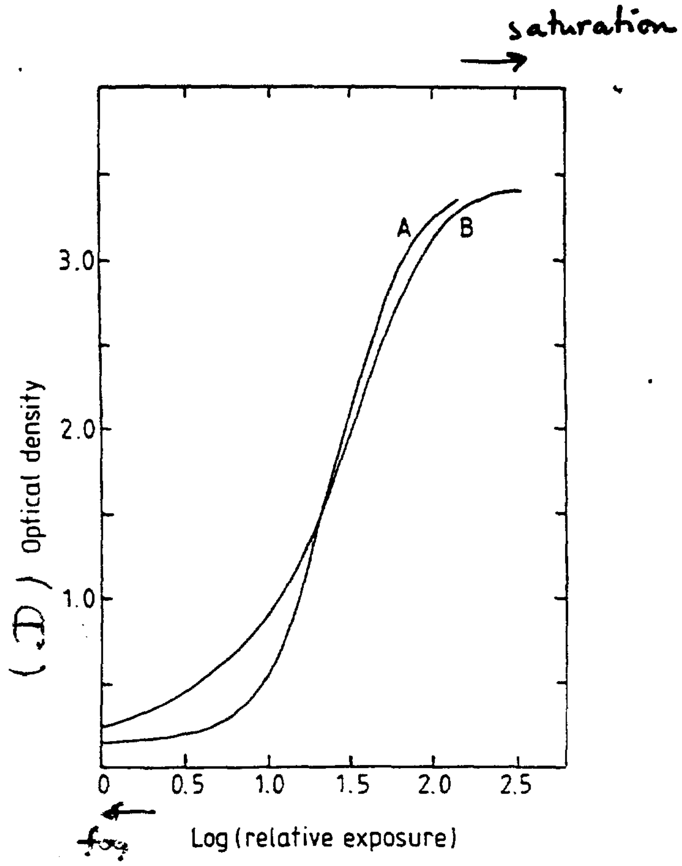

Figure 2.17 Film characteristics for a direct-exposure x-ray film (curve A, equation (2.31)) and for a screen film (curve B). The speed of the direct exposure film has been increased so that the shapes of the two curves can be compared. The two films have the same fog level and maximum density.

from: D. Dance "Diagnostic Radiology with X-rays", In: The Physics of Medical Imaging, S. Webb (Ed.)

- $D = \log_{10}(I_0/I)$
- $D = D_{MAX}\left[1 - \exp(-kX)\right]$
- film latitude

Γ (film gamma) $\sim 2-3$

$$D \sim \Gamma \log_{10} \frac{X}{X_0}$$

X-ray radiology **diagnostic range**: 10 -100 keV

film:
- high spatial resolution (few μm)
- high contrast (curve A, high Γ, narrow latitude)
- low efficiency (20 μm)

film+screen

calcium tungstate
terbium activated rare-earth oxysulphide (X_2O_2S) phosphors

X = gadolinium
lantanium
or yttrium

- moderate high spatial resolution (10-20μm)
- good contrast (curveB, low Γ, wide latitude)
- high efficiency
  typical values: 100% at 10 keV
  45% at 40 keV
  10% at 70 keV

noise
- quantum mottle
- variation in energy absorbed per interacting photon
- inhomogeneities in phosphor coating (structure mottle)
- fluctuations in light fluorescent photons yield
- fluctuations in the number of silver halide grains in the emulsion (film granularity)

$$\text{DQE} = \text{Detective quantum efficiency} = \left[\frac{\text{SNR (out)}}{\text{SNR (in)}}\right]^2 \quad (\leq 1)$$

$$\text{DQE}_{tot} = \text{DQE}_1 * \text{DQE}_2 \ldots\ldots * \text{DQE}_N$$

Main film limitations:

- Limited dynamic range (narrow latitude)
- Lack of digital processing

Transducers for digital imaging:

AREA EXPOSURE

- Digital screen-film system

  Illumination of the film w/ light followed by a visual assessment of variation in transmittance (viewing box)

- TV camera

  Standard viewing box and digitising by TV frame
  - cheap and easy
  - bandwidth and dynamic range limitations

- Laser scanner

  Raster scanner of the X-ray film by small focussed spot (10 μm minimum, 100-200 μm standard)

- Image Intensifier + Television system

  CsI phosphor

- Photostimulable luminescence

DIRECT DIGITAL IMAGING

(2-D, 1-D and point scanning)

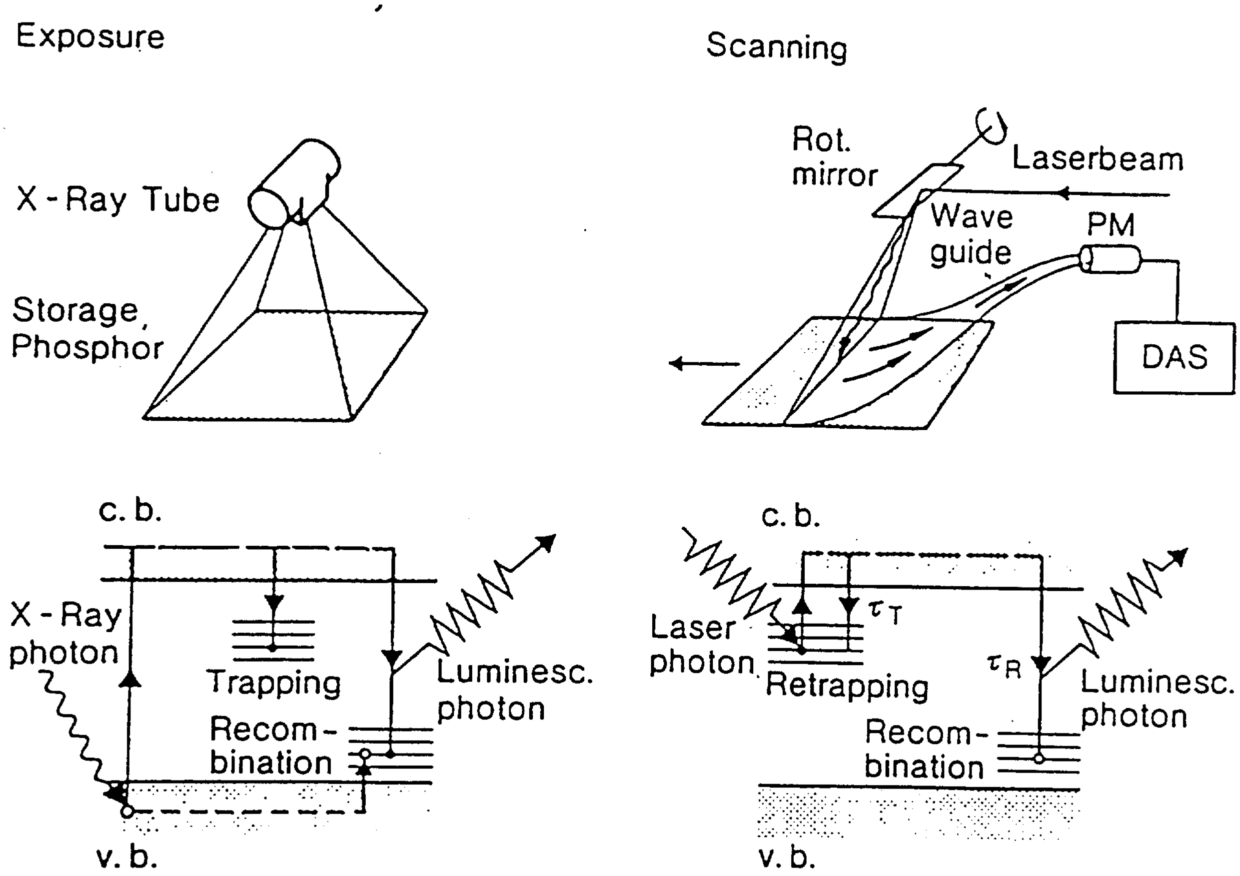

Fig. 1 – X-ray imaging via storage phosphors. Upper half: Scheme of apparatus. Lower half: Physical principle.

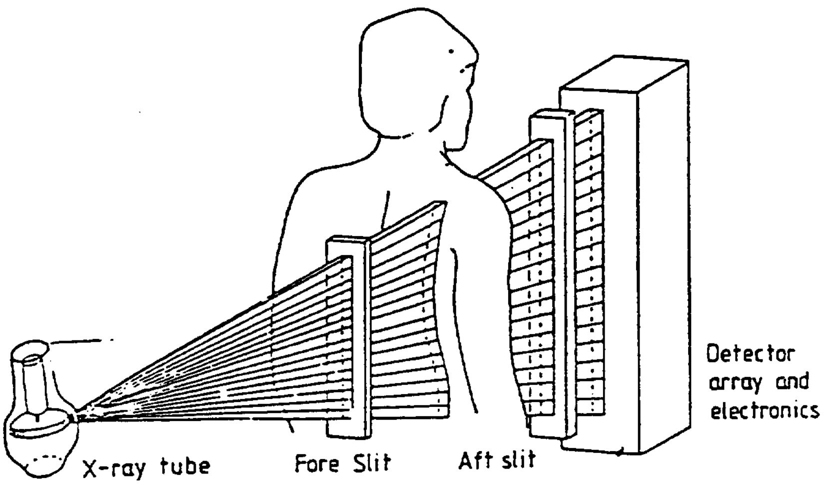

Fig. 4. A prototype digital radiography system for examination of the chest. The X-ray beam is collimated to a narrow fan beam by two mechanically connected vertical slits. [Courtesy Picker International Ltd and Radiology 148 (1983) 259.]

Gaseous and Semiconductor Detectors for Digital Medical Imaging

Single photon counting

Gaseous	**MultiWire Proportional Chamber** **MicroStrip Gas Chamber**
Semiconductor	Microstrip solid state crystal (Si, Ge, HgI_2) Pixel solid state crystal (Si, GaAs, CdTe)

Integrating

Semiconductor	CCD matrices Photosensitive diode arrays Amorphous silicon

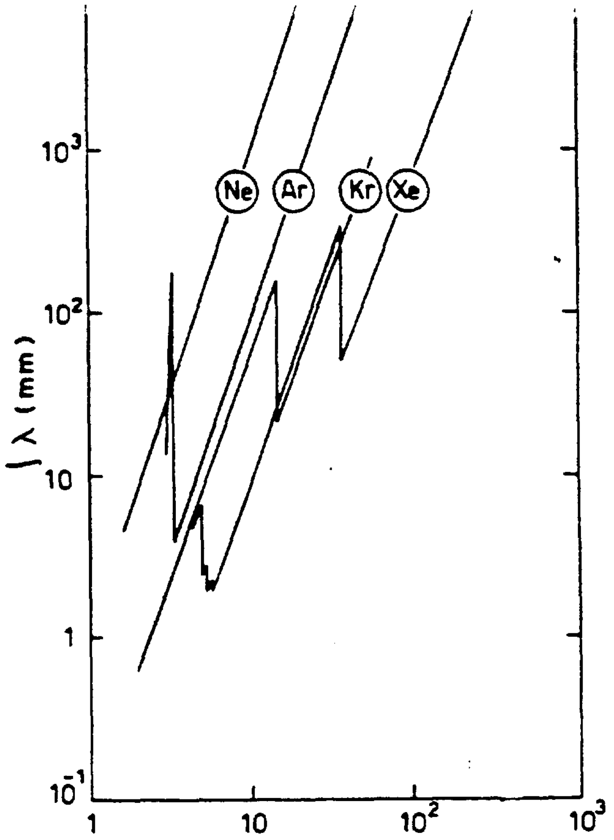

Fig. 2 - Cammino libero medio della radiazione in alcuni gas nobili, alla pressione di 1 atmosfera (2).

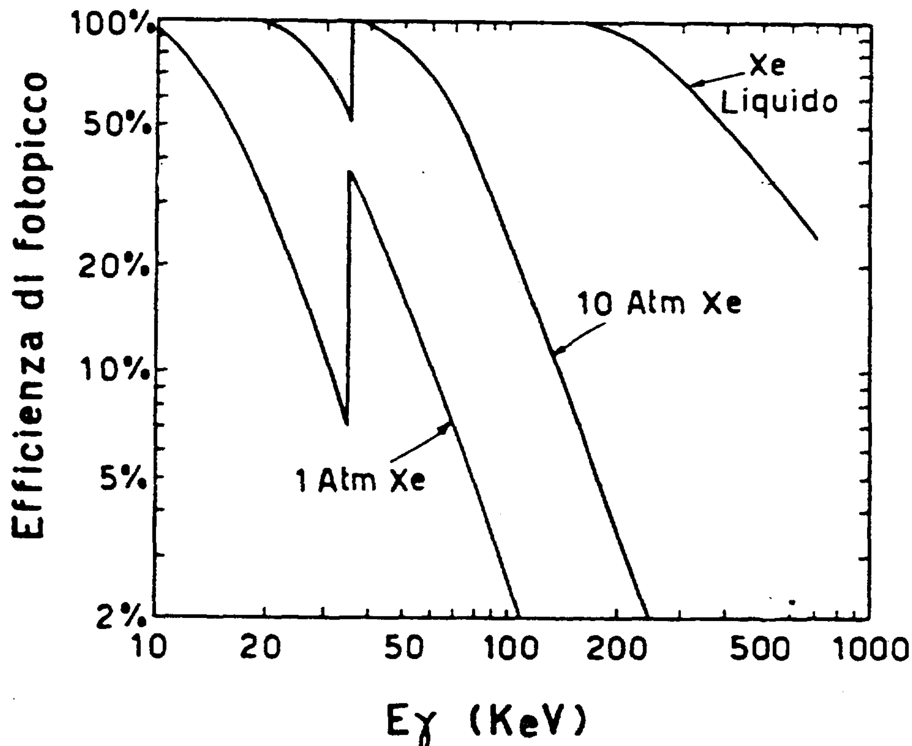

Fig. 3 - Efficienza di fotopicco in funzione dell'energia per una MWPC di spessore 2.5 cm con riempimento: a Xenon gassoso (a 1 atm e a 10 atm) e a Xenon liquido (10).

Table 1
Physical characteristics of the semiconductors

Semi-conductor	ρ [g/cm³]	Z	E_{gap} [eV]	ϵ [eV]	$T_{working}$ [K]	K-edge [keV]	ρ_e [Ω cm]	$\mu_{e,h}\tau_{e,h}$ [cm²/V]
Si	2.33	14	1.12	3.6 [1]	300	1.8	$\approx 10^3$	0.42, 0.22
Ge	5.33	32	0.67	2.9 [3]	77	11.1	$\approx 10^2$	0.72, 0.84
GaSe	4.55	31, 34	2.03	4.5 [4]	300	10.3, 12.6		10^{-7}, 10^{-7} 1.5×10^{-6}, 2.5×10^{-6}
InP	4.78	49, 15	1.30	4.2 [6]	300	27.9, 2.1	$\approx 10^7$	4.8×10^{-6}, $\leq 10^{-7}$
CdS	4.84	48, 16	2.60	7.3 [15]	300	26.7, 2.4		
GaAs	5.32	31, 33	1.43	4.3 [3]	300	10.3, 11.8	$\approx 10^7$	8.6×10^{-6}, 4.0×10^{-7} 8.6×10^{-5}, 4.0×10^{-6}
InSb	5.77	49, 51	0.20	0.6 [15]	4	27.9, 30.4		10^{-5}, 7.5×10^{-6}
CdSe	5.80	48, 34	1.73	5.5 [a]	300	26.7, 12.6		2.0×10^{-5}, 1.5×10^{-6}
CdTe	6.20	48, 52	1.44	4.7 [3]	300	26.7, 31.8	$\approx 10^9$	2.0×10^{-3}, 4.0×10^{-4}
PbI_2	6.20	82, 53	2.55	7.7 [a]	300	88.0, 33.2	$> 10^{13}$	8.0×10^{-6}, 2.0×10^{-7}
HgI_2	6.40	80, 53	2.13	4.2 [7]	300	83.1, 33.2	10^{13}	10^{-4}, 10^{-5}
TlBr	7.56	81, 35	2.68	6.5 [18]	300	85.5, 13.5	$\approx 10^{12}$	1.6×10^{-5}, 1.5×10^{-6}

[a] Calculated from Klein's empirical formula [4].

from: W. Bencivelli et al
Nucl. Instr Meth A310 (1991) 210

Table 2.2 Doses for some common radiological examinations.

Examination[a]	Dose (mGy)
CC breast	1.2
AP chest	0.3
AP lumbar spine	9.2
AP pelvis	6.6
AP skull	4.4

[a] CC = cranio-caudad view or projection.
AP = antero-posterior view or projection.

Table 2.3 Effective dose equivalent (mSv) and organ doses (mGy) (breast, red bone marrow, lung, thyroid, skin, ovaries and testes) for selected radiological examinations.

Examination	Doses per examination							
	Eff. dose equiv.	Breast	RBM	Lung	Thyroid	Skin	Ovary	Testes
Barium meal	3.8	2.2	2.6	8.7	1.1	2.1	3.6	0.3
Barium enema	7.7	0.7	8.2	3.2	0.2	5.1	16.0	3.4
IVU[a]	4.4	0.7	1.9	7.0	0.2	1.9	0.8	0.1
Cholecystography	1.0	0.4	0.8	1.6	0.1	0.8	0.4	0.0

[a] Intravenous urography.

AVALANCHE GROWTH AND SIGNAL FORMATION

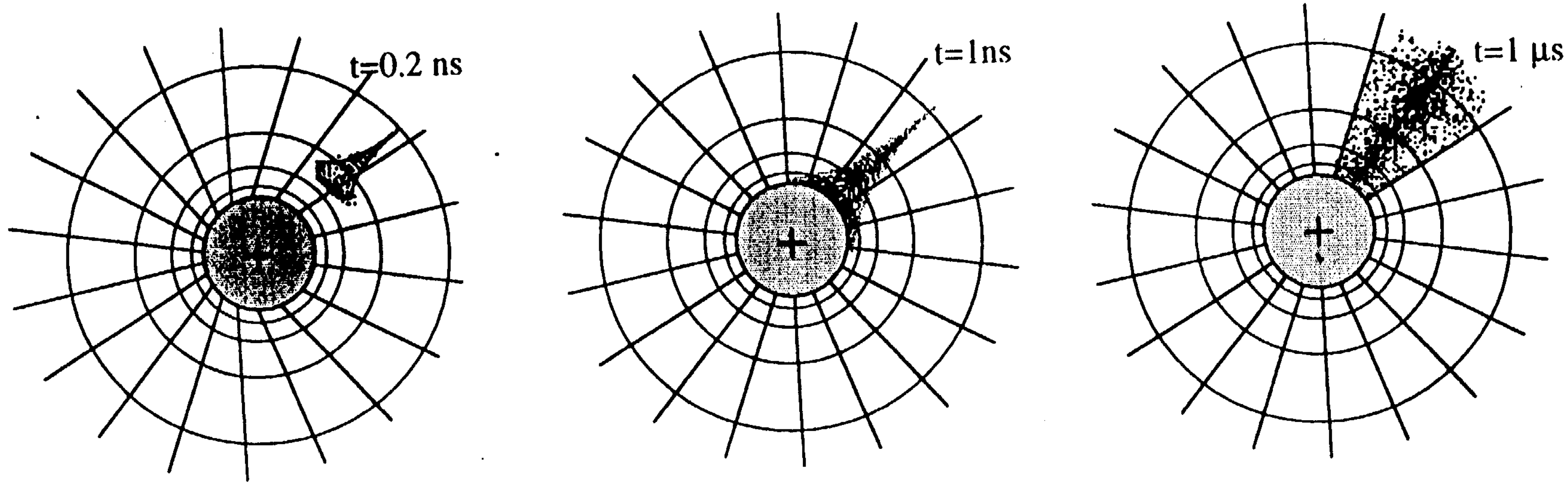

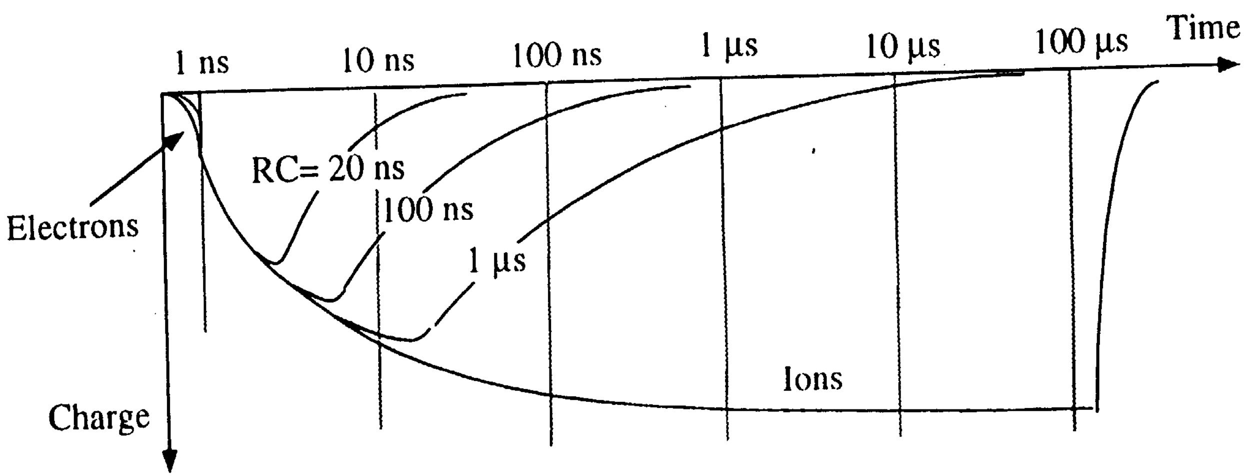

METHODS OF POSITION READOUT

(A) AMPLIFIER-ENCODER/WIRE ON ANODE WIRES OR CATHODE STRIPS REQUIRES MUCH ELECTRONICS. NEED CENTER OF GRAVITY SENSING.

(B) CHARGE DIVISION. INTERCONNECT CATHODE STRIPS BY CAPACITORS OR RESISTORS. MEASURE CHARGE AT BOTH ENDS OF CHAMBER. MODERATE POSITION ACCURACY. LIMITATION: ONLY ONE IONIZING TRACK CAN BE READ ON EACH EVENT. TWO OR MORE TRACKS ARE READOUT AS AN AVERAGE POSITION.

(C) DELAY LINE READOUT. CONNECT DELAY LINE CAPACITATIVELY TO ORTHOGONAL PLANES OF CATHODE WIRES OR TO ANODE WIRES AS WELL. BY TIMING ARRIVAL OF SIGNALS TO BOTH ENDS CAN DETERMINE POSITION TO ACCURACY OF 0.1 MM. MAIN LIMITATION X,Y AMBIGUITY WHEN MULTIPLE TRACKS OCCUR.

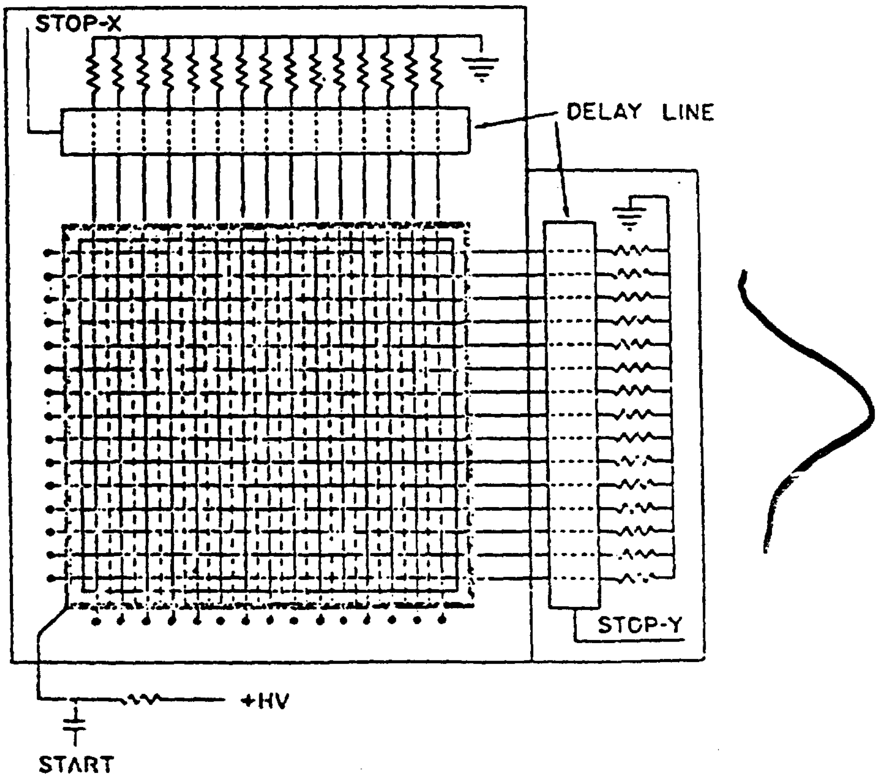

2.3 - Bone densitometry: Rationale

Passive (film) detection has an unparalleled resolution in densitometry studies. However, the radiographic film suffers from the intrinsic chemical fog which diminishes the sensitivity and the density resolution of this technique.

⇒ a MWPC with

1. good detection efficiency ⇒ Xenon (4 atm)
2. good spatial resolution ⇒ monochromatic source just above the Xe K-edge (34.6 keV)
3. high rate capability ⇒ fast TDC's and histogramming memories

Parameters*:

Active area	128 mm x 128 mm
Anode wire pitch	1 mm
Anode-cathode gap	3 mm
Cathode strips with fast delay line read-out	50 ns/cm
Xenon (80%)-CO_2(20%)	4 atm
Entrance window	300 μm - 0.07 g/cm^3 - 300 μm G-10 - Rohacell 71 - G-10
Read out system	Charge sensitive preamplifier Fast shaping amplifier Constant Fraction Discriminator 2-TDC's (500 ns conversion time) 1 dedicated two-D 128x128 pixels histogramming CAMAC memory

* R.Bellazzini, A.Brez, A.Del Guerra , et al. Nucl Instr Meth Phys Res1984, 228, 193-200

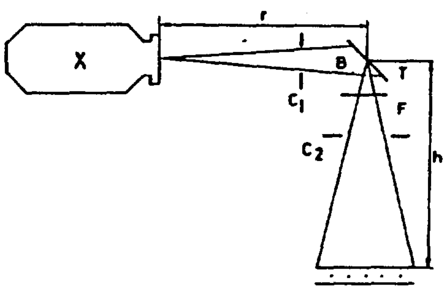

Fig. 1. A scheme of the fluorescent X-ray source: C1: entrance collimator, C2: exit collimator, T: target, F: filter.

Table 1
X-ray energy selection.

Target	samarium	gadolinium	dysprosium
Filter	neodymium	samarium	gadolinium
Energy	40 keV	42 keV	45 keV

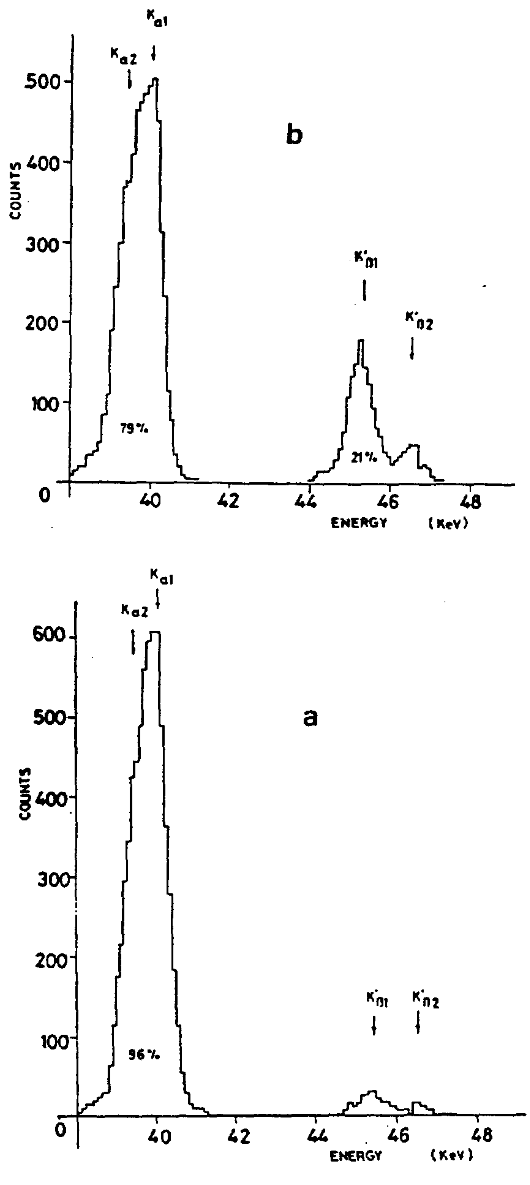

SAMARIUM TARGET

SAMARIUM TARGET + NEODYMIUM FILTER

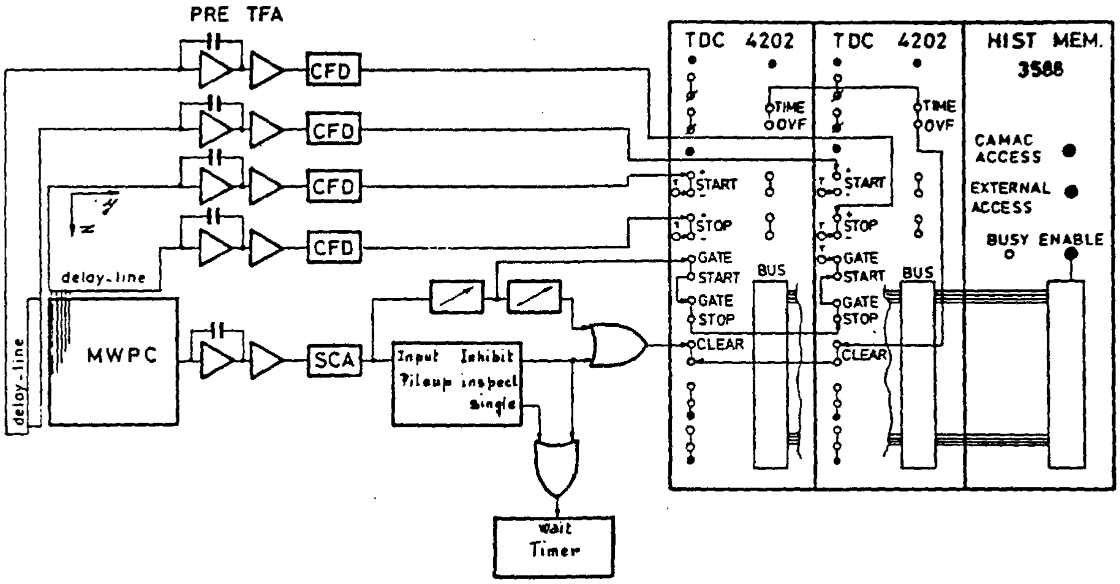

Block diagram of the position read-out system.

Read write → 1.2 μs
800 kHz

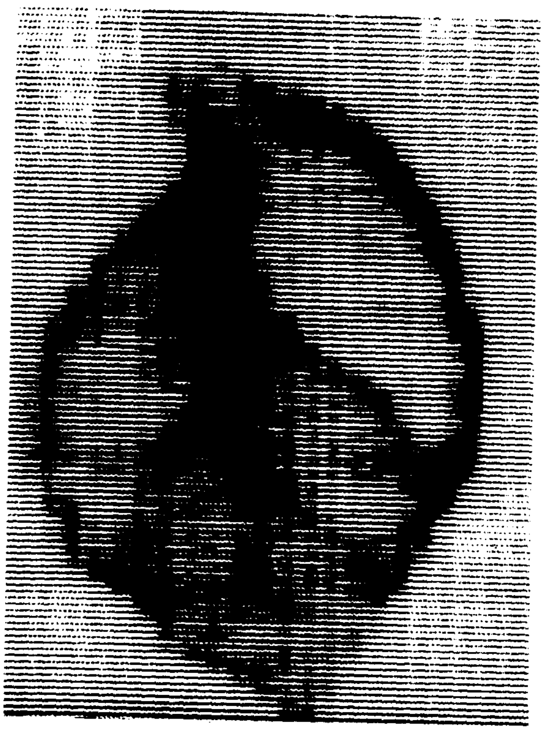

Fig. 13. A MWPC shell radiography.

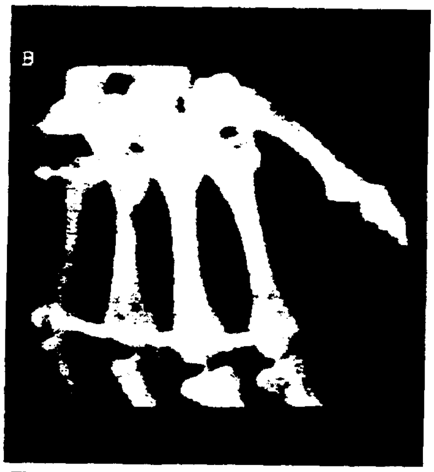

Fig. 6. The two dimensional bone mass distribution of a wrist of a human skeleton.

The system is now under clinical trial, as single photon absorptiometer at the energies of both I-125 (27.4 keV) and Gd-153 (42 and 100 keV) or as dual photon absorptiometer using one of the two pairs of isotopes (I-125,Gd-153) or (I-125, Am-241). Compared to standard DPA the MWPC system has a much lower repositioning error ⇒ this allows its use in regions with a large gradient of bone mineral density, such as the calcaneus or the very distal site of the forearm (both can be imaged in a few minutes), which seem superior in identifying early osteoporosis.

* F. Angelini, R.Bellazzini, A.Brez et al. Bone densitometry of the Pheripheral Skeleton with a new photon counting and imaging device. Investigative Radiology, 1989, 24(9), 684-691.

DIGITAL RADIOGRAPHY WITH MWPC:

Budker Institute for Nuclear Physics, Novosibirsk (Russia)
S. Baru et al, Nucl. Instr. Methods A283 (1989) 431
E. Babichev et al, Nucl. Instr. Methods A323 (1992) 49

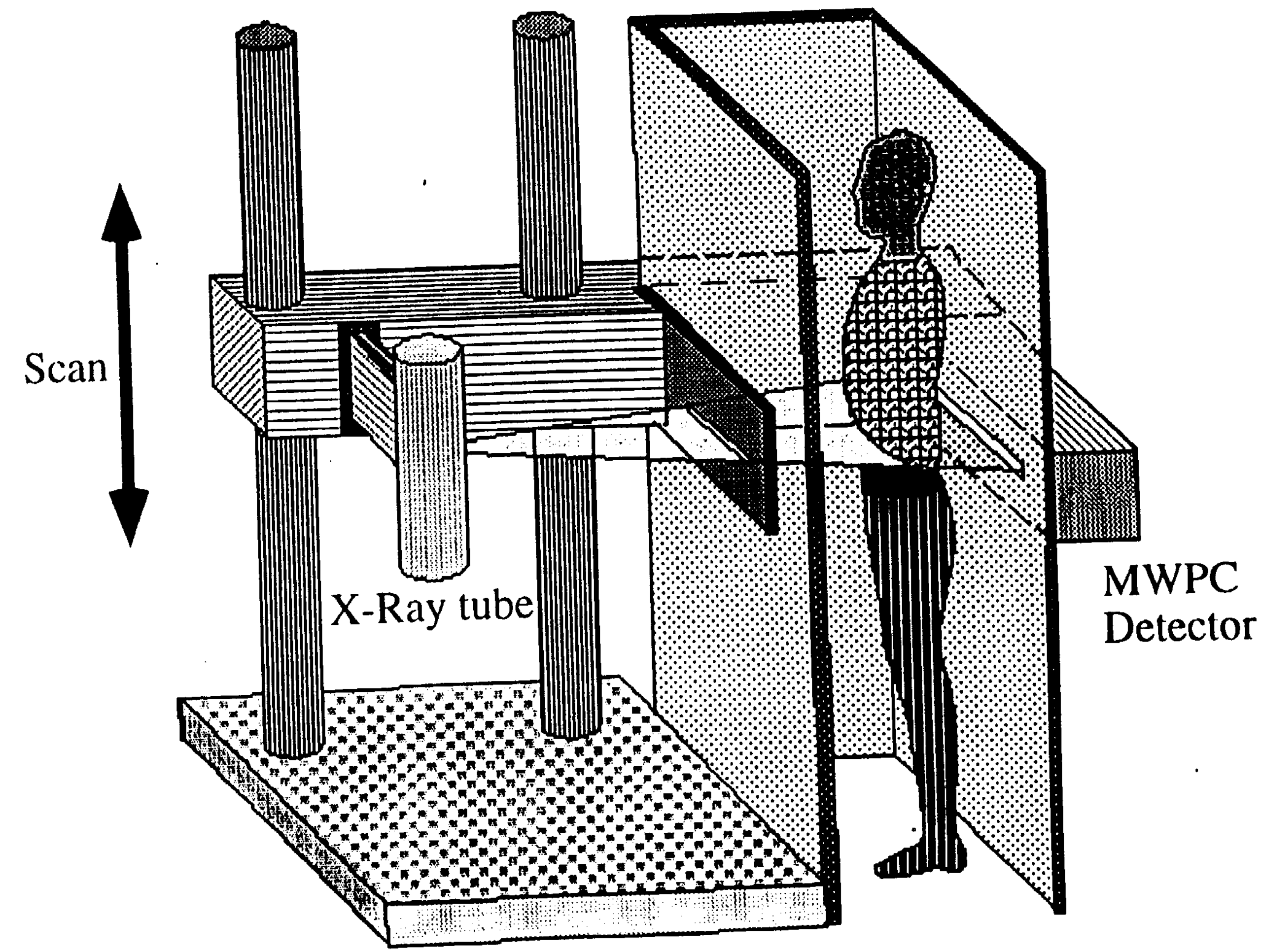

DIGITAL X-RAY MWPC DETECTOR:

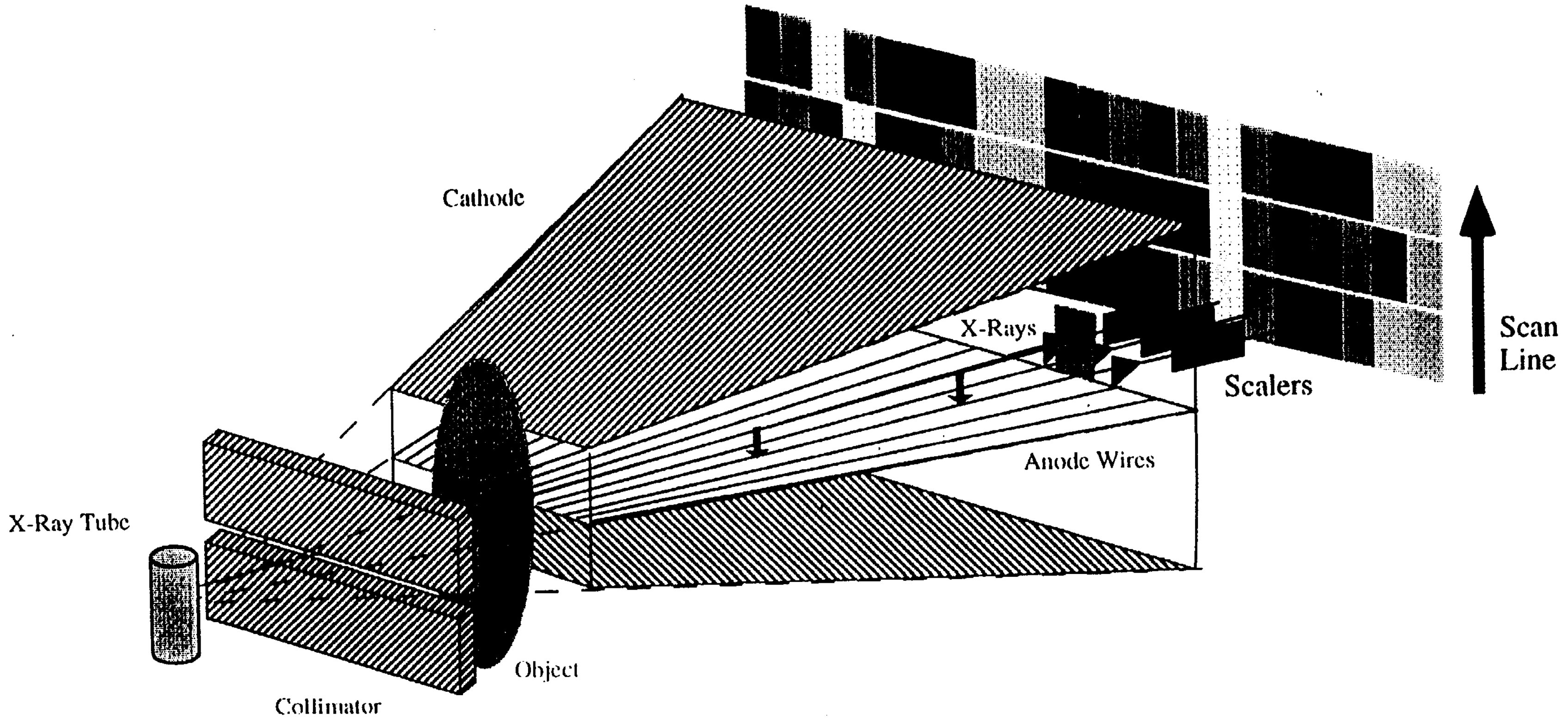

C940612D

Fig. 5 – Image of the pelvis of a pregnant woman (photo from a TV monitor).

Fig. 6 – Image of the chest (photo from a TV monitor).

SIBERIAN DIGITAL RADIOGRAPHY DEVICE (SDRD)

MWPC: 1 mm wire spacing
50 mm absorption
Xe-CO_2 at 3 Atmospheres
Efficiency 30% at 60 keV

Max Data Rate: 600 kHz per channel

Image Size: 320 x 256 pixels, $1mm^2$

Typical exposure times: 30 ms per line
10 s per image

THRESHOLD CONTRAST COMPARISON AS A FUNCTION OF DOSE:

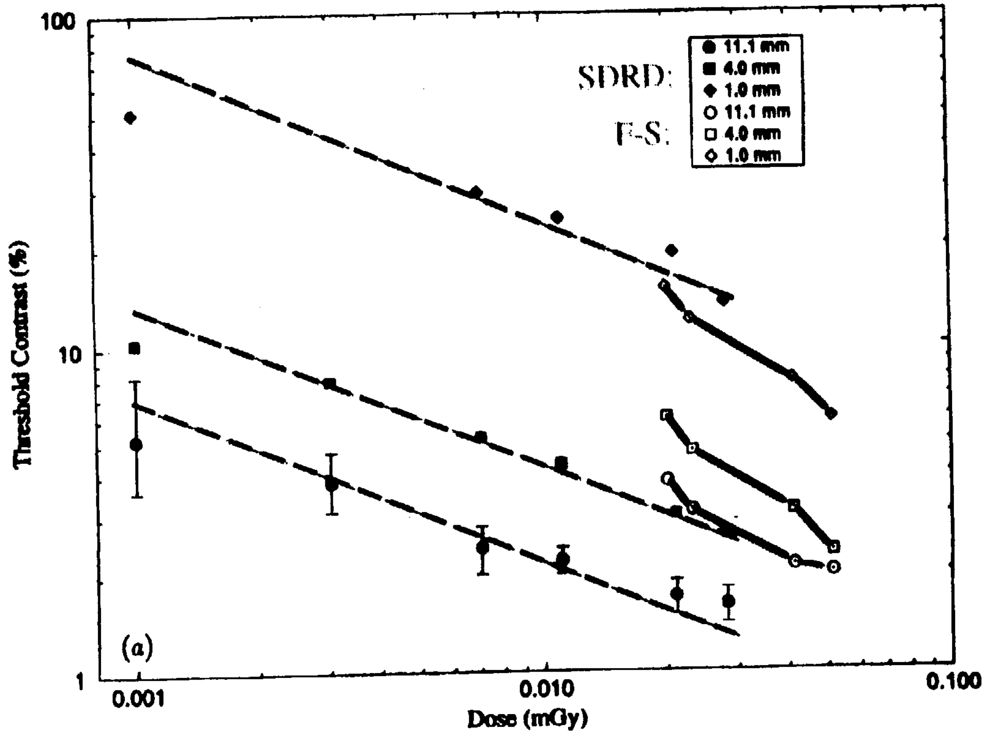

SDRD: SIBERIAN DIGITAL RADIOGRAPHY DEVICE
F-S: UK FILM-SCREEN SYSTEM

EXPOSURES FOR CLINICAL EXAMINATIONS
(ENTRANCE SKIN DOSES IN mGy) :

	SDRD	F-S (NRPB)
Chest	0.015	0.23
Abdomen	0.03	8.43
Lumbar Spine	0.292	22.80

A. Martinez-Davalos, R.D. Speller, J.A. Horrocks, D.J. Miller, S.E. Baru, A.G. Khabakhpashev, O.A. Ponomarev, L.I. Shekhtman
Phys. Med. Biol. 38 (1993) 1419

36

MICRO-STRIP GAS CHAMBER

A. Oed, 1988

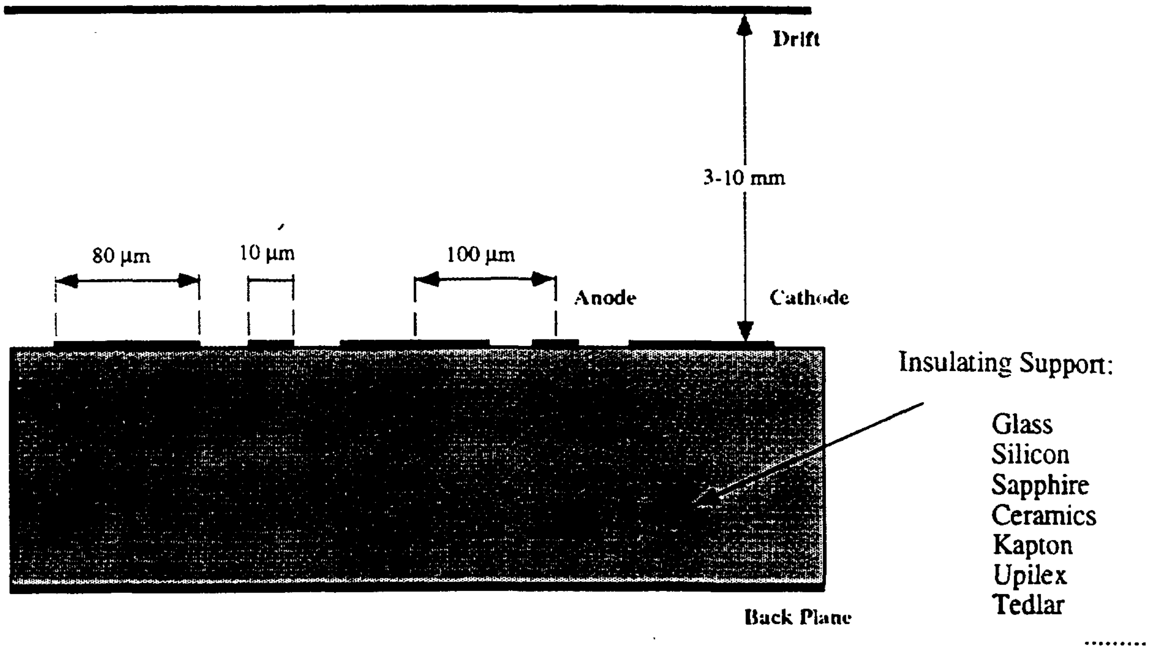

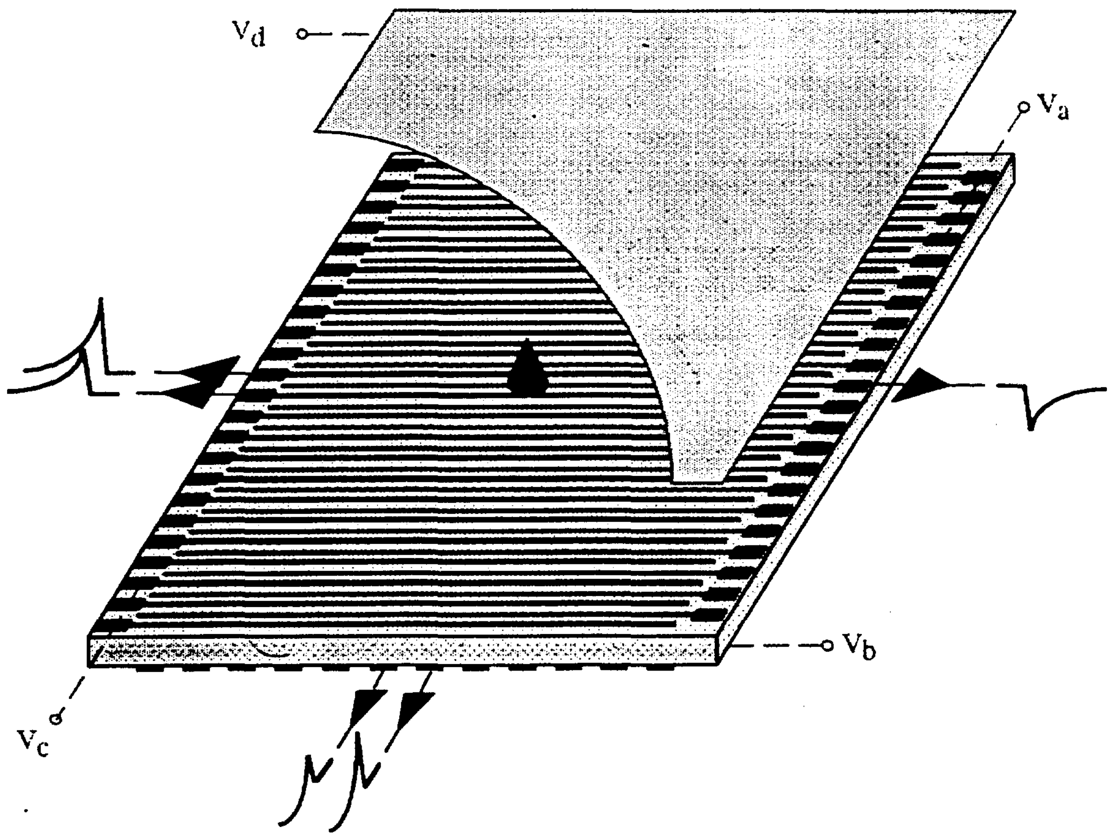

2-D and 3-D MSGC

A. Oed, Nucl. Instrum. Methods A263 (1988) 35

MULTIWIRE PROPORTIONAL CHAMBER

George Charpak (1968)

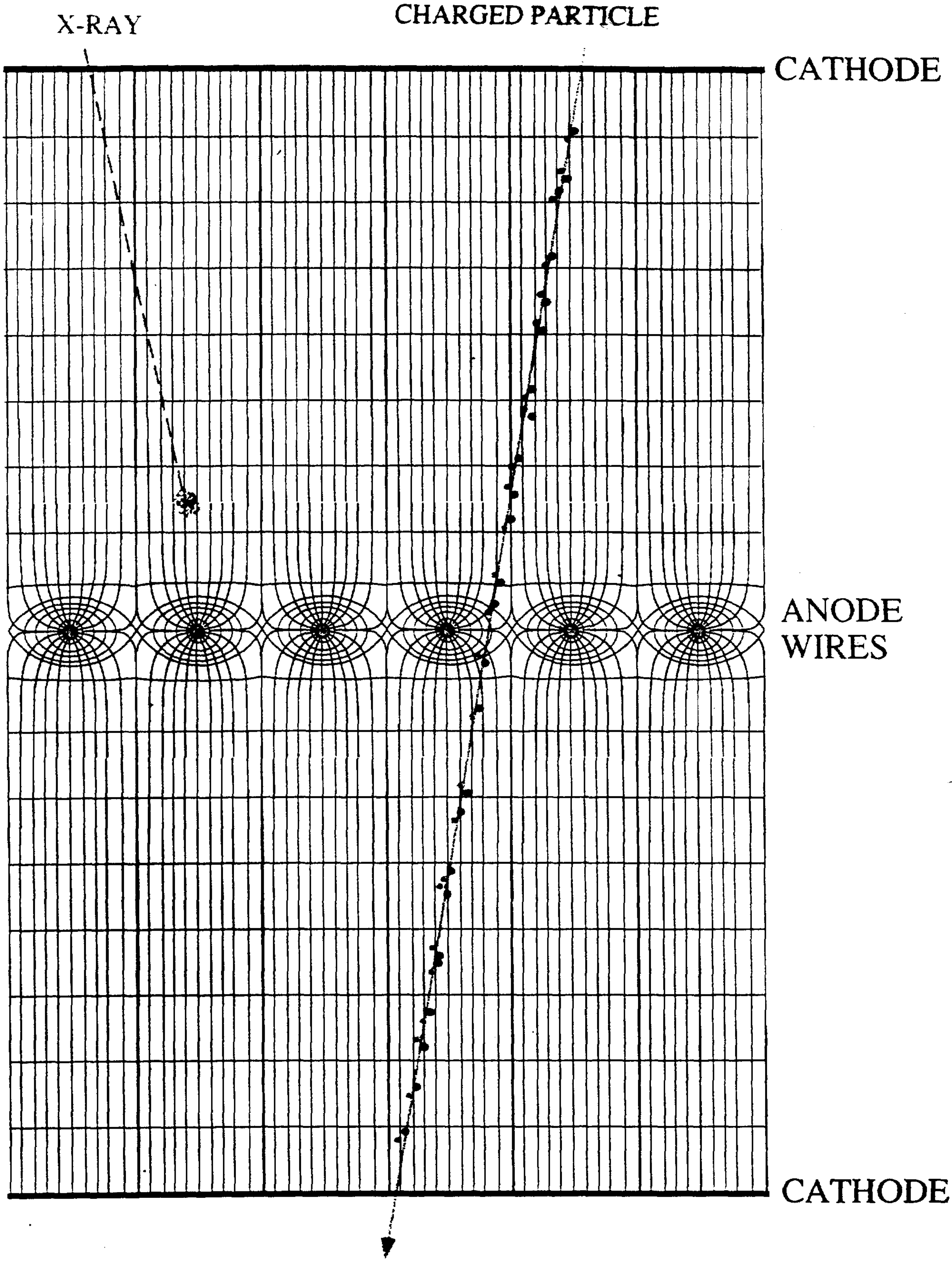

FIELD LINES AND EQUIPOTENTIALS IN THE MSGC:

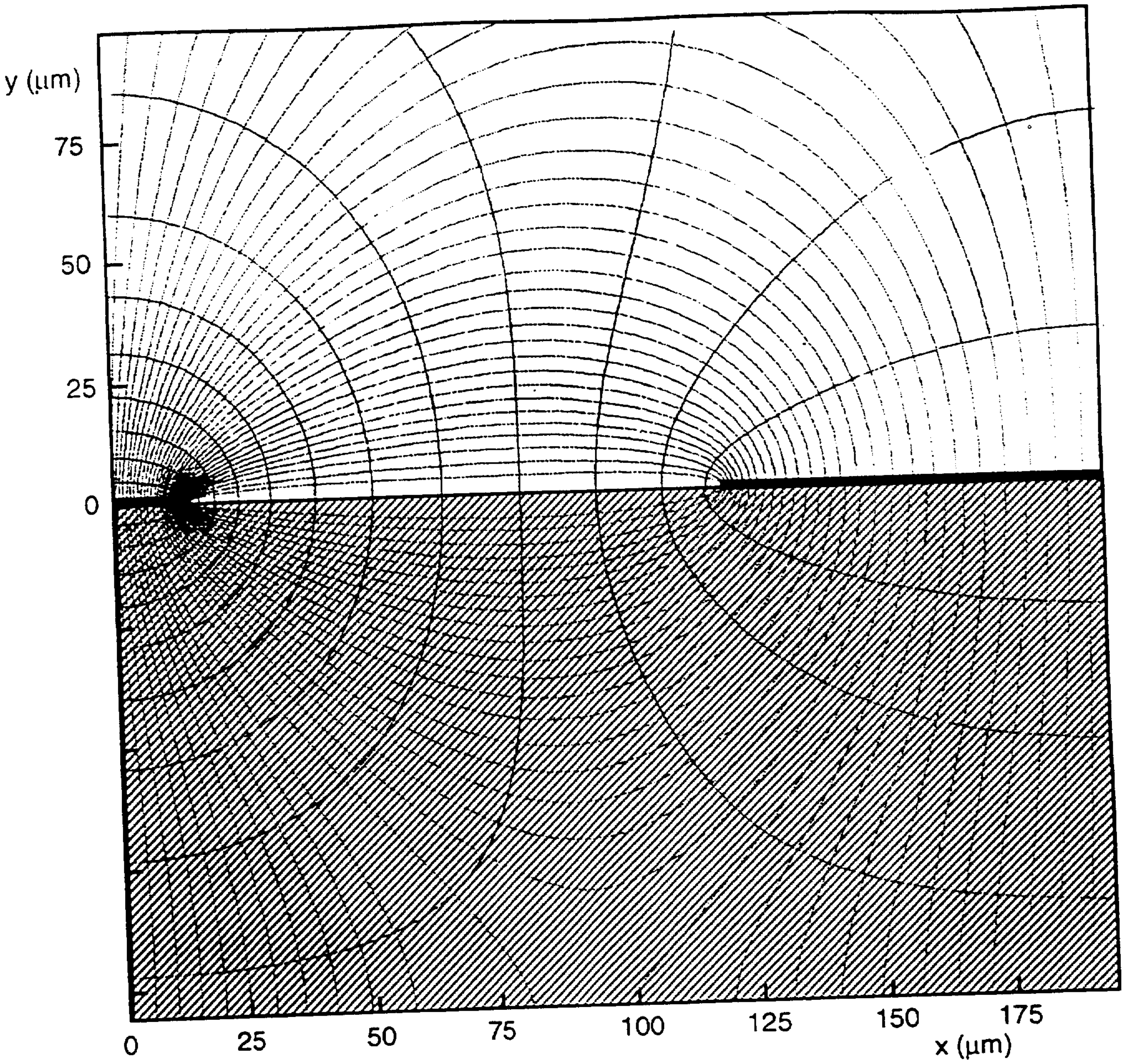

J.J. Florent, J. Gaudaen, L. Ropelewski and F. Sauli, Nucl. Instrum. Methods **A329** (1993) 125.

C940621B

ELECTRIC FIELD LINES IN MSGC:

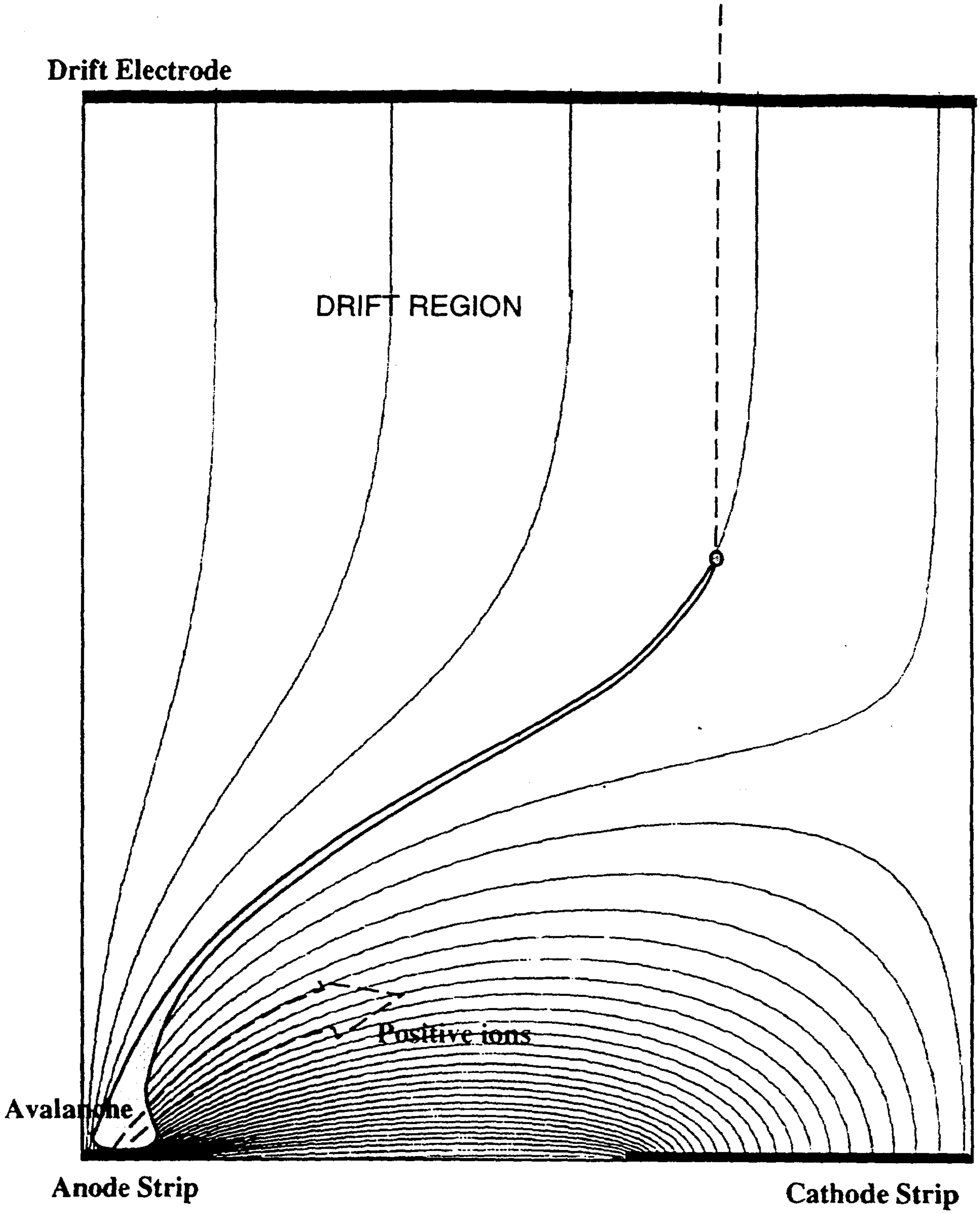

MSGC FIELD AND IONS

GLASS MSGC

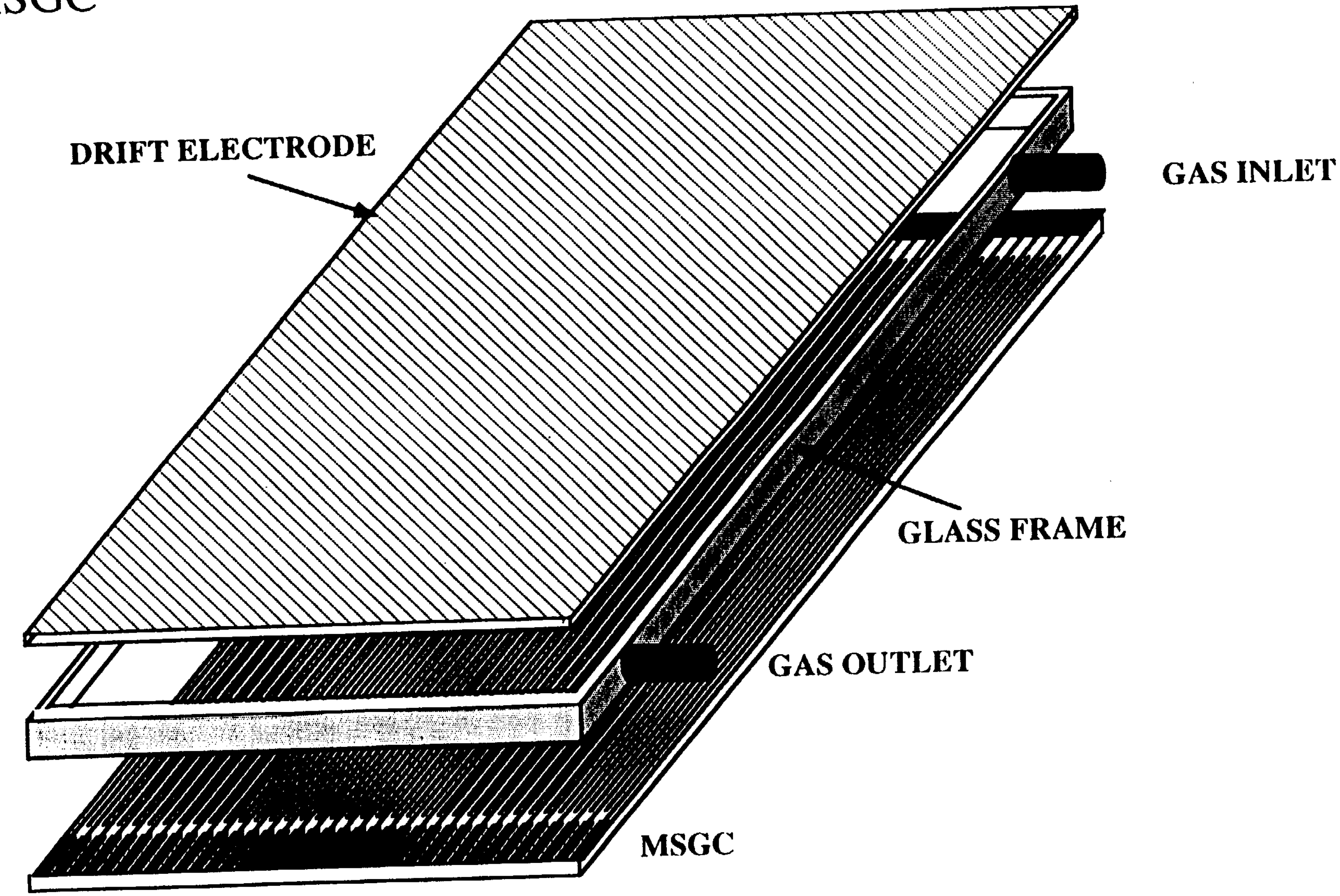

41

MSGC: VERY GOOD ENERGY RESOLUTION

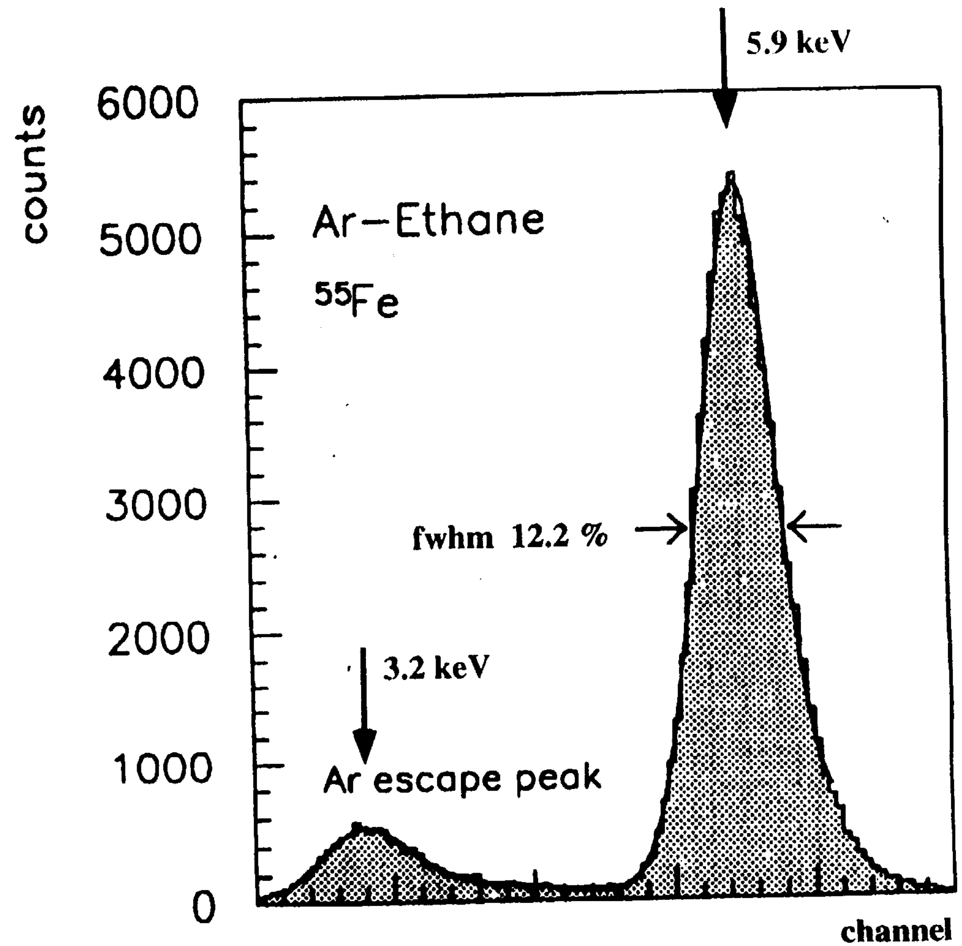

Energy resolution (low energy region):

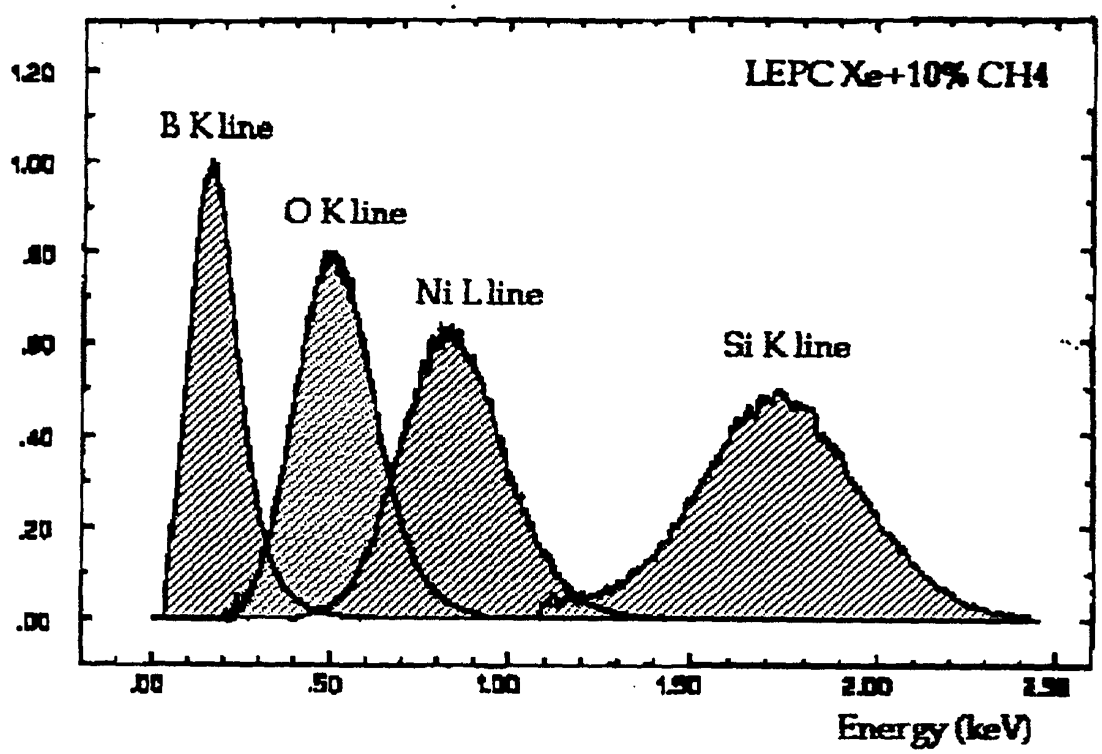

Energy resolution (high energy region):

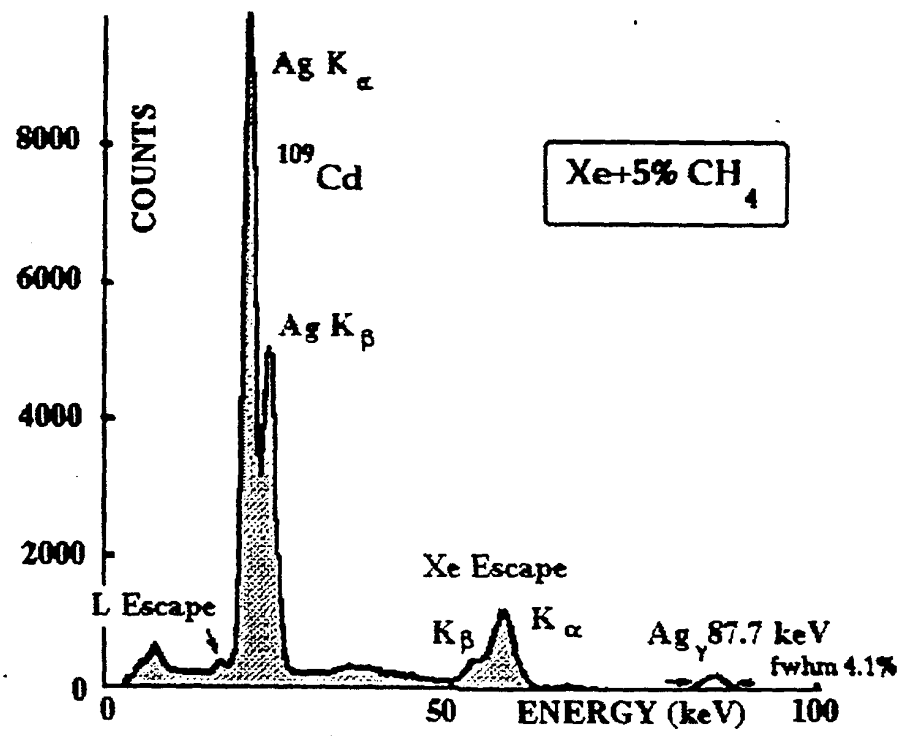

C. Budtz-Jørgensen, Rev. Sci. Instrum. 63 (1992) 1

MICRO-STRIP GAS CHAMBER STRIP RESPONSE FUNCTION

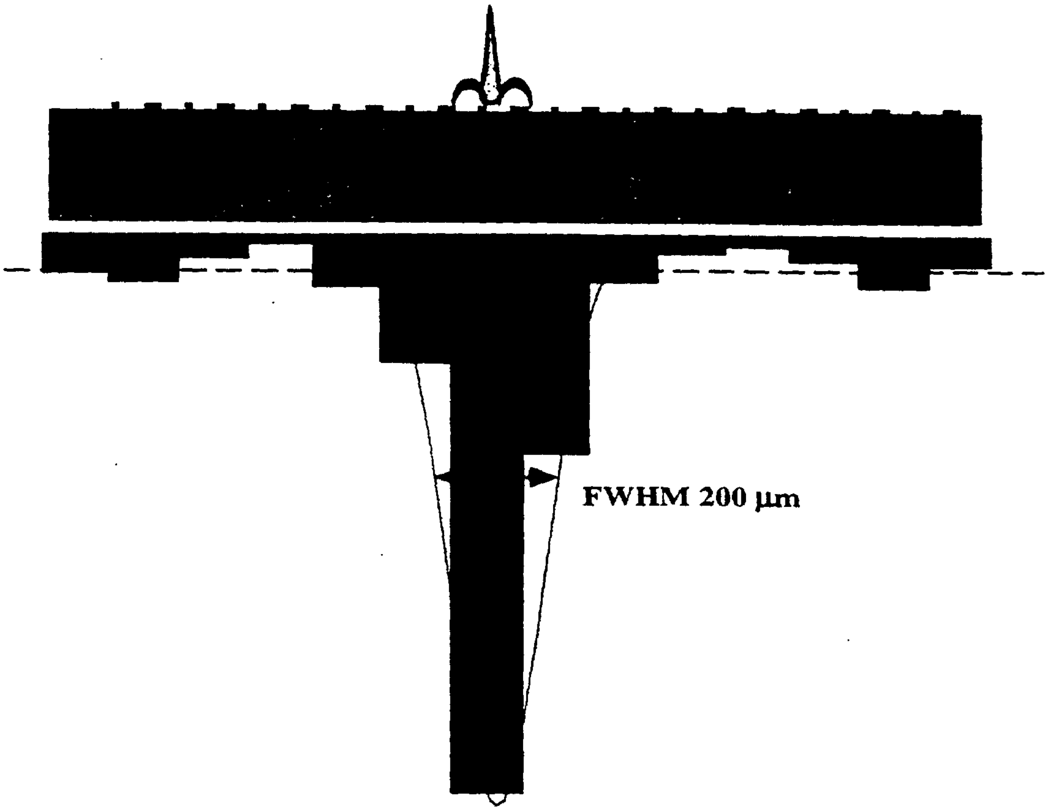

LOCALIZATION ACCURACY (MINIMUM IONIZING TRACKS):

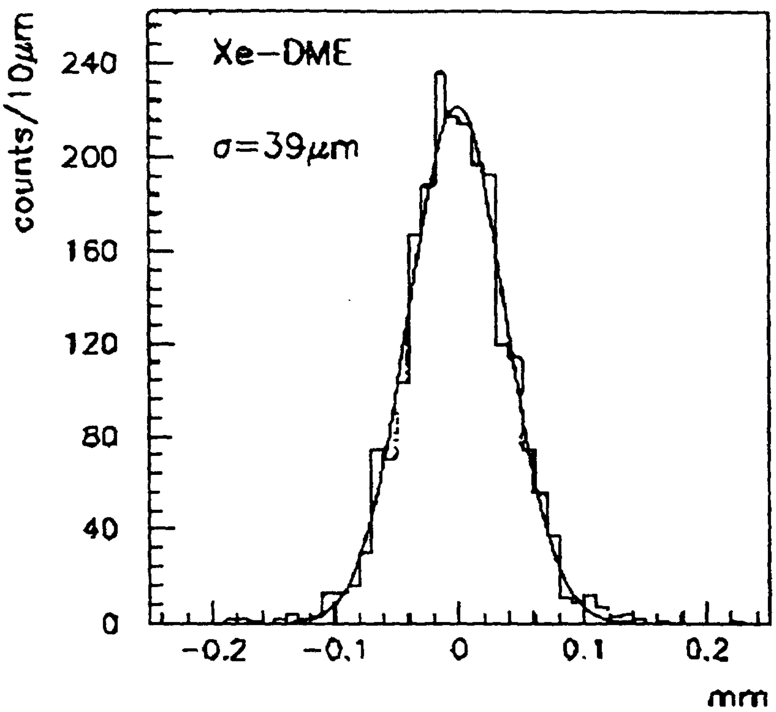

MSGC PRF

F. Angelini et al, Nucl. Physics 23 (1991) 254

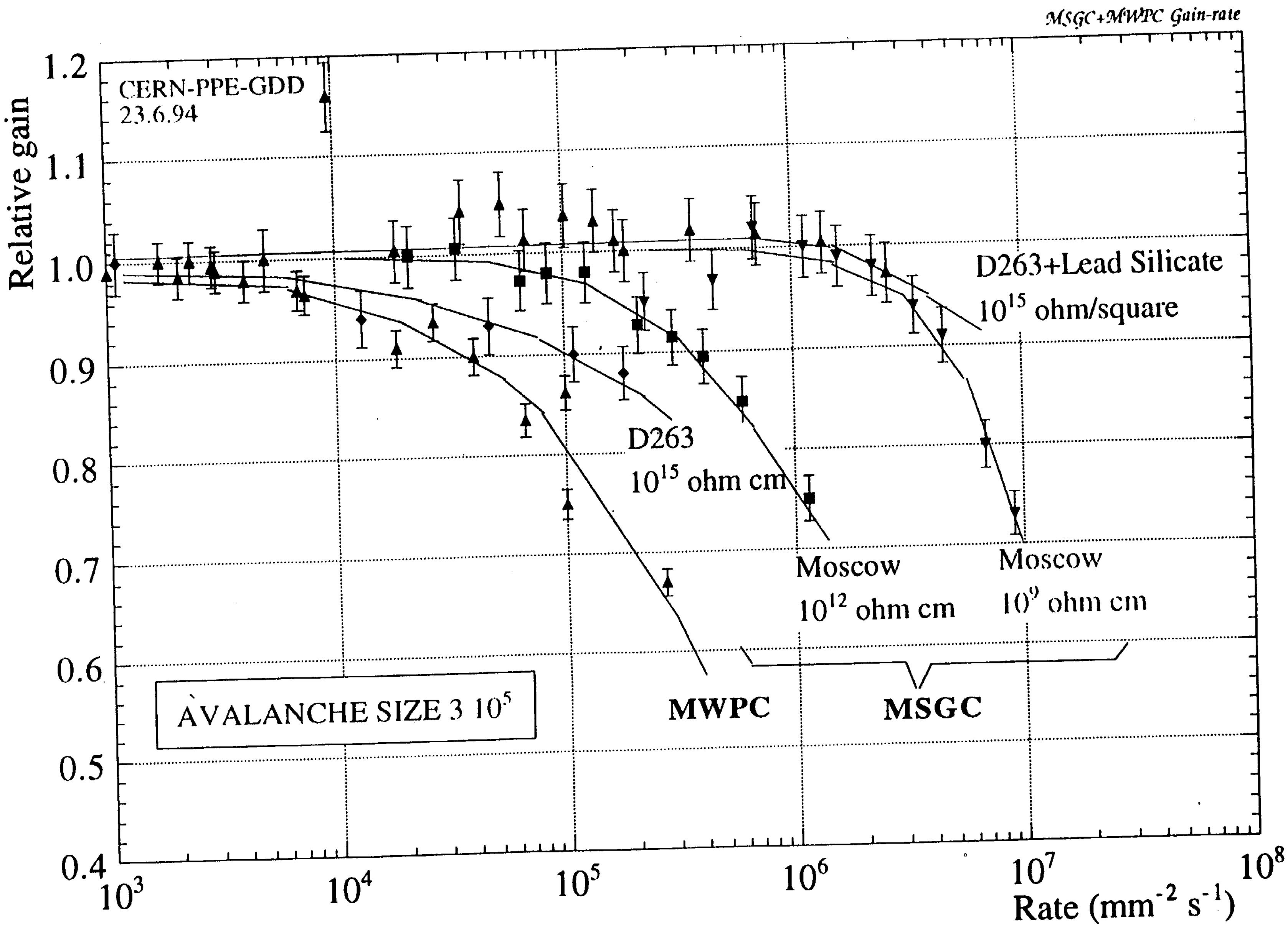
MSGC+MWPC Gain-rate
CERN-PPE-GDD
23.6.94
Relative gain
1.2
1.1
1.0
0.9
0.8
0.7
0.6
0.5
0.4
D263+Lead Silicate
10^15 ohm/square
D263
10^15 ohm cm
Moscow
10^12 ohm cm
Moscow
10^9 ohm cm
MWPC
MSGC
AVALANCHE SIZE 3 10^5
10^3
10^4
10^5
10^6
10^7
10^8
Rate (mm^-2 s^-1)

45

OPERATION OF MSGC AT HIGH PRESSURES:

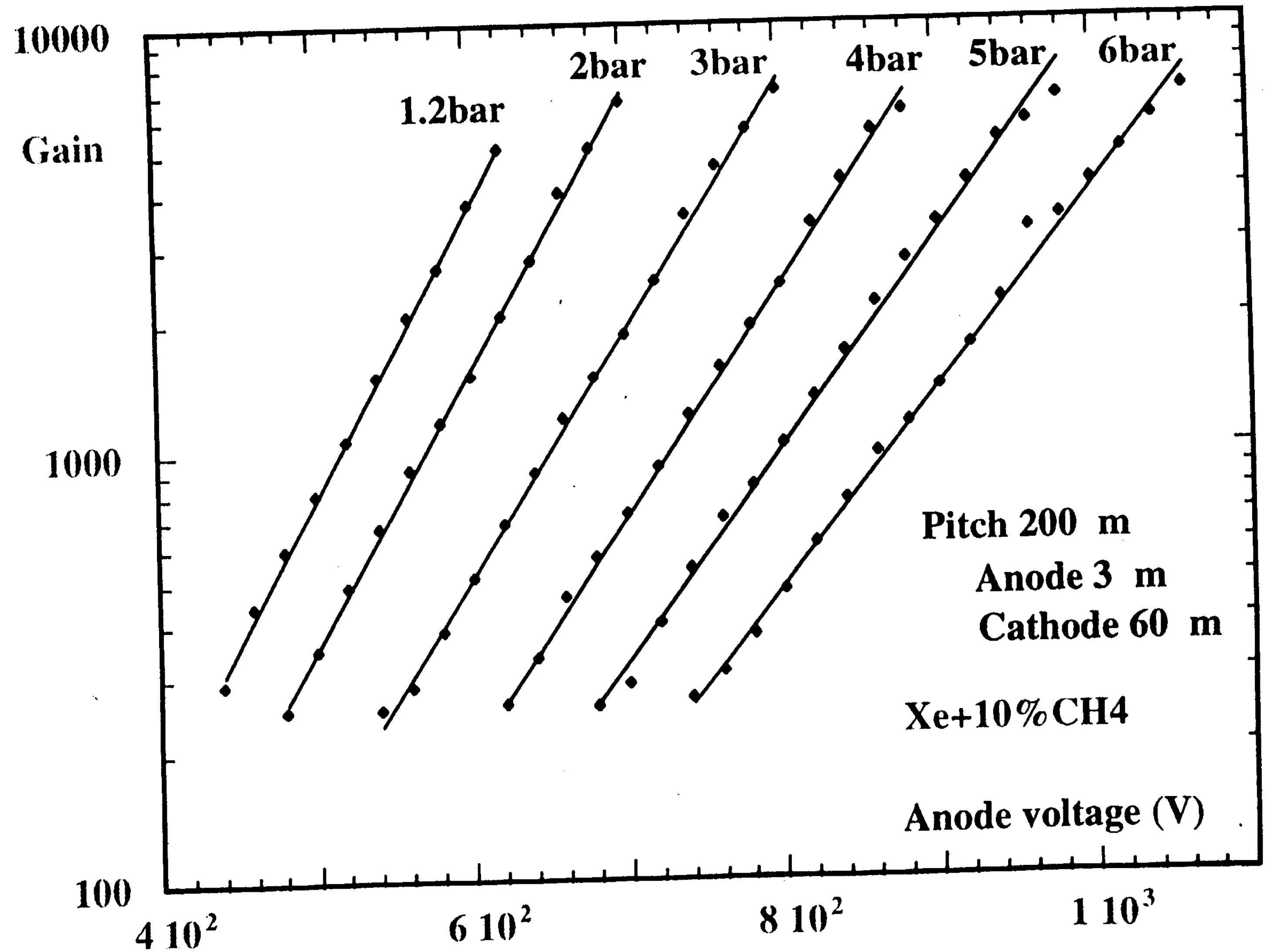

G.D. Minakov et al, Nucl. Instrum. Methods A326 (1993) 566

HIGH PRESSURE MSGC GAIN

46

DIGITAL X-RAY MSGC DETECTOR:

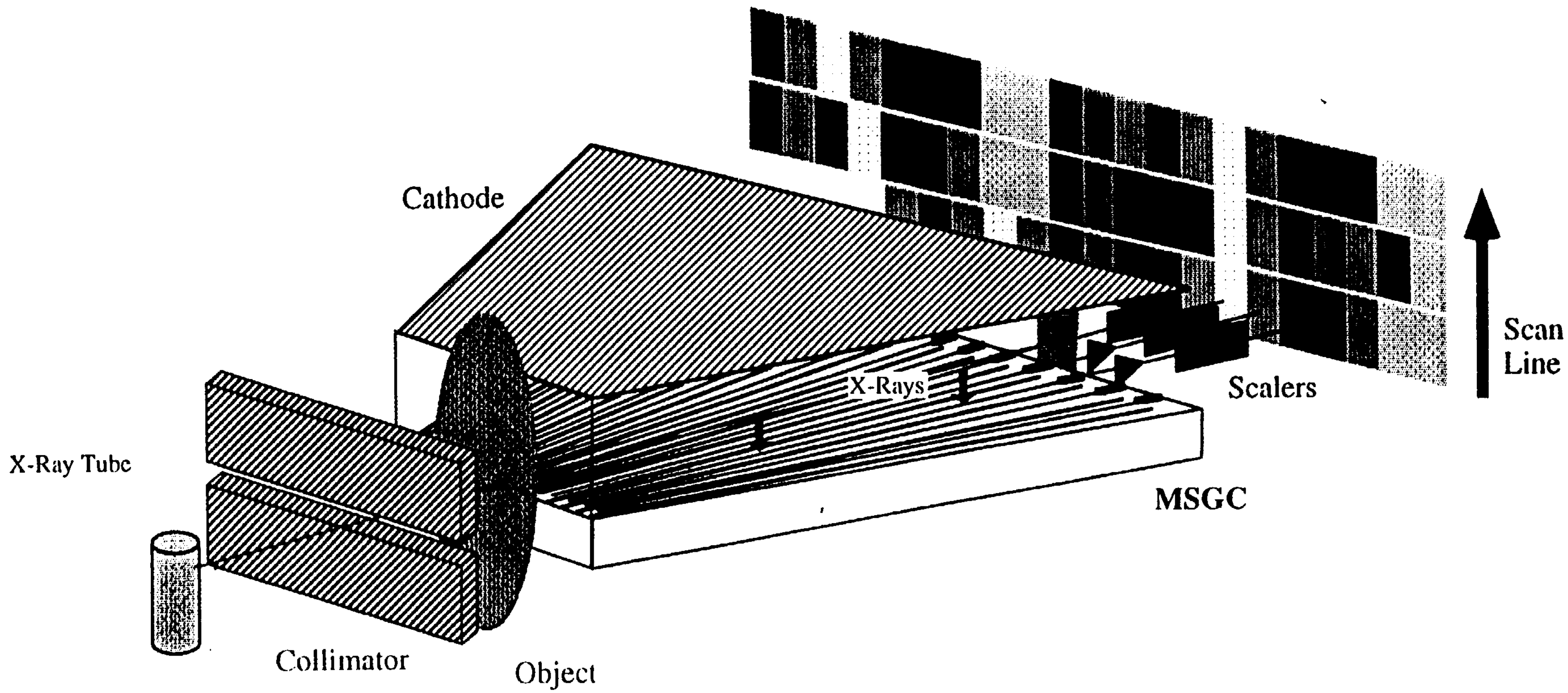

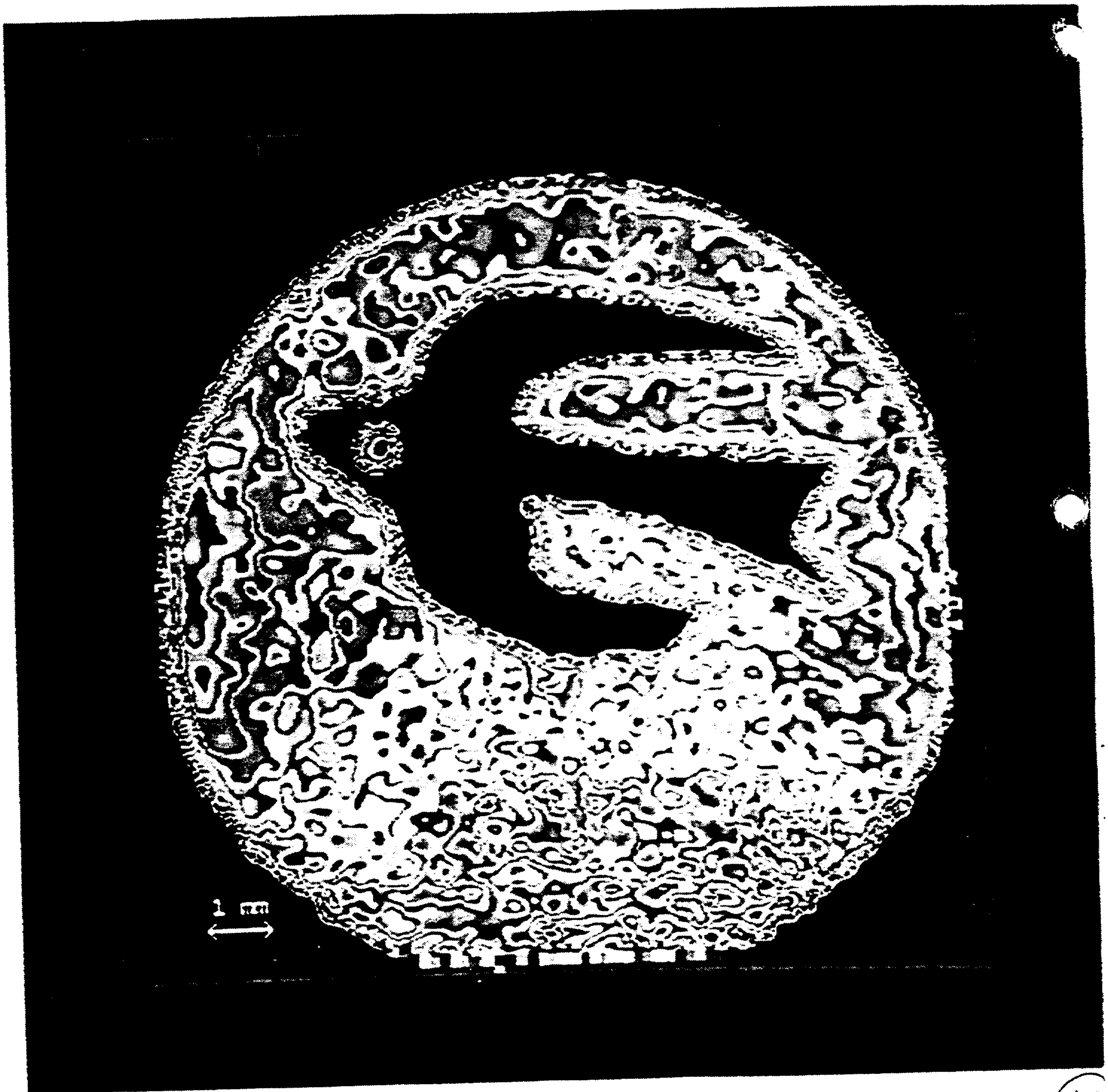

48

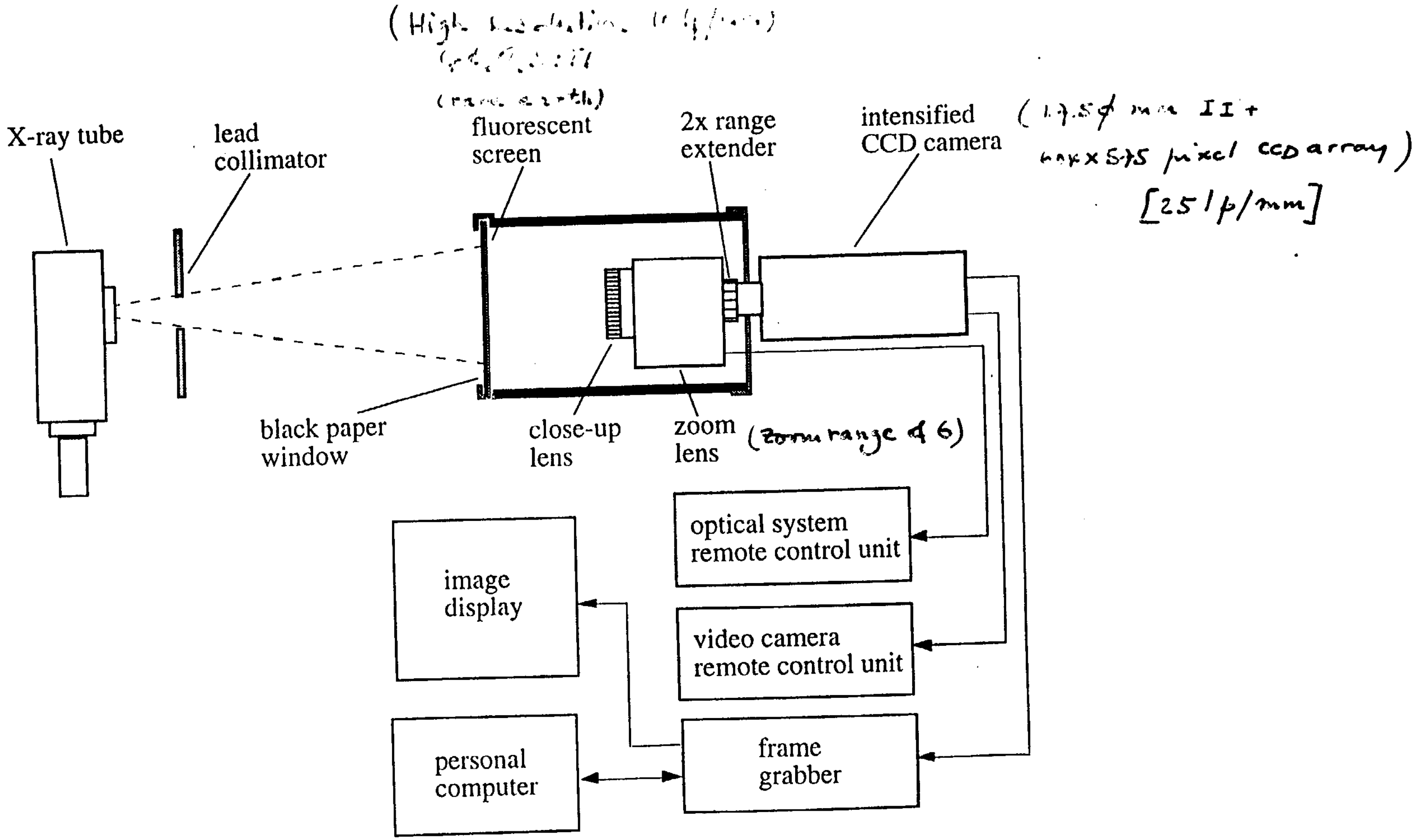

from { Gambaccini et al. 1994 SPIE proceedings 2132, 295-300.
Gambaccini et al. 1994, Physica Medica X(2)(1994)47

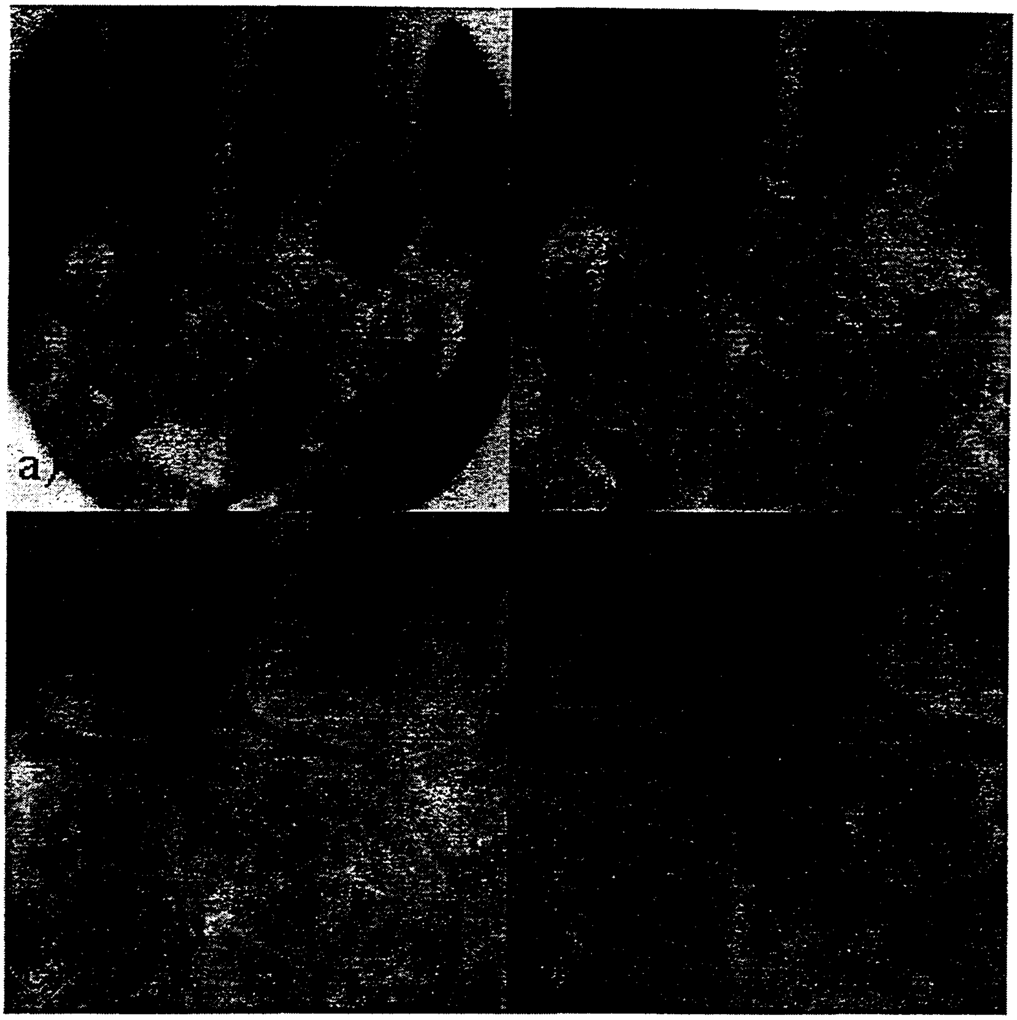

Fig. 3. Radiographic images of the phanton of a hand. Zoom factors: a) 1 x; b) 1.7 x; c) 2.8 x; d) 4.6 x.

SILICON MICRO-STRIP DETECTOR:

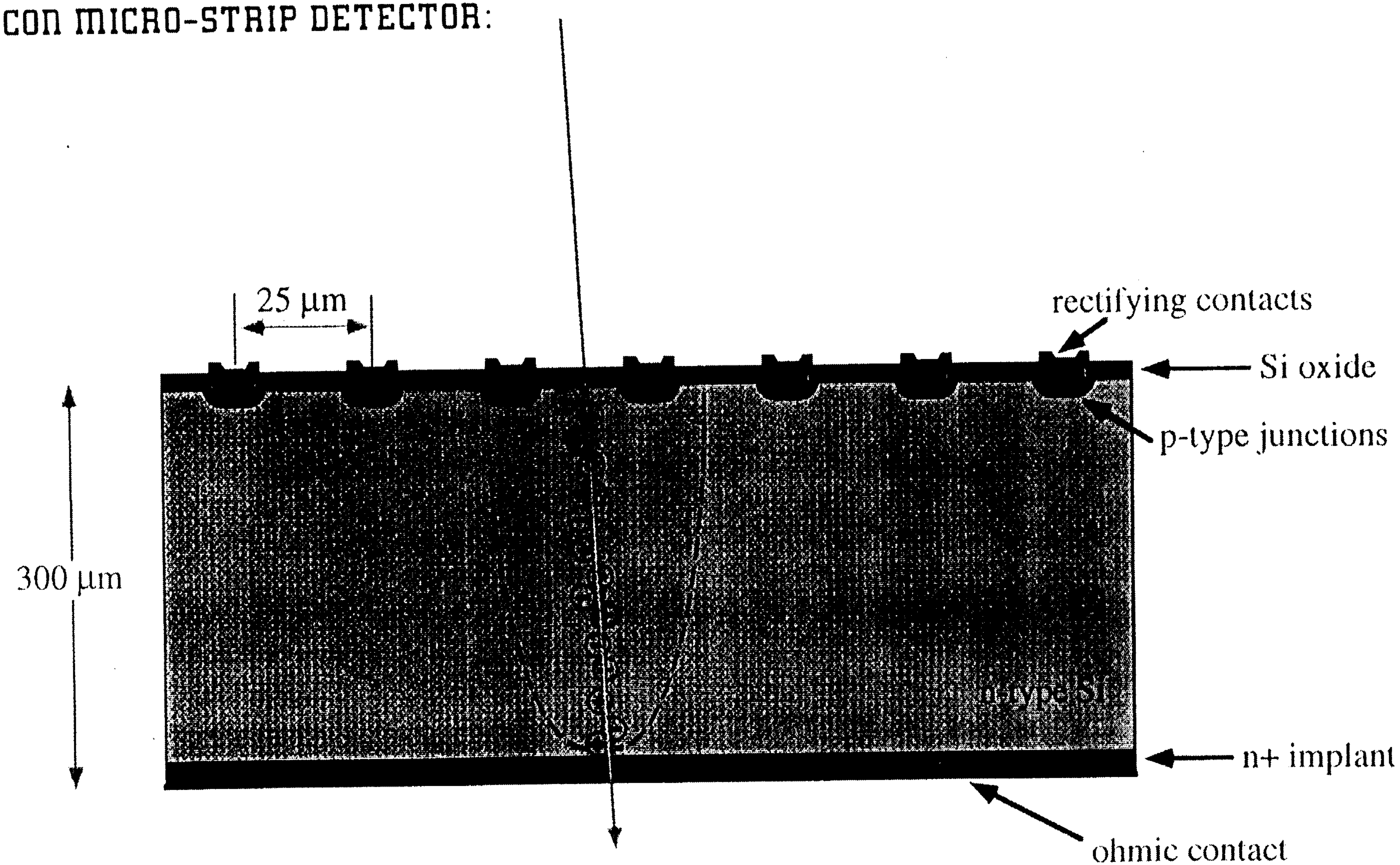

J. Kemmer, Nucl. Instrum. Methods 169 (1980) 499

TWO-DIMENSIONAL SILICON MICROSTRIP

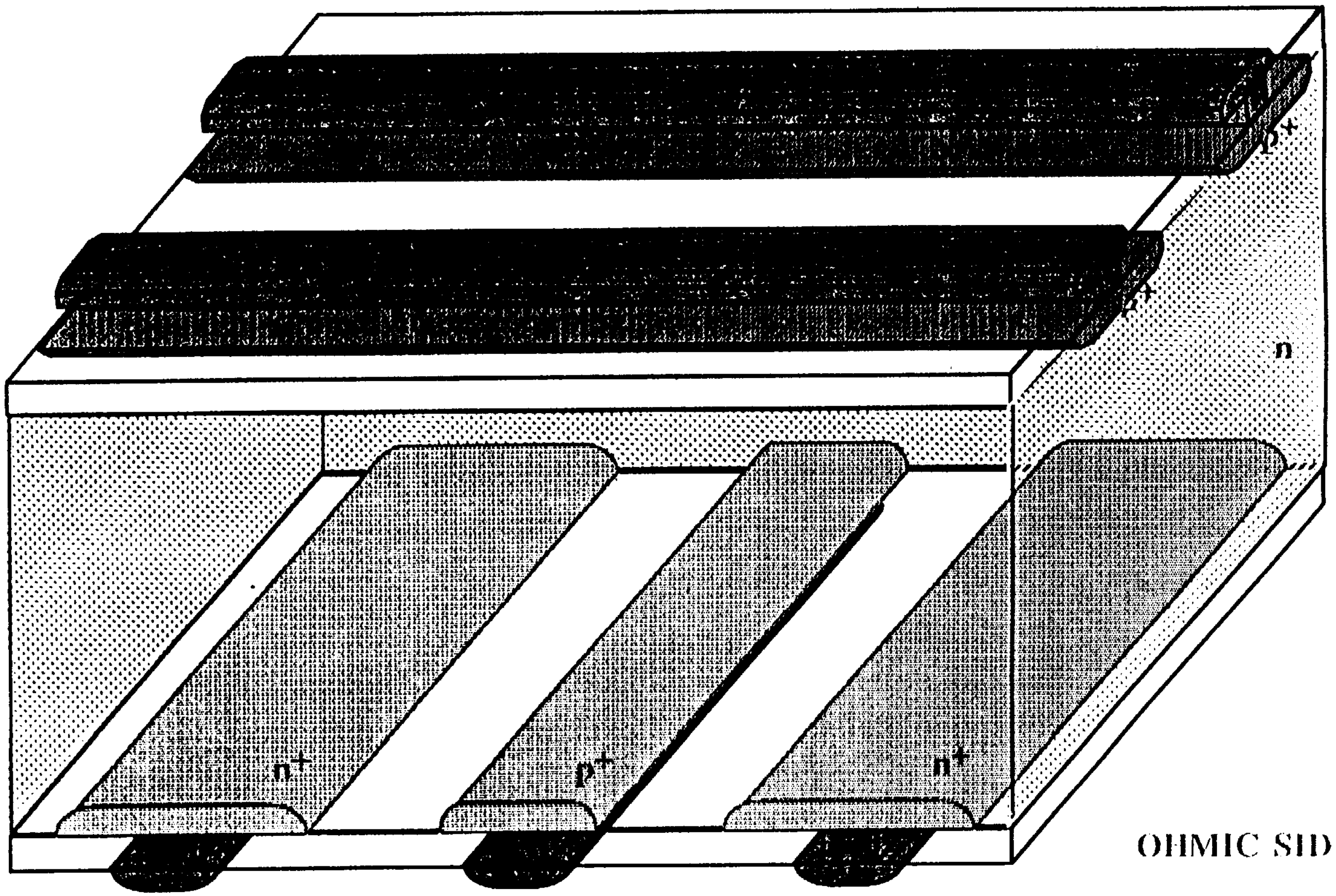

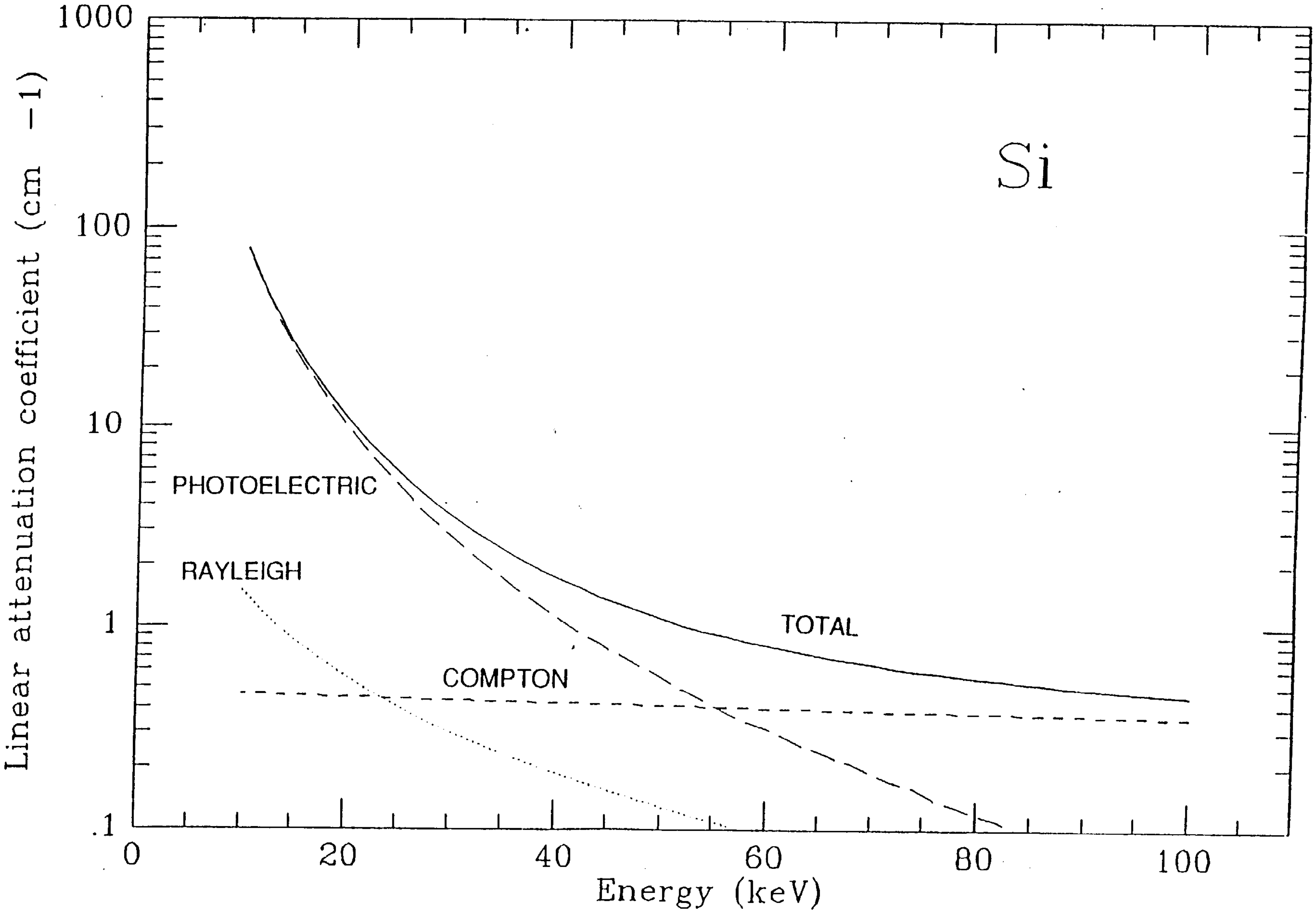

Si
1000
100
10
1
.1
0
20
40
60
80
100
Linear attenuation coefficient (cm -1)
Energy (keV)
PHOTOELECTRIC
RAYLEIGH
COMPTON
TOTAL

53

X-RAY ABSORPTION LENGTH AND EFFICIENCY OF SILICON

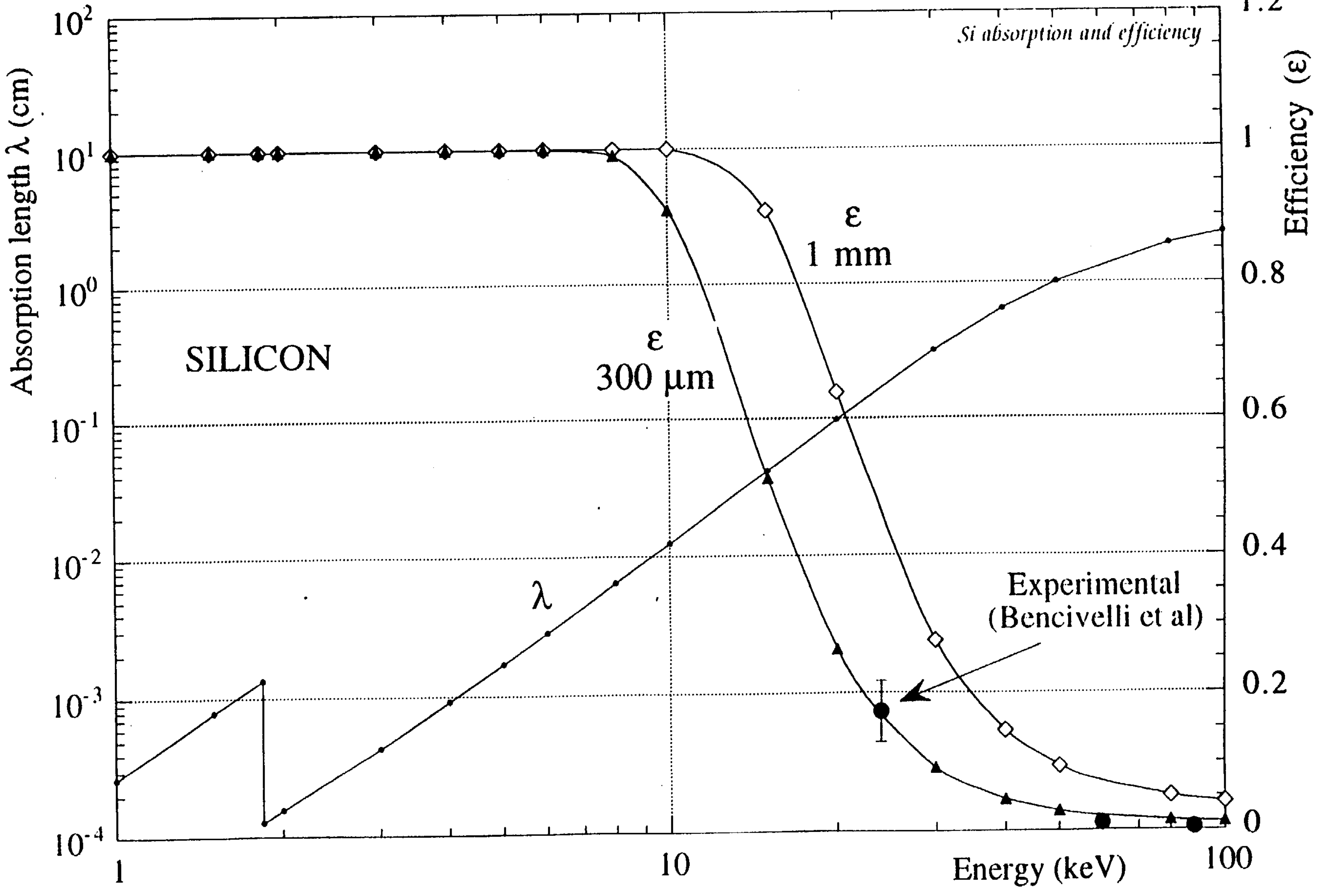

54

SUMMARY OF EGS4 CAPABILITIES AND FEATURES

* The radiation transport of electrons (+ or -) or photons can be simulated in any element, compound or mixture.

* The dynamic range of charged particles goes from 10 keV to a few thousand GeV, while the dynamic range of photon energies lies between 1 keV and several thousand GeV.

* The following physical processes are taken into account by the EGS4 Code System:

  - Bremsstrahlung production
  - Positron annihilation in flight and at rest
  - Molière multiple scattering
  - Møller ($e^- e^-$) and Bhabha ($e^- e^+$) scattering
  - Continuous energy loss applied to charged particle tracks
  - Pair production
  - Compton scattering
  - Coherent (Rayleigh) scattering
  - Photoelectric effect

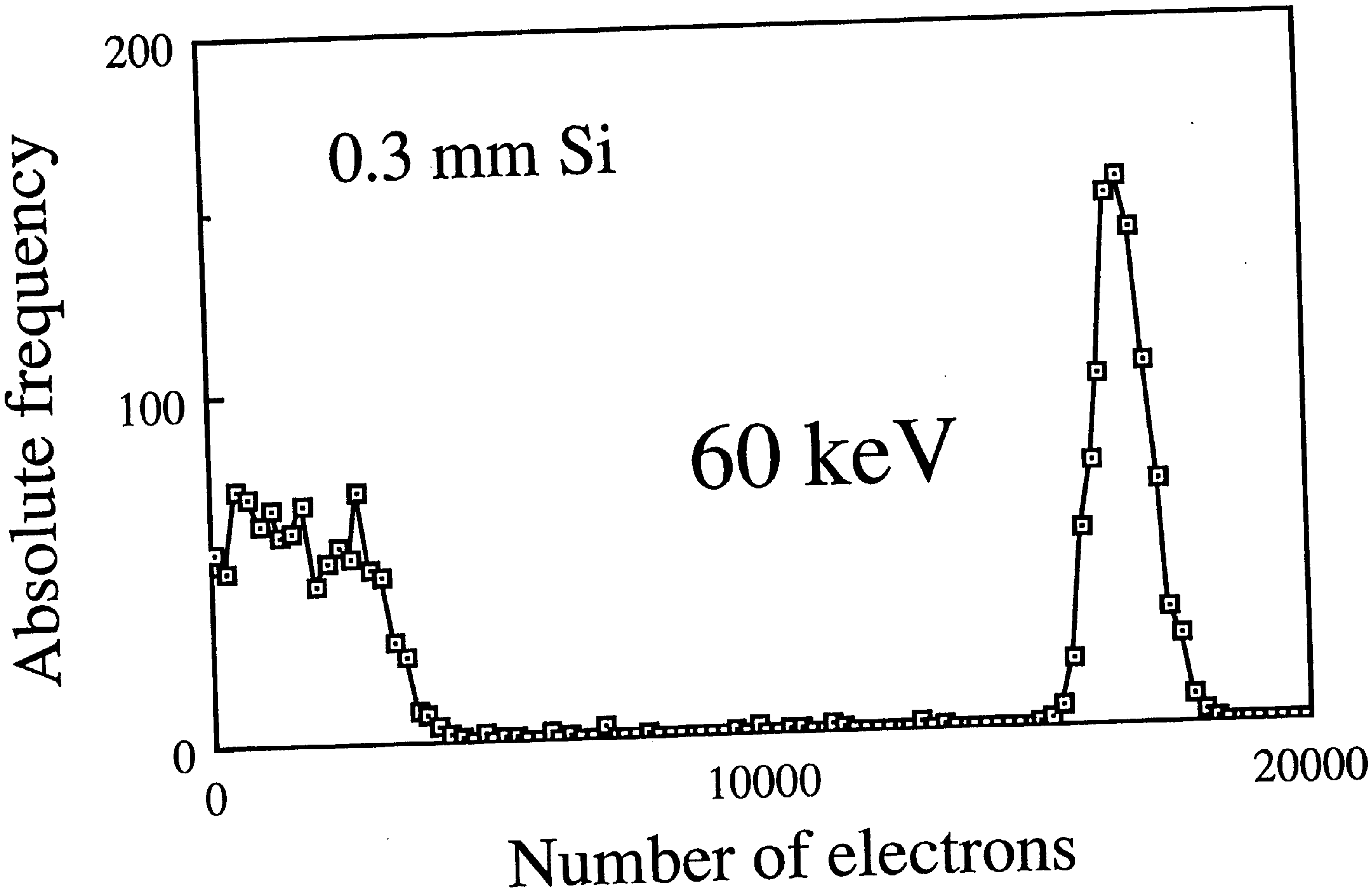

Fig. 6a: Charge deposit for 60 keV incident photons

56

$(^{241}Am \rightarrow 60\ keV)$

$(^{109}Cd \rightarrow \simeq 22\ keV,\ \simeq 80\ keV)$

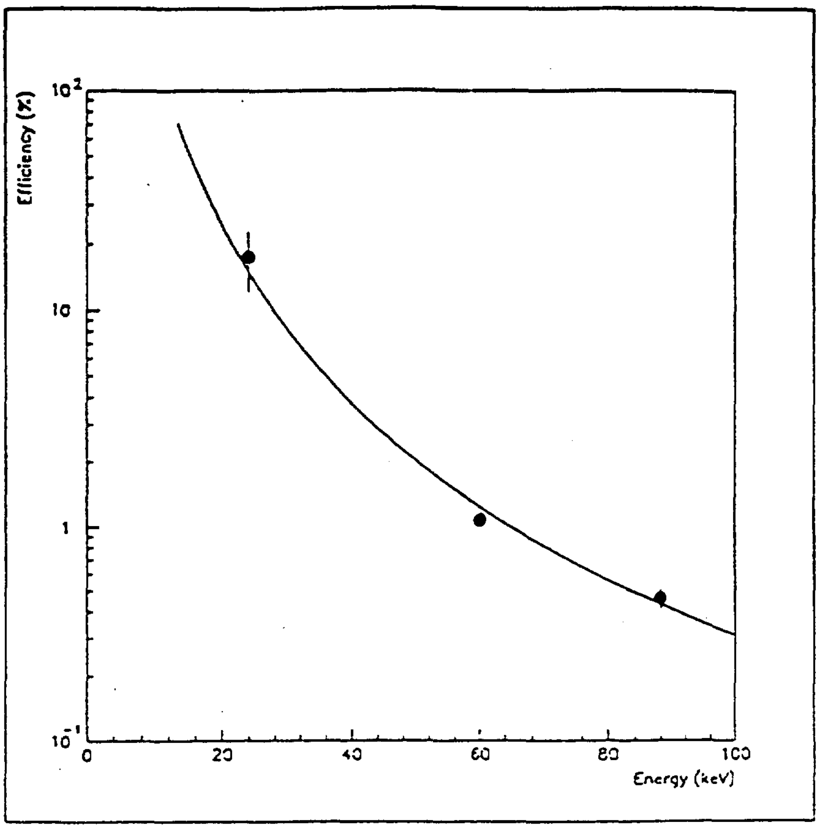

Figure 6: Experimental efficiency (%) for 24, 60 and 88 keV photons. The solid line represents the MonteCarlo simulation.

• Energy resolution $\sigma/E \sim 13\%$

A. Baudettini et al, IEEE Trans. Nucl. Sci. NS40 (1993) 983

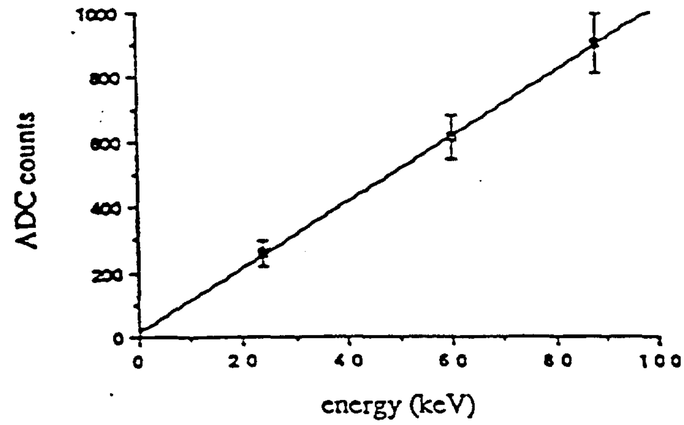

Figure 1. Charge released in the crystal (ADC counts) versus photon energy. The vertical bars are the standard deviations as calculated by a Gaussian fit to the charge distribution.

• Spatial resolution

$\sigma = 8\ \mu m - 22\ \mu m$

B. Alfano et al, Phys. Med. Biol. 37 (1992) 1167

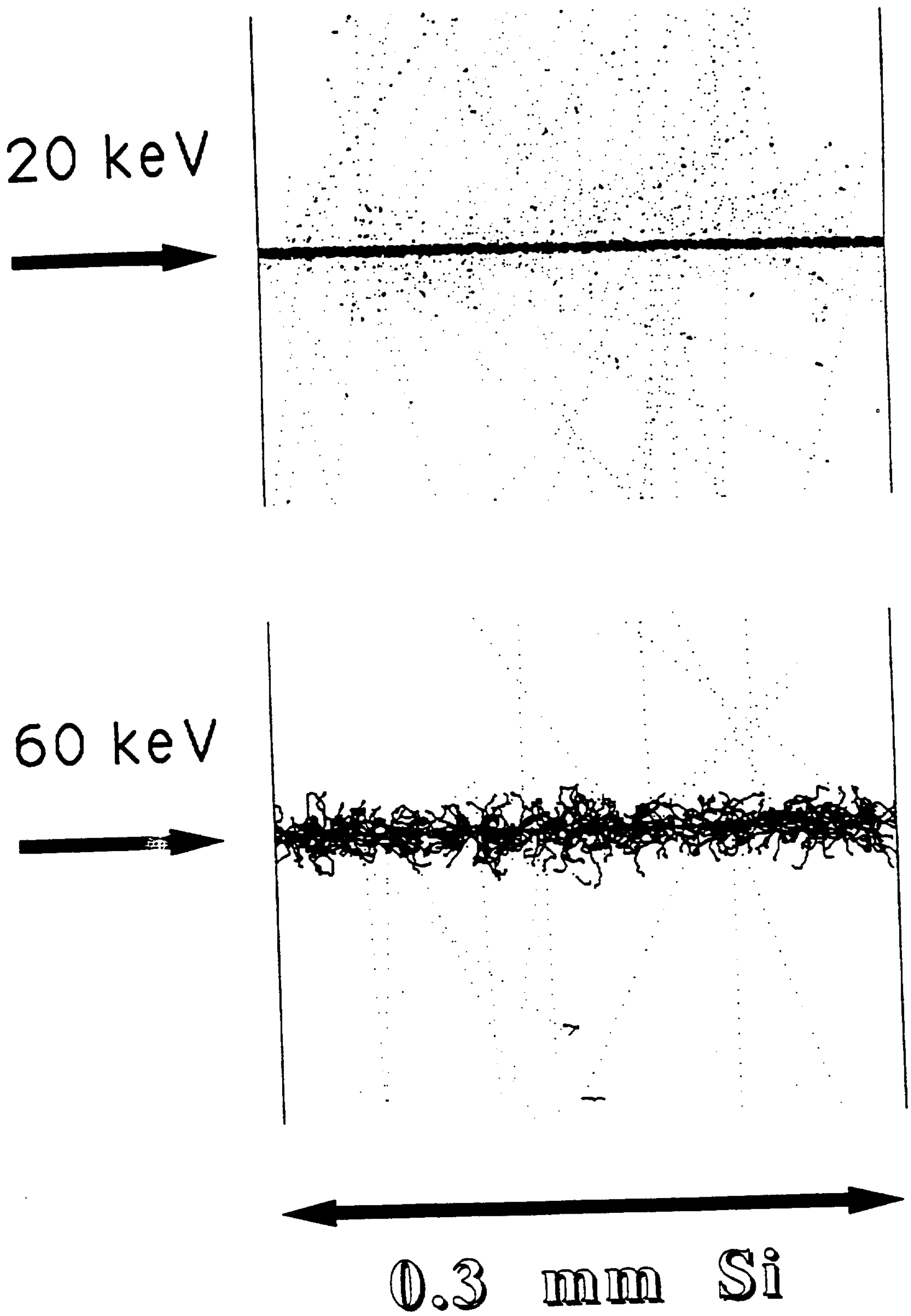

Fig. 7: Plot (side view) of 20000 tracks of photons (dotted) and electrons inside a 0.3 mm thick Si crystal.

[illegible] et al. Nucl. Instr. Meth. A[illegible] (199[illegible]) 574.

A new 2-Dimensional High Resolution Si Detector for ß- and γ-Radiography

A. Czermak[1], P. Jalocha[1], A. Kjensmo[2], G. Malamud[3], E. Nygård[4], C. Rönnqvist[5], F. Santos[6], J. Straver[2] and P. Weilhammer[3]

1. IFJ, Cracow, Poland
2. IDE AS, Oslo, Norway
3. CERN, Geneva, Switzerland
4. University of Oslo, Norway
5. SEFT, Helsinki, Finland
6. Federal Univ. of Rio de Janeiro, Rio de Janeiro, Brazil

A double-sided silicon microstrip detector read out by a CMOS low noise self-triggering 128-channel chip has successfully been tested with low energy γ- and X-rays and ß-emitting sources for imaging of simple patterns. The readout chip is described in detail, as well as the detector, the ancillary electronics and the data acquisition. Images of the size of 6.4 x 6.4 mm^2 are presented. The readout pitch is 50 μm in both the x- and the y-direction. The energy resolution for the 44.23 keV K_α-line from Tb is measured to 0.86 keV (240 e^- rms). For ß-patterns with ^{35}S, the spatial spread is in good correlation with the range of the particles (130 μm).

Contribution to 6th Pisa
Meeting on Advanced Detectors
22-28 May 1994, La Biodola
Isola d'Elba

59

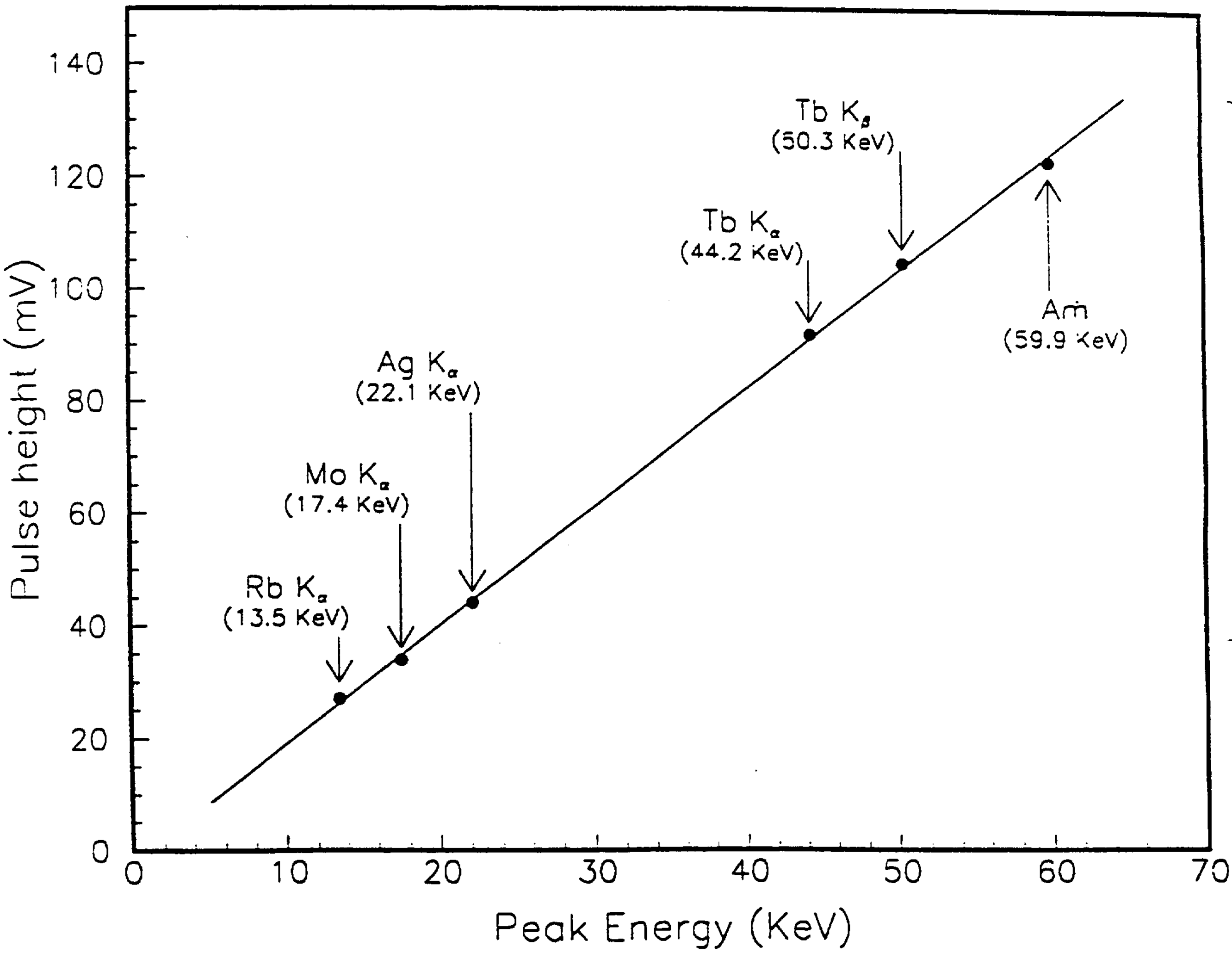

Pulse height (mV)
Peak Energy (KeV)
Rb K_α (13.5 KeV)
Mo K_α (17.4 KeV)
Ag K_α (22.1 KeV)
Tb K_α (44.2 KeV)
Tb K_β (50.3 KeV)
Am (59.9 KeV)
0 20 40 60 80 100 120 140
0 10 20 30 40 50 60 70

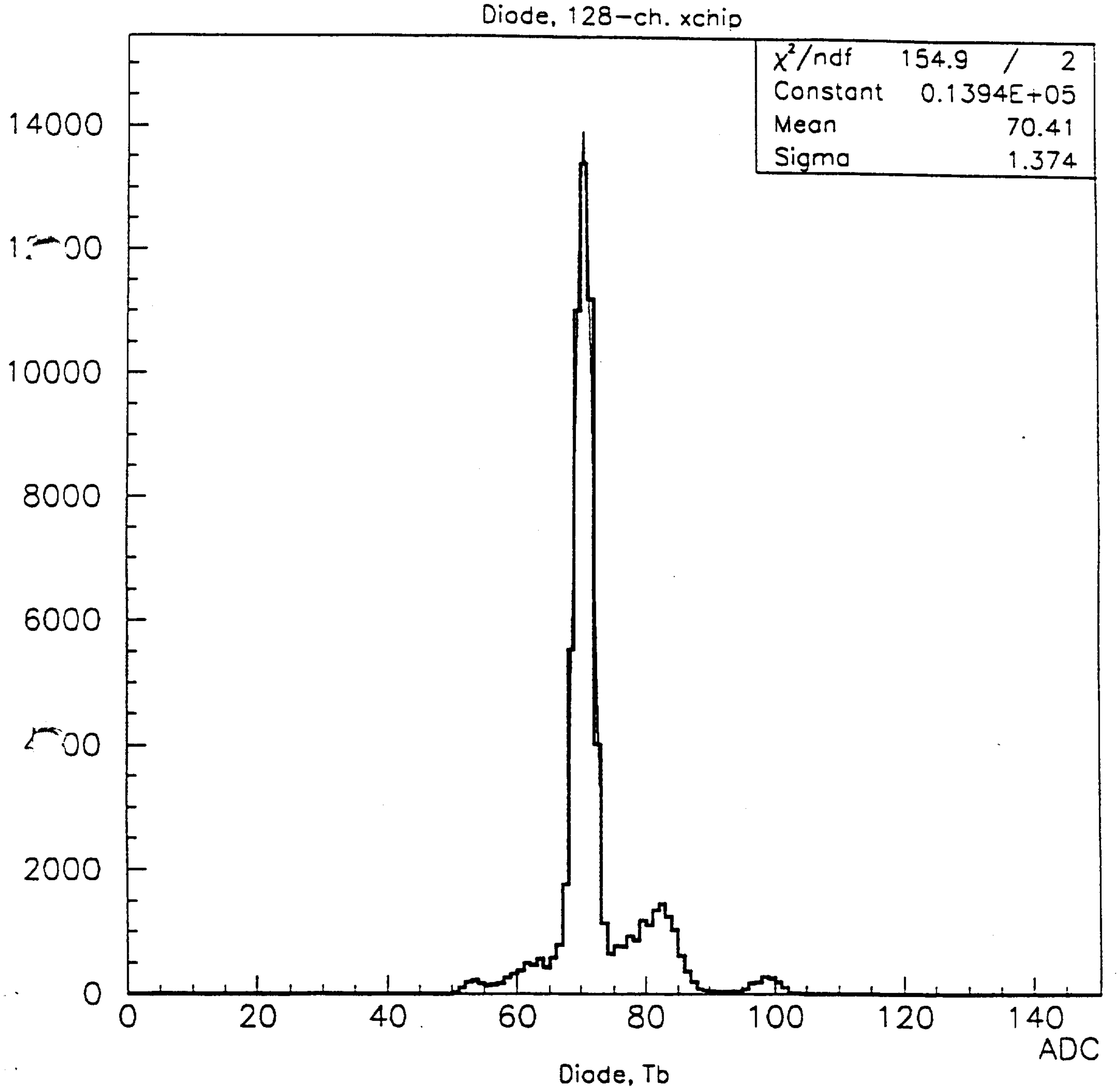

Diode, 128−ch. xchip
χ^2/ndf 154.9 / 2
Constant 0.1394E+05
Mean 70.41
Sigma 1.374
14000
10000
8000
6000
2000
0
0
20
40
60
80
100
120
140
ADC
Diode, Tb

61

diode-a.tif

Imaging Test with an X-ray Tube

- X-ray tube operated at 30 kV and 15 mA with a molybdenum target and molybdenum filtration
- Energy spectrum: 10-30 keV,

  K peaks: 17.4, 19.6 keV
- Photon flux: 6.4 10^5 s^{-1} mm^{-2}

- Net acquisition time ≈ 100 ms (1/10 s)
- Strip read-out pitch 100 μm, 20x20 pixels

- Phantoms:

  steel sphere (700 μm)

  hole (500 μm) in lead slab

  square wave test pattern (50 μm thick Pb)

SLIDE

63

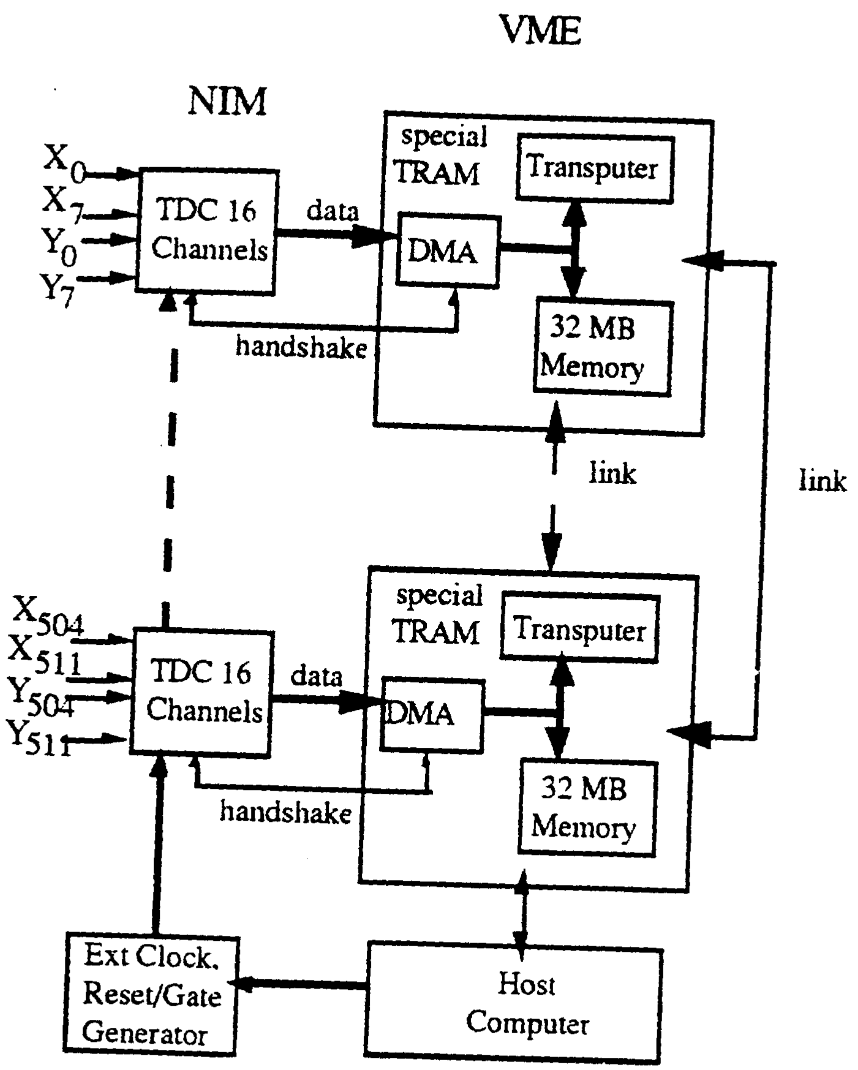
VME
NIM
X0
X7
Y0
Y7
TDC 16 Channels
data
special TRAM
Transputer
DMA
handshake
32 MB Memory
link
link
X504
X511
Y504
Y511
TDC 16 Channels
data
special TRAM
Transputer
DMA
handshake
32 MB Memory
Ext Clock. Reset/Gate Generator
Host Computer

Rationale:

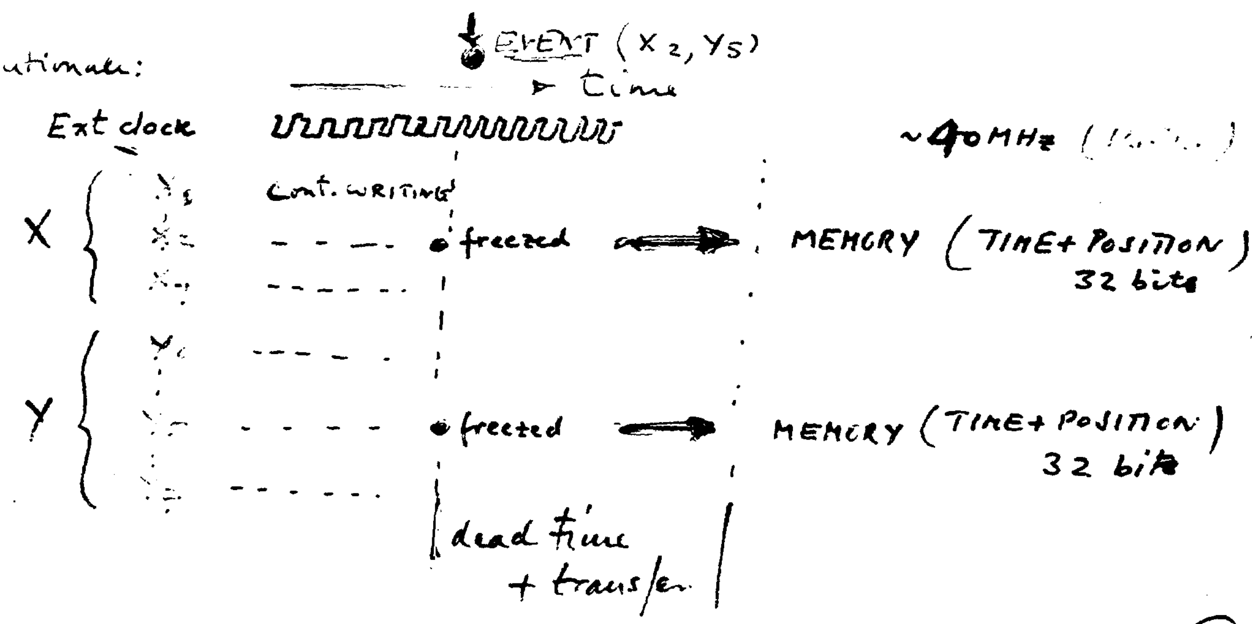
EVENT (X2, Y5)
time
Ext clock
~40 MHz
cont. writing
X
freezed
MEMORY (TIME+POSITION)
32 bits
Y
freezed
MEMORY (TIME+POSITION)
32 bits
dead time
+ transfer

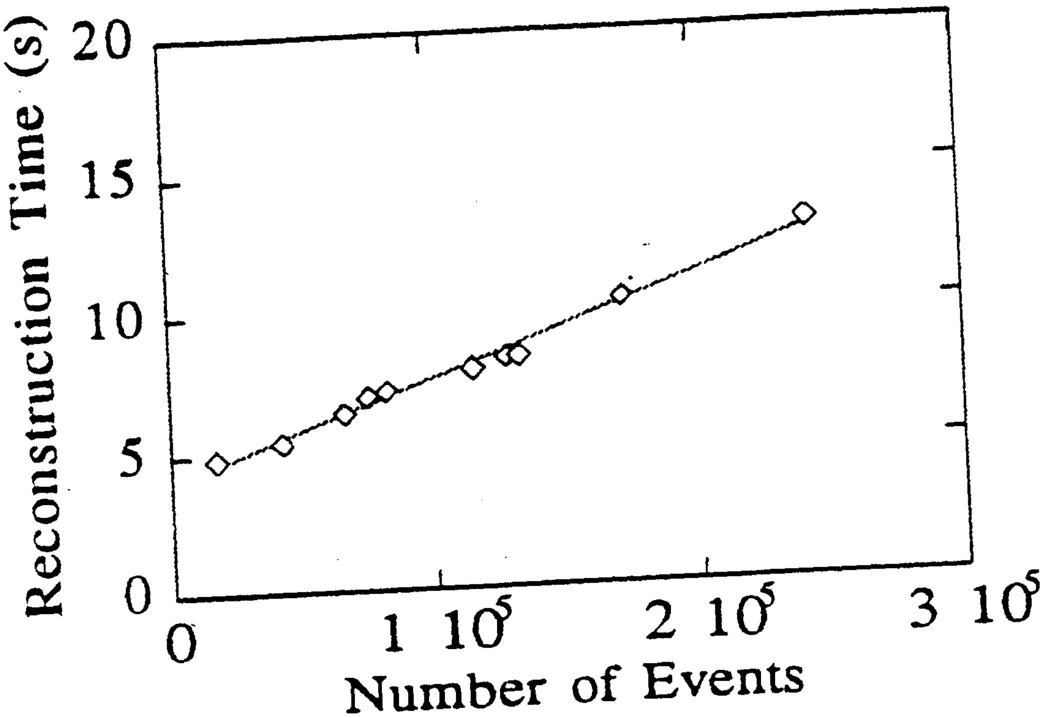

Figure 2: Reconstruction time versus number of events stored in the memory of each transputer

5s for images presented

~ 45' for 5x5 cm^2 goal

⇒ T9000 × 1/10

i 860 ×

Software ×

} Real time < 5'

M. Conti et al., IEEE Trans. Nucl. Sci. NS41 (1994) 1522

65

(The very first image
June 1992)

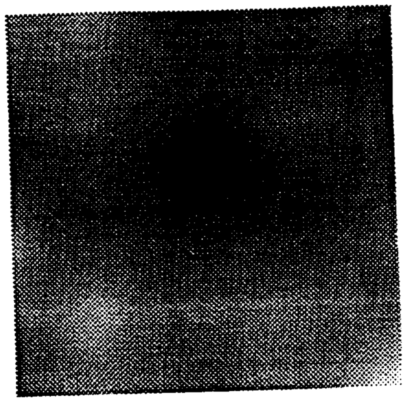

500 μm hole in lead

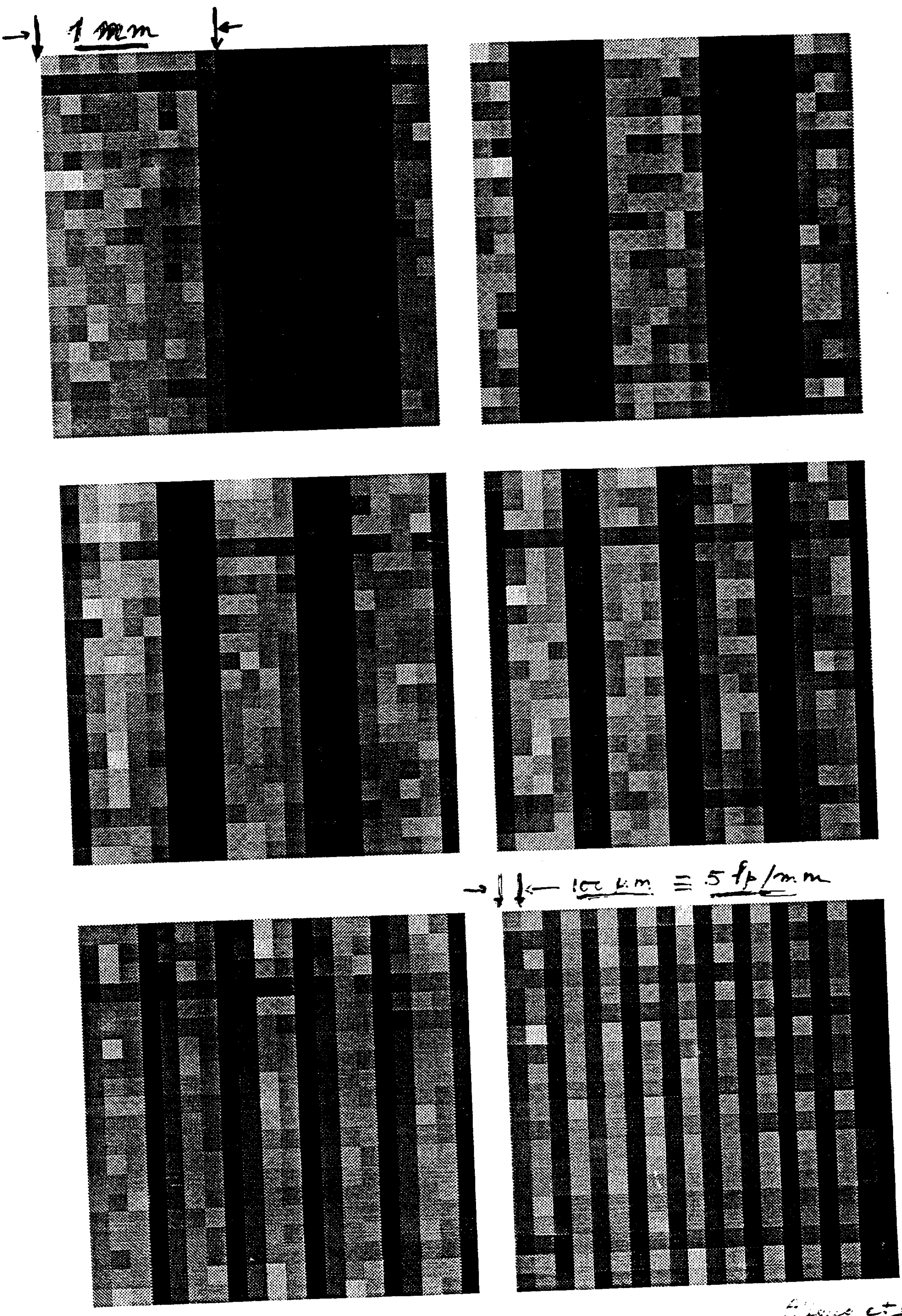

Albano et al
67

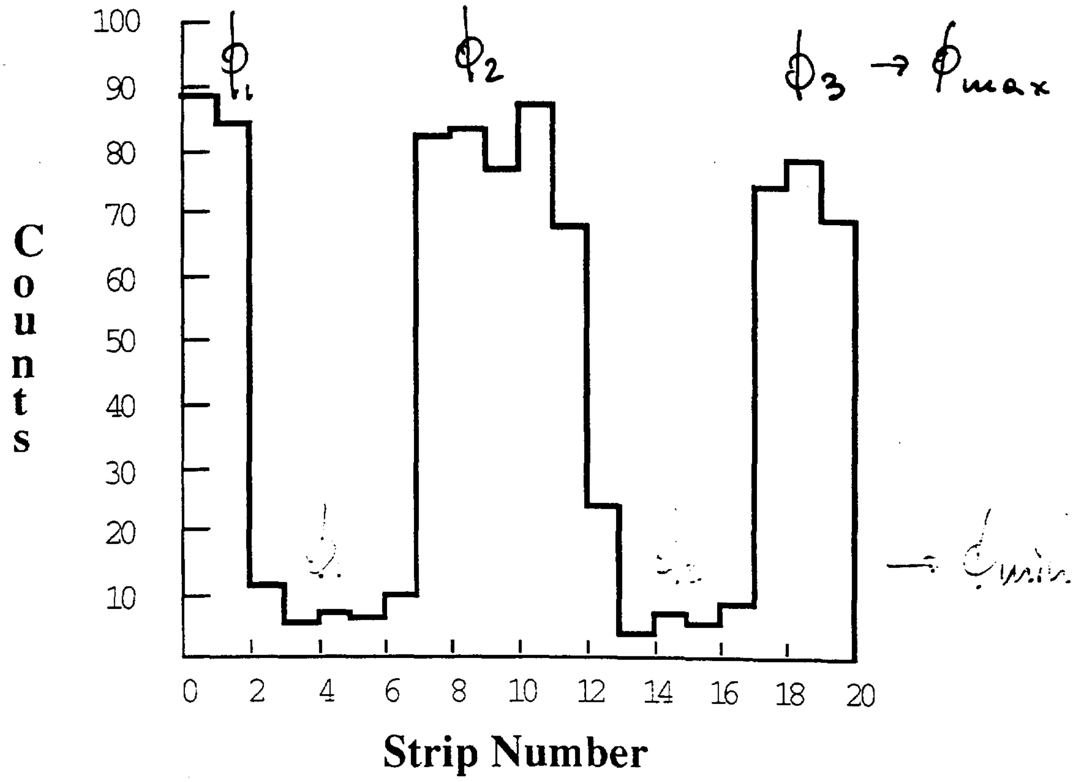

Image profile along the J direction obtained with an 1 line pair per mm square wave test pattern. The vertical axis shows the average pixel content for an 100 ms acquisition time.

From profiles we obtain Contrast:

$$C_{output} = (\Phi_{max} - \Phi_{min})/(\Phi_{max} + \Phi_{min})$$

Φ_{max} is the average number of counts at the maxima Φ_{min} the corresponding average at the minima for each frequency

Contrast Transfer Function

$$CTF(\nu) = \frac{C_{output}(\nu)}{C_{input}}$$

C_{output} is defined as $(\Phi_{max} - \Phi_{min})/(\Phi_{max} + \Phi_{min})$,
Φ_{max} is the average number of counts at the maxima,
Φ_{min} the corresponding average at the minima for each frequency,

C_{input} is defined as $(\Phi_{air} - \Phi_{Pb})/(\Phi_{air} + \Phi_{Pb})$,
Φ_{air} is the average number of counts obtained with no test pattern,
Φ_{Pb} the average number of counts obtained with a Pb slab as thick as the test pattern (50 μm) in front of the detector,

We measured for C_{input} a value of 0.94.

Allan et al
IEEE Trans Nucl. Sci
NS40 (1993) 987

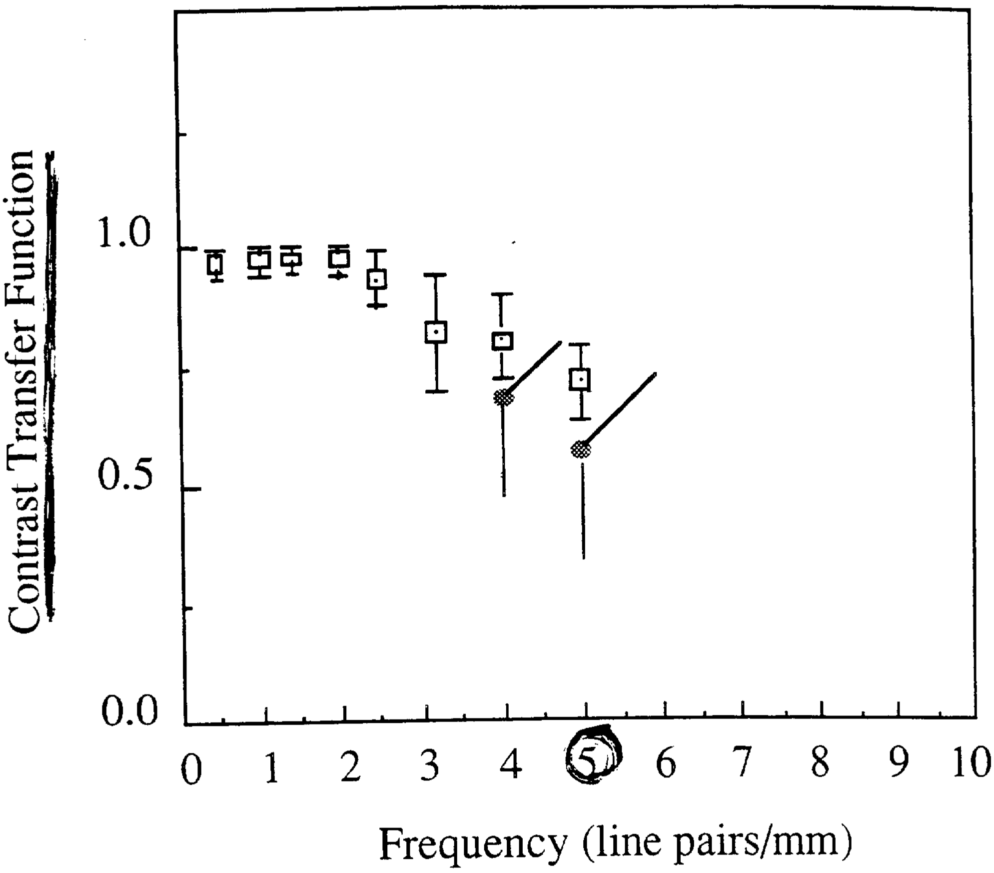

Figure 6 : Contrast Transfer Function

Frequency (lp/mm)	Contrast
Measurements in phase	
0.5	0.96 ± 0.03
1.0	0.97 ± 0.03
1.4	0.97 ± 0.03
2.0	0.97 ± 0.03
2.5	0.93 ± 0.05
3.2	0.82 ± 0.12
4.0	0.80 ± 0.09
(100 μm) 5.0	0.71 ± 0.08
Measurements out of phase	
4.0	0.68 ± 0.18
5.0	0.57 ± 0.16

tooth pitch 270 μm

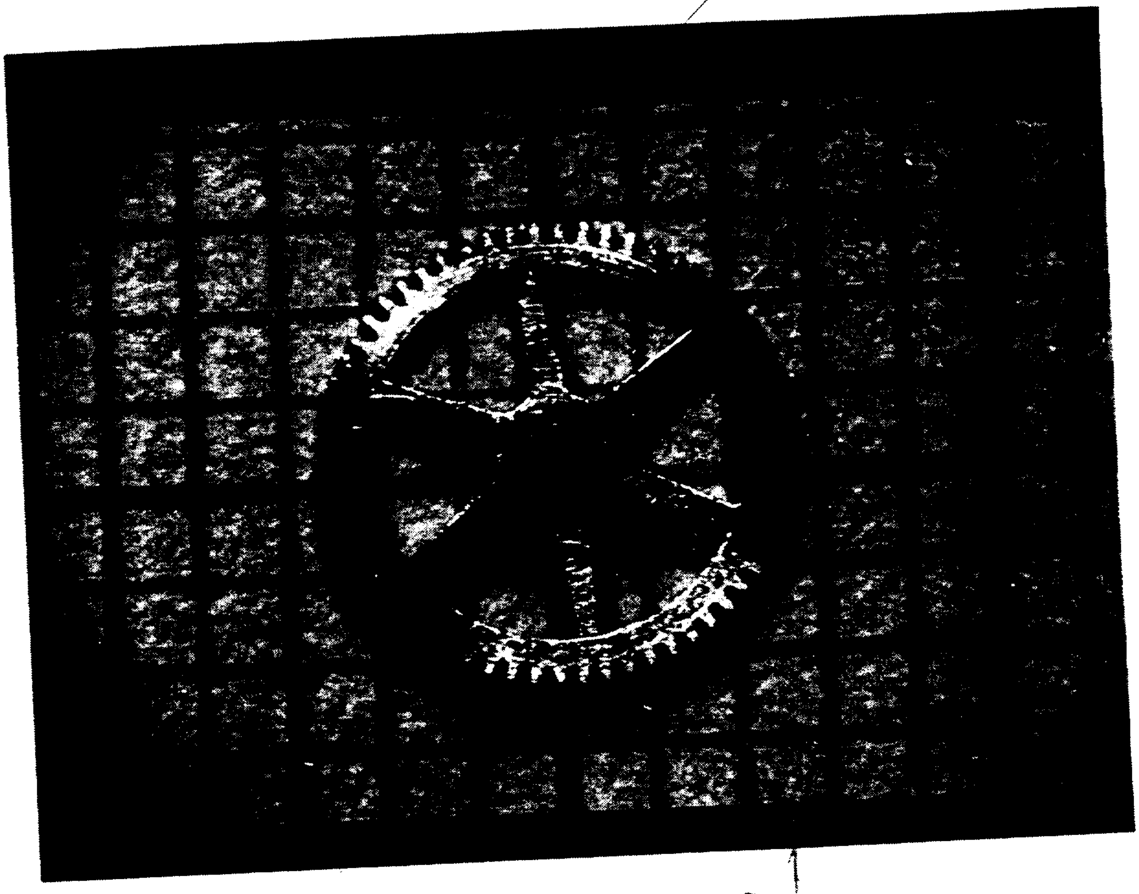

5.36 mm

ACQUISIZIONE IN LISTA

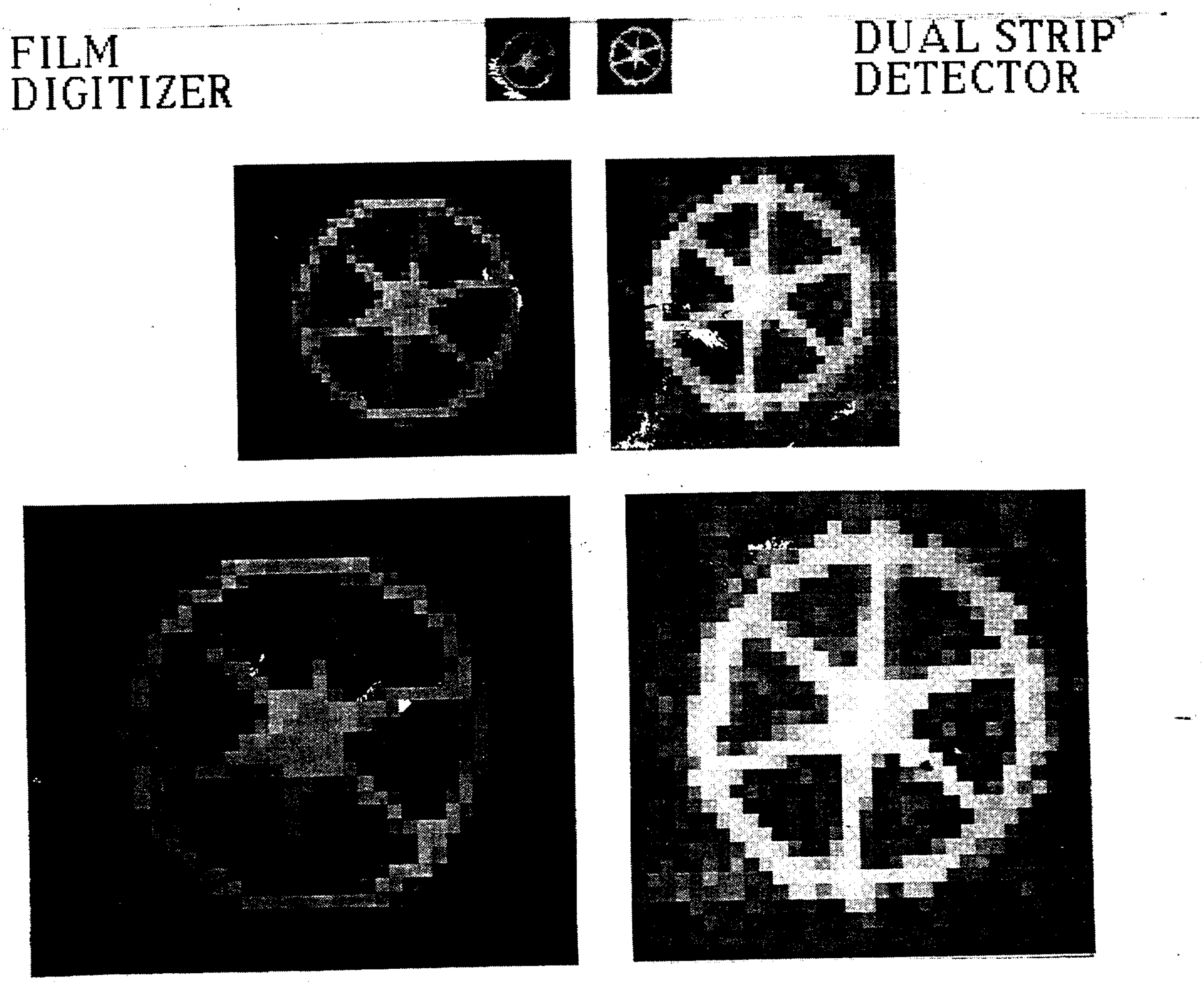

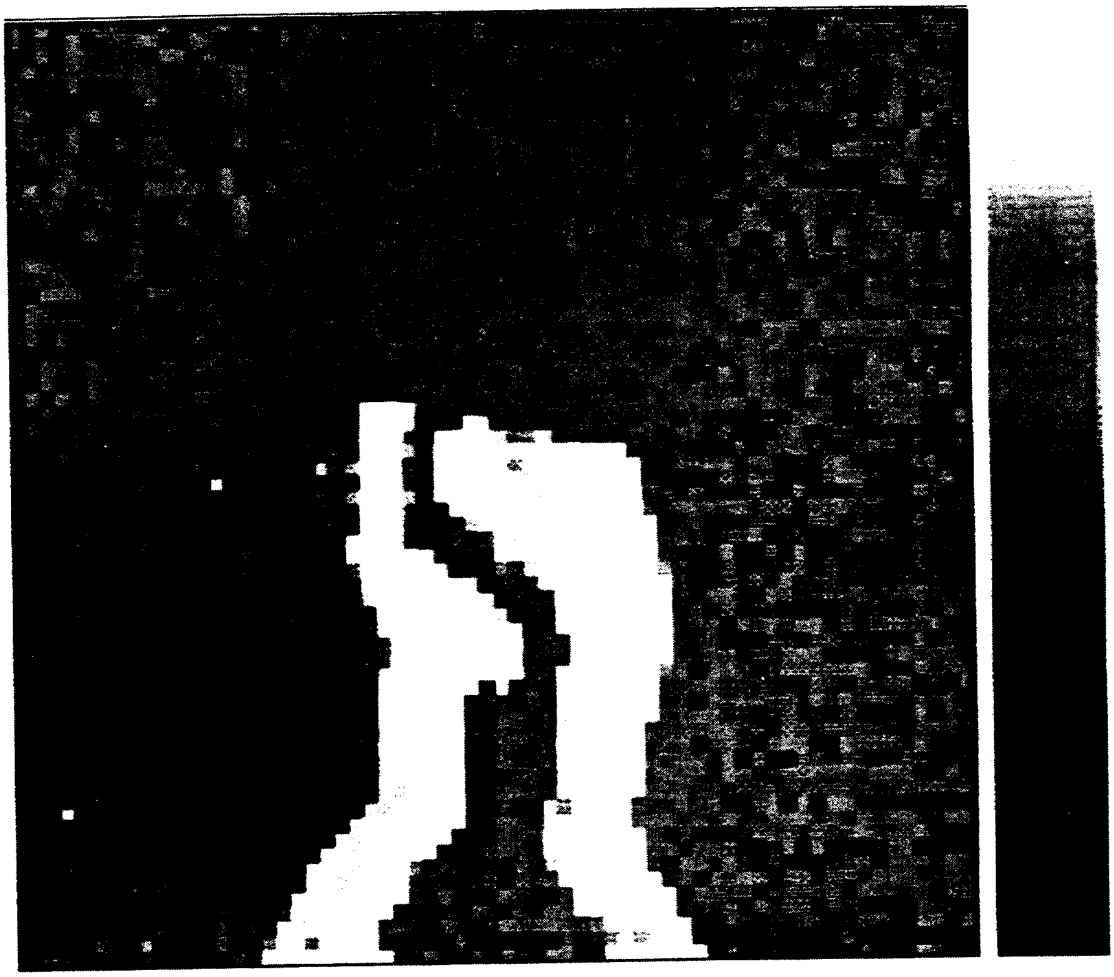

Holes in alluminium slab

diameters 1 mm

depth 1 mm, 0.5 mm

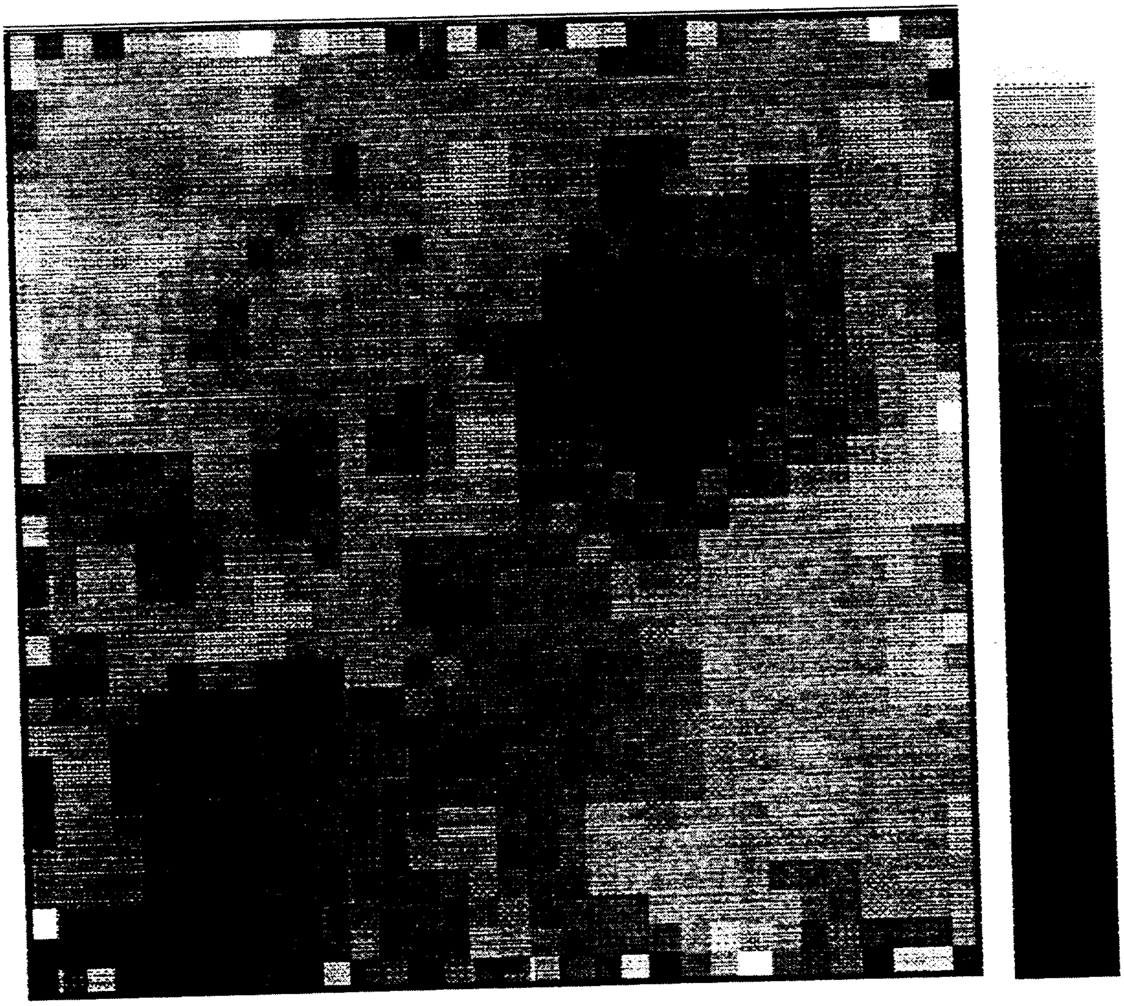

SCR =(34 ± 2) % SNR =10.1 ± 0.5

SCR =(13 ± 2) % SNR = 3.8 ± 0.5

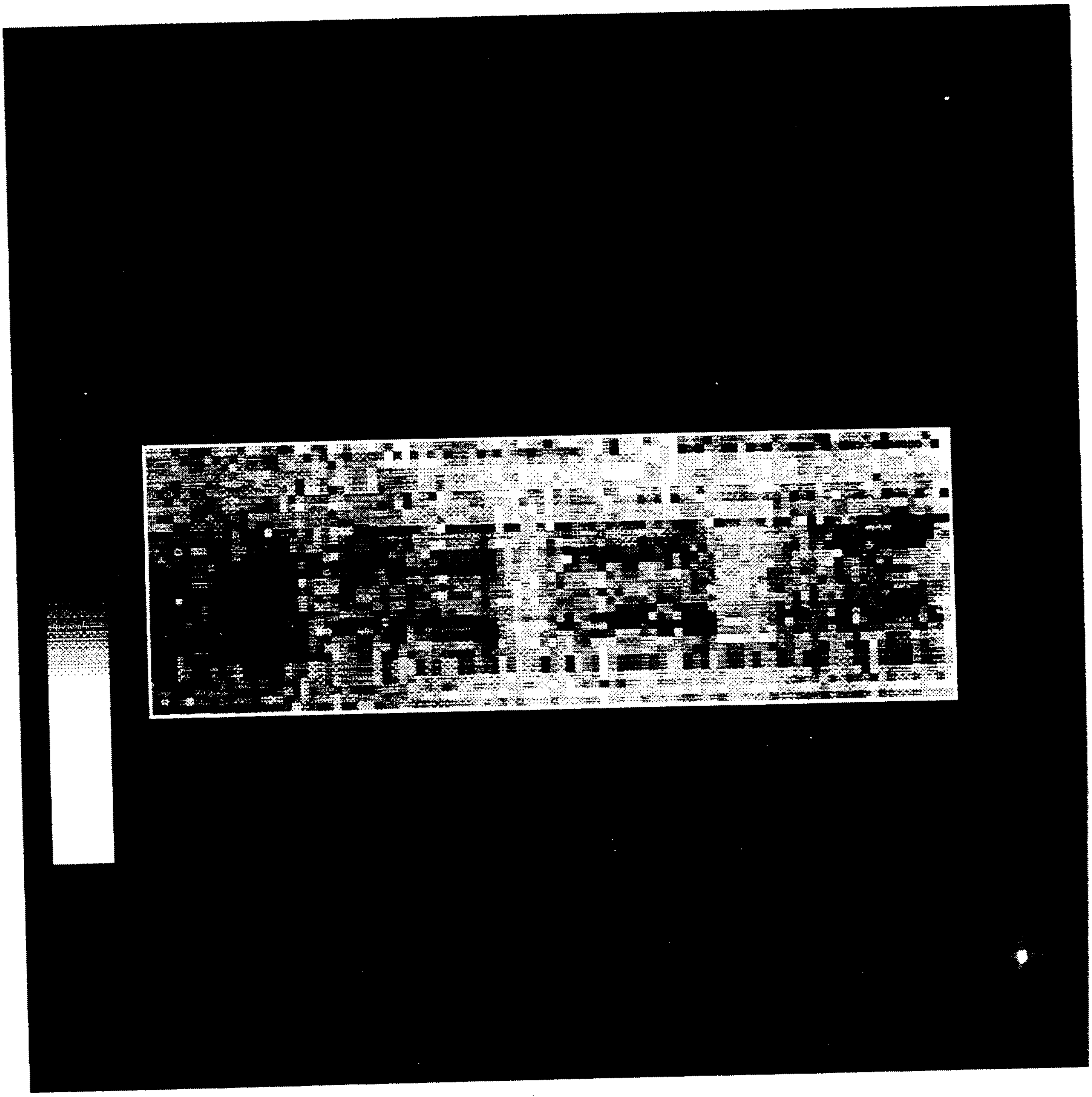

ONE PROBLEM OF THE MICROSTRIPS GEOMETRY: DOUBLE OR MULTIPLE HITS

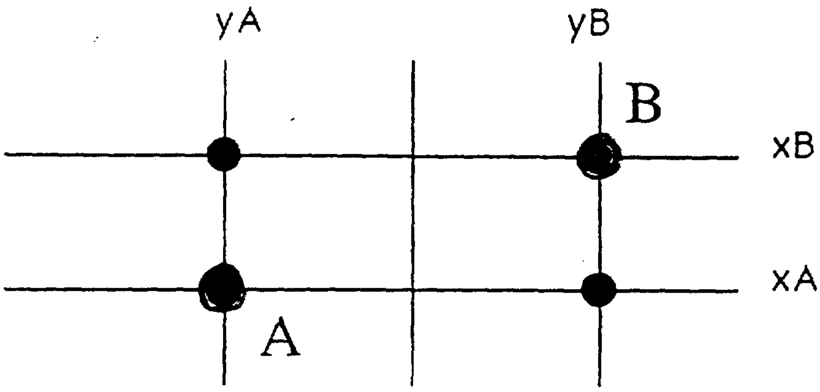

- (XA, YA), (XB, YB) RIGHT COMBINATION
- (XB, YA), (XA, YB) WRONG COMBINATION (GHOSTS)

THE EFFECTS ARE ARTIFACTS ON THE IMAGES.

REMEDIES:

- SOFTWARE FILTERS (NN),
- VERY FAST ELECTRONICS TO MAKE THE RIGHT COINCIDENCES IN A VERY SHORT TIME.

We studied the effect of these double counting as applied to mammography examination for a 300 μm silicon crystal

$N_T = 5 * 10^4$ photons/mm2 $T_{exposure} = 1$ s
$E\gamma \approx 20$ keV $T_{sampling} = 10$ ns (coincidence resolution)

To be taken into account:

- Poisson statistic
- Efficiency of the detector
- Effects due to $|T_\Omega - T_J|$ and to the time slew

$\Downarrow$

i.e.

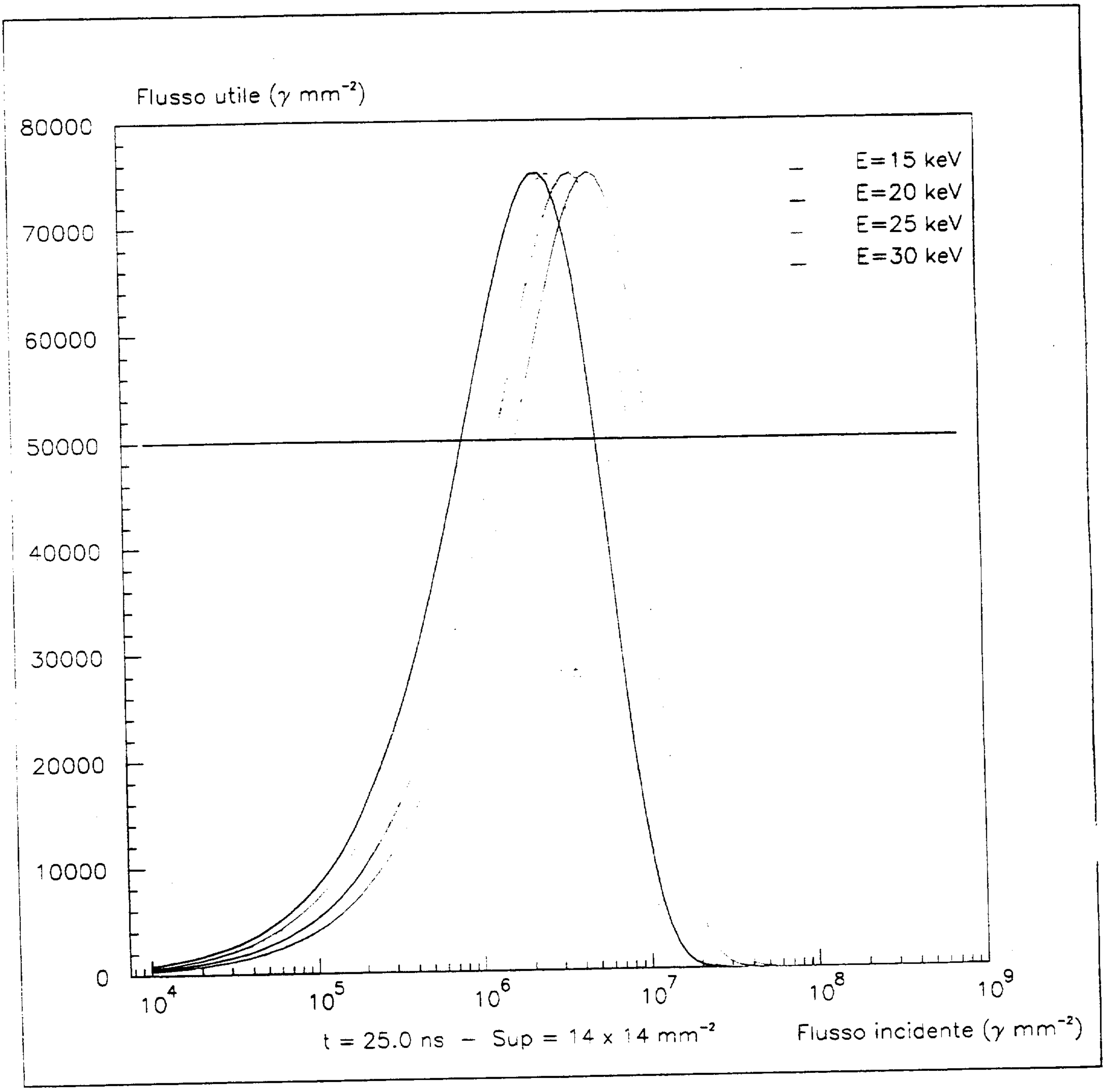
Flusso utile (γ mm^{-2})
80000
70000
60000
50000
40000
30000
20000
10000
0
E=15 keV
E=20 keV
E=25 keV
E=30 keV
10^4
10^5
10^6
10^7
10^8
10^9
t = 25.0 ns – Sup = 14 x 14 mm^{-2}
Flusso incidente (γ mm^{-2})

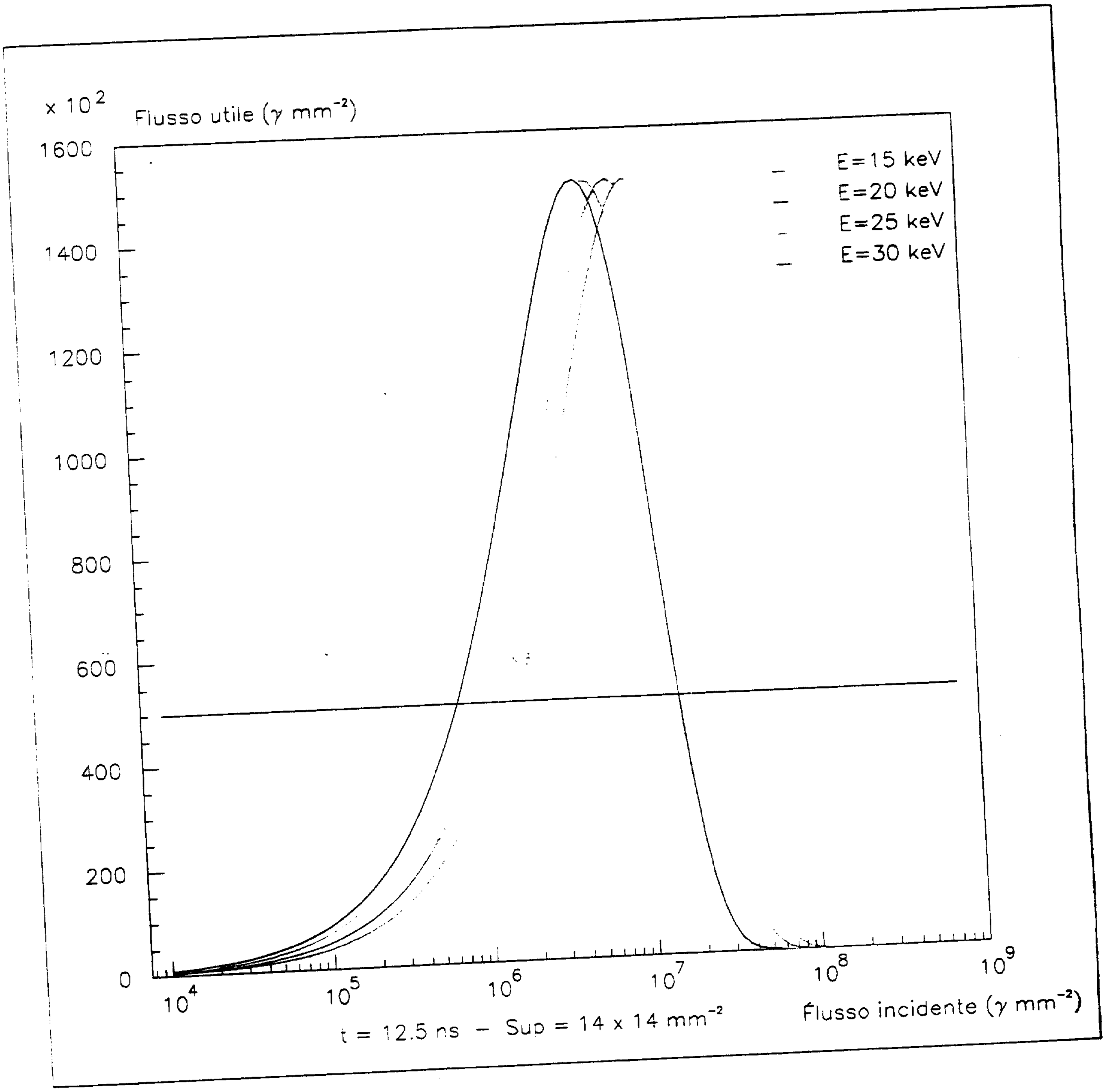

x 10 2
Flusso utile (γ mm⁻²)
1600
1400
1200
1000
800
600
400
200
0
E=15 keV
E=20 keV
E=25 keV
E=30 keV
10 4
10 5
10 6
10 7
10 8
10 9
Flusso incidente (γ mm⁻²)
t = 12.5 ns – Sup = 14 x 14 mm⁻²

RECONSTRUCTION ALGORITHMS

- Singles: one event per time slot (type **1**)
- Doubles: two (maximum) events per time slot (type **2**)

ALGORITHM **I** (examines only one time slot)

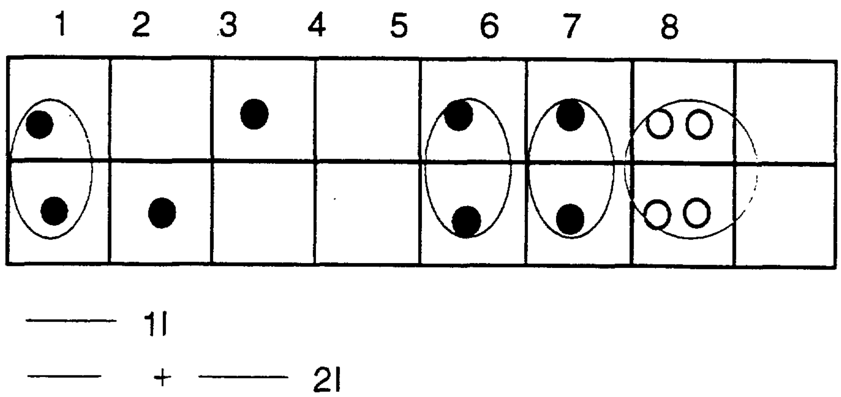

ALGORITHM **X** (examines two adjacent time slots)

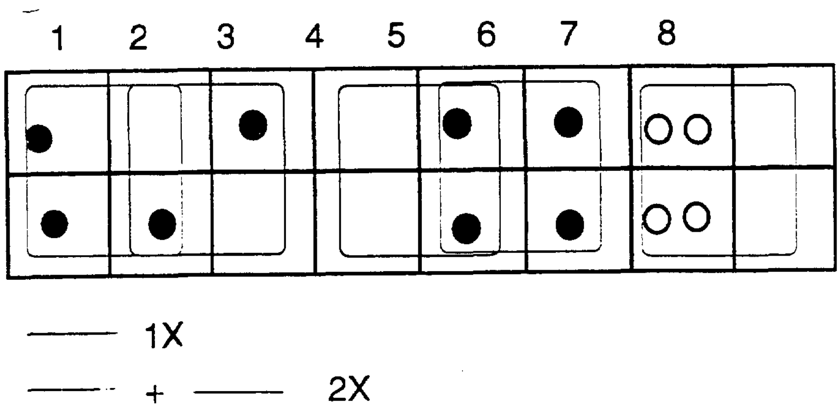

Combination of X with I (1X1I,1X2I,2X2I...)
Software simulation
Hardware implementation (VLSI)

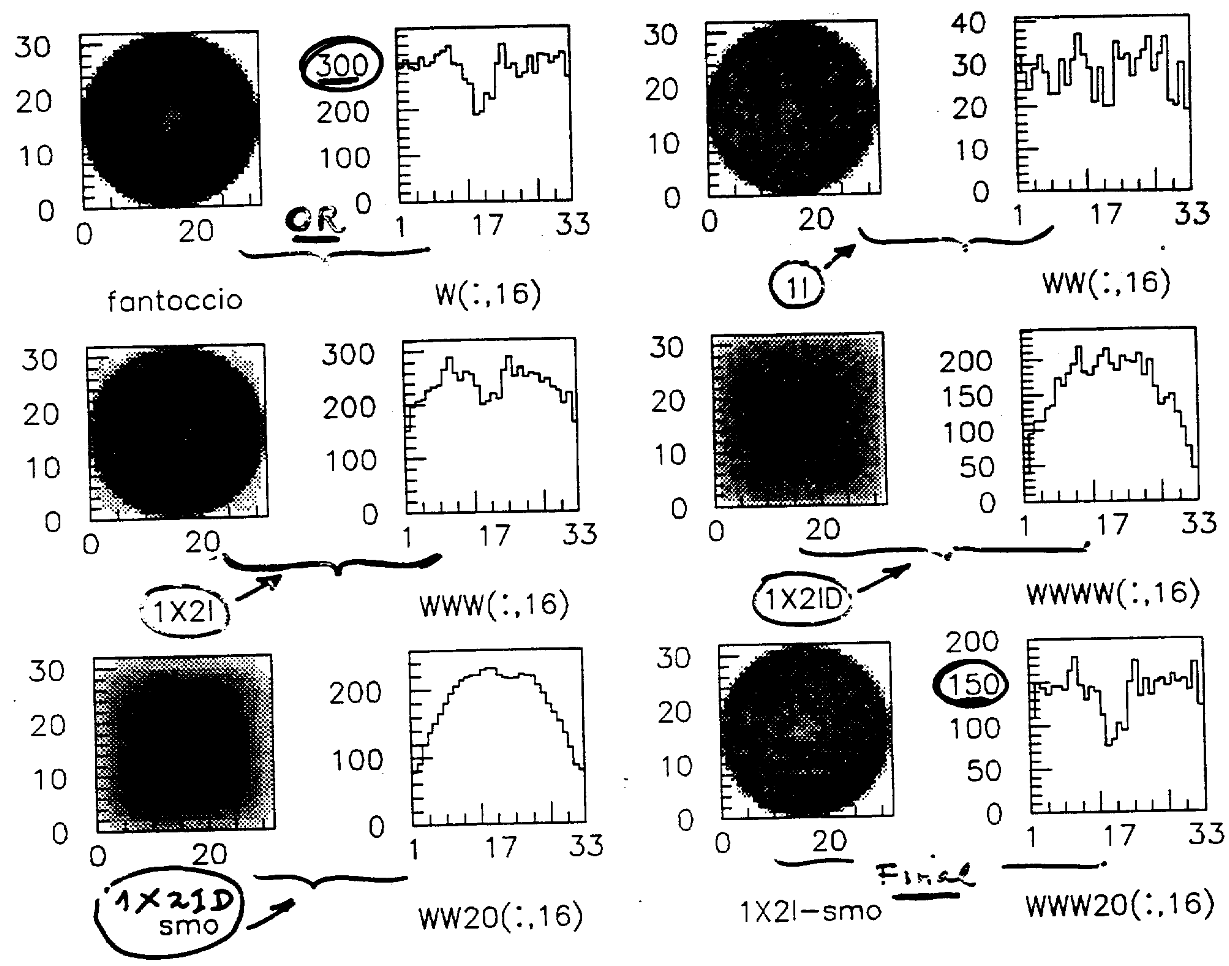

fantoccio
W(:,16)
OR
300
11
WW(:,16)
1X2I
WWW(:,16)
1X2ID
WWWW(:,16)
1X2ID smo
WW20(:,16)
1X2I-smo
Final
150
WWW20(:,16)

- DAQ in frame

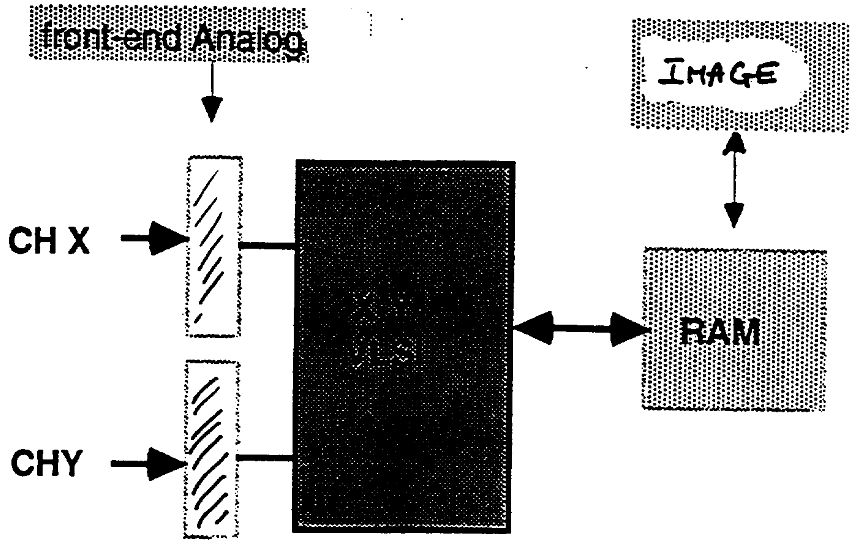

- Pipeline Architecture

(synchronous clock at 100 MHz) $\Rightarrow t_{sampling} = 10$ ns)

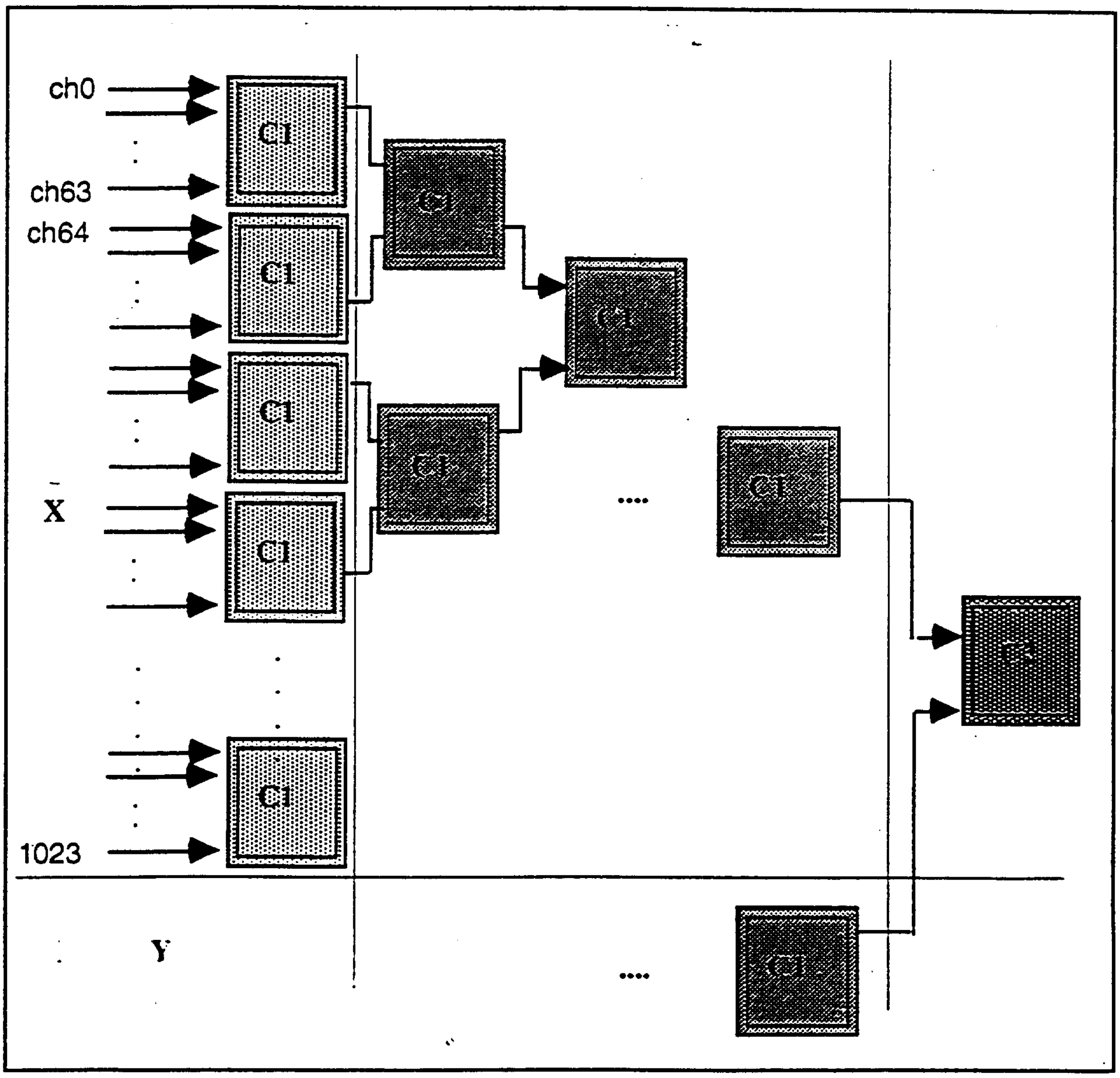

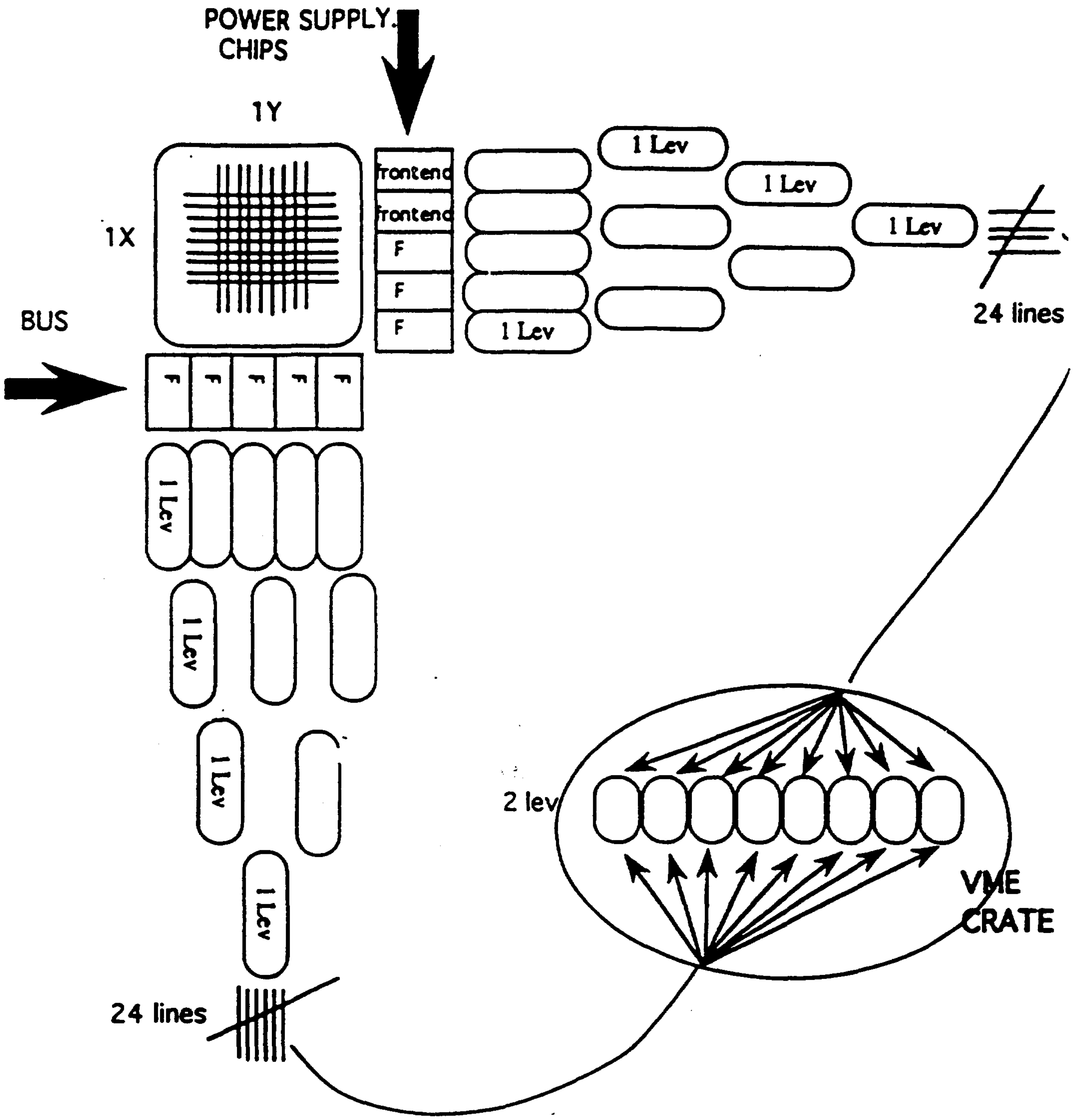

64 STRIPS PER CHIP

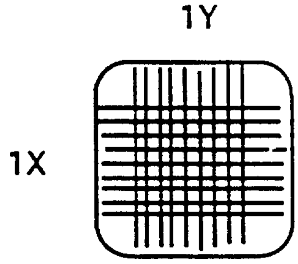
1Y
1X

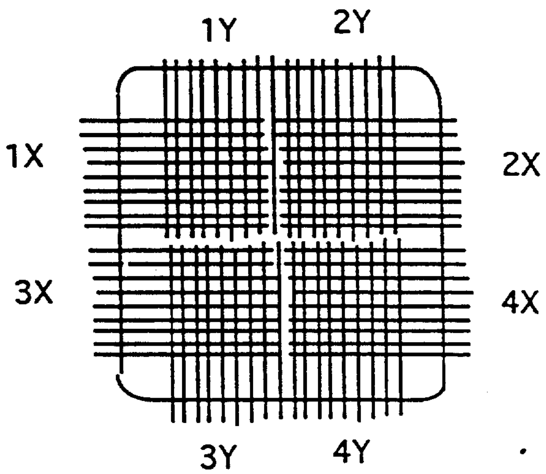
1Y
2Y
1X
2X
3X
4X
3Y
4Y

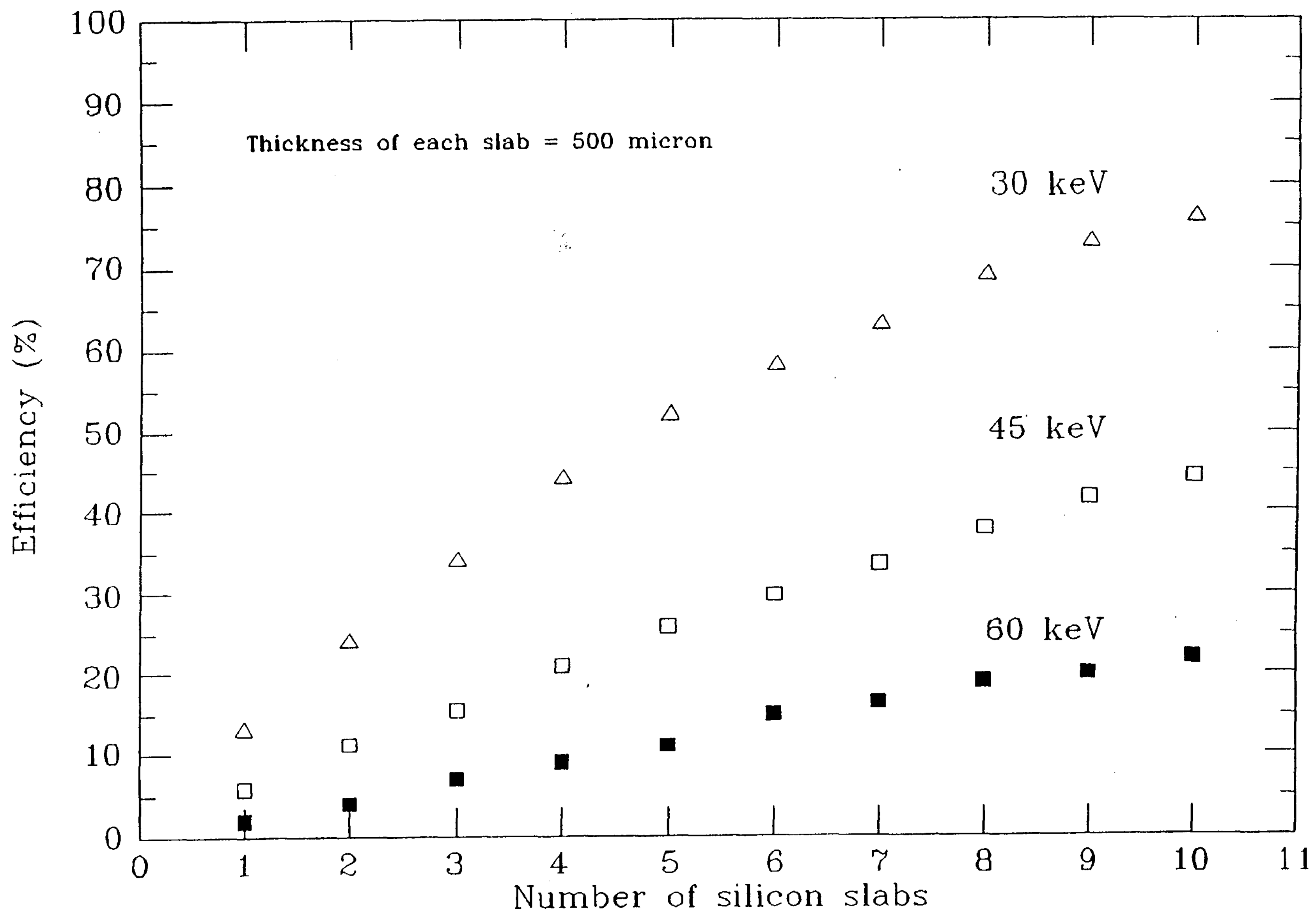
Thickness of each slab = 500 micron
30 keV
45 keV
60 keV
Efficiency (%)
Number of silicon slabs
0
10
20
30
40
50
60
70
80
90
100
0
1
2
3
4
5
6
7
8
9
10
11

SILICON PIXEL DETECTOR

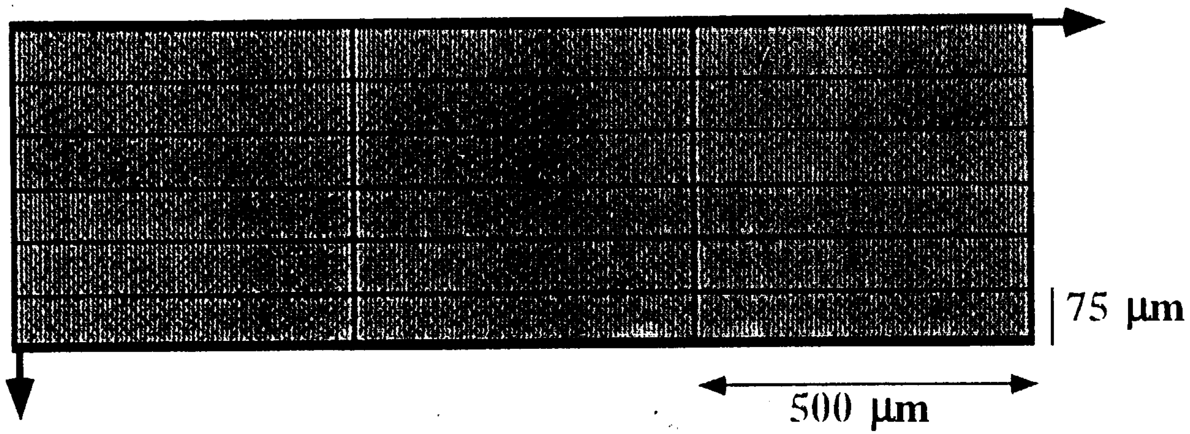

The detector is bump-bonded to the read-out chips:

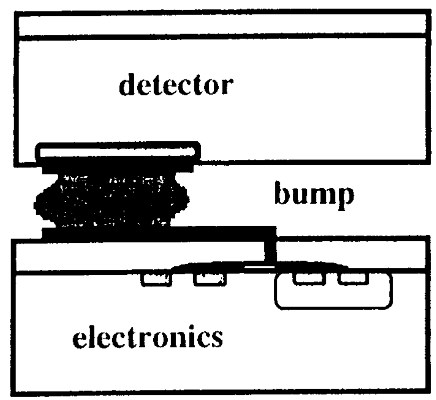

CERN RD-19 (E. Heijne) and WA-97

M. Campbell et al. Nucl. Instrum. Methods A342 (1994) 52

E. Heijne, Phisica Medica 9 (1993) 109

Physica Medica IX (1993) 109

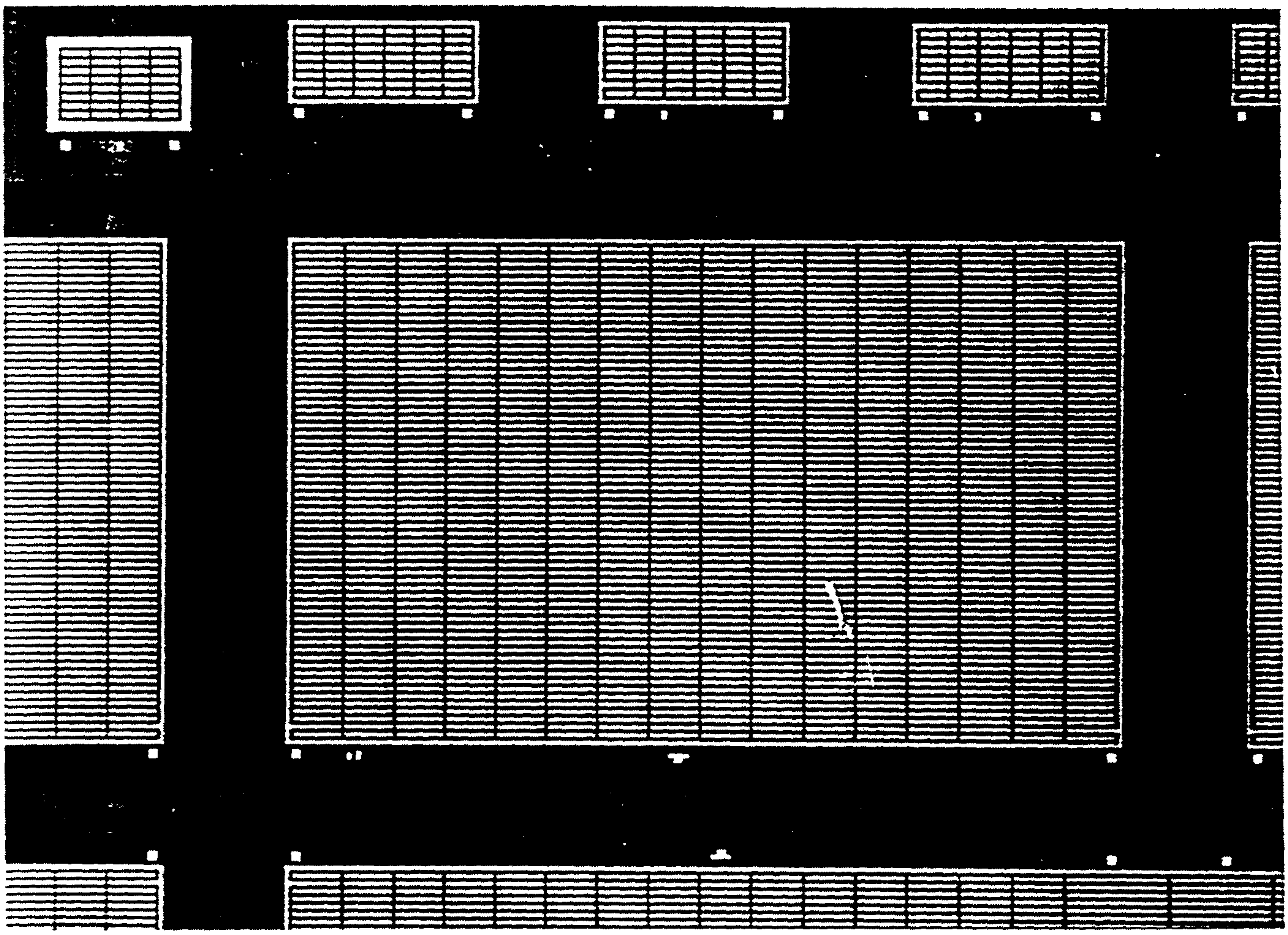

Fig. 1 – Photograph of a part of a processed detector wafer. In the middle is shown a large silicon detector (8.3 mm x 6.6 mm) with 2-dimensional segmentation. Each segment (pixel) has dimension 75 μm x 500 μm and is an individual diode element. The separation between segments is achieved by an oxide layer. Under total depletion condition 100% efficiency is obtained without any insensitive region between the segments. The various smaller structures seen around the main detector are test detectors to be cut off.

PIXEL AMPLIFIERS WITH BUMP BONDS

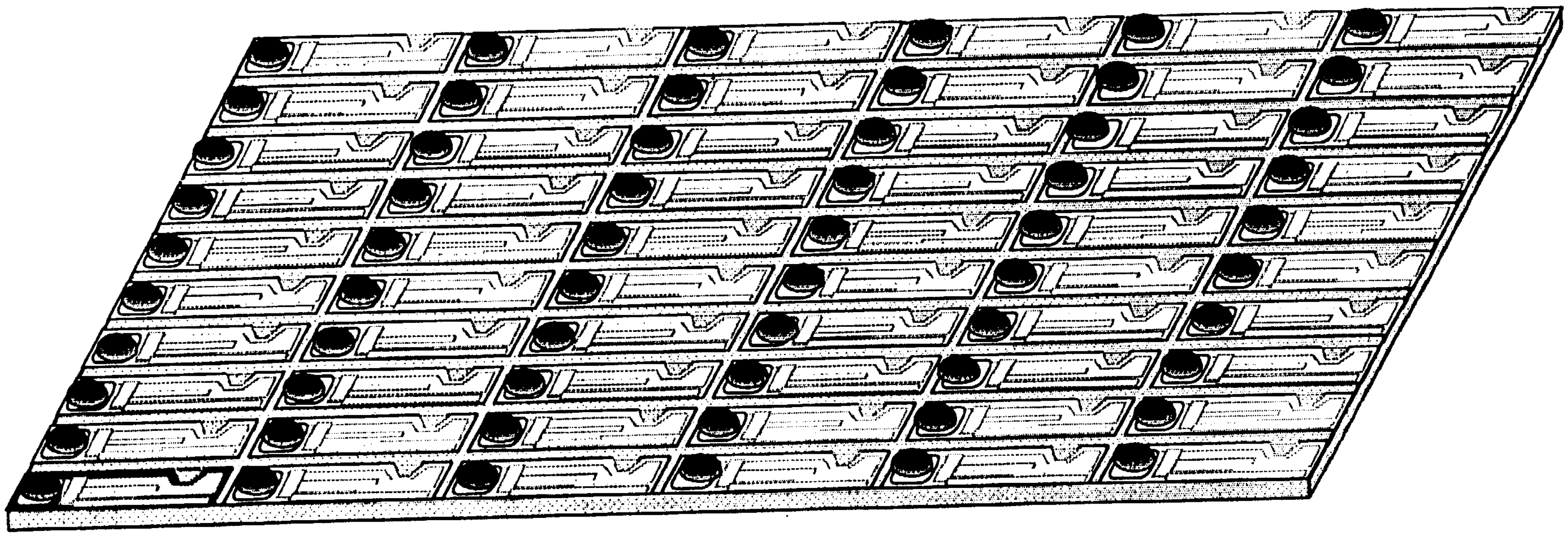

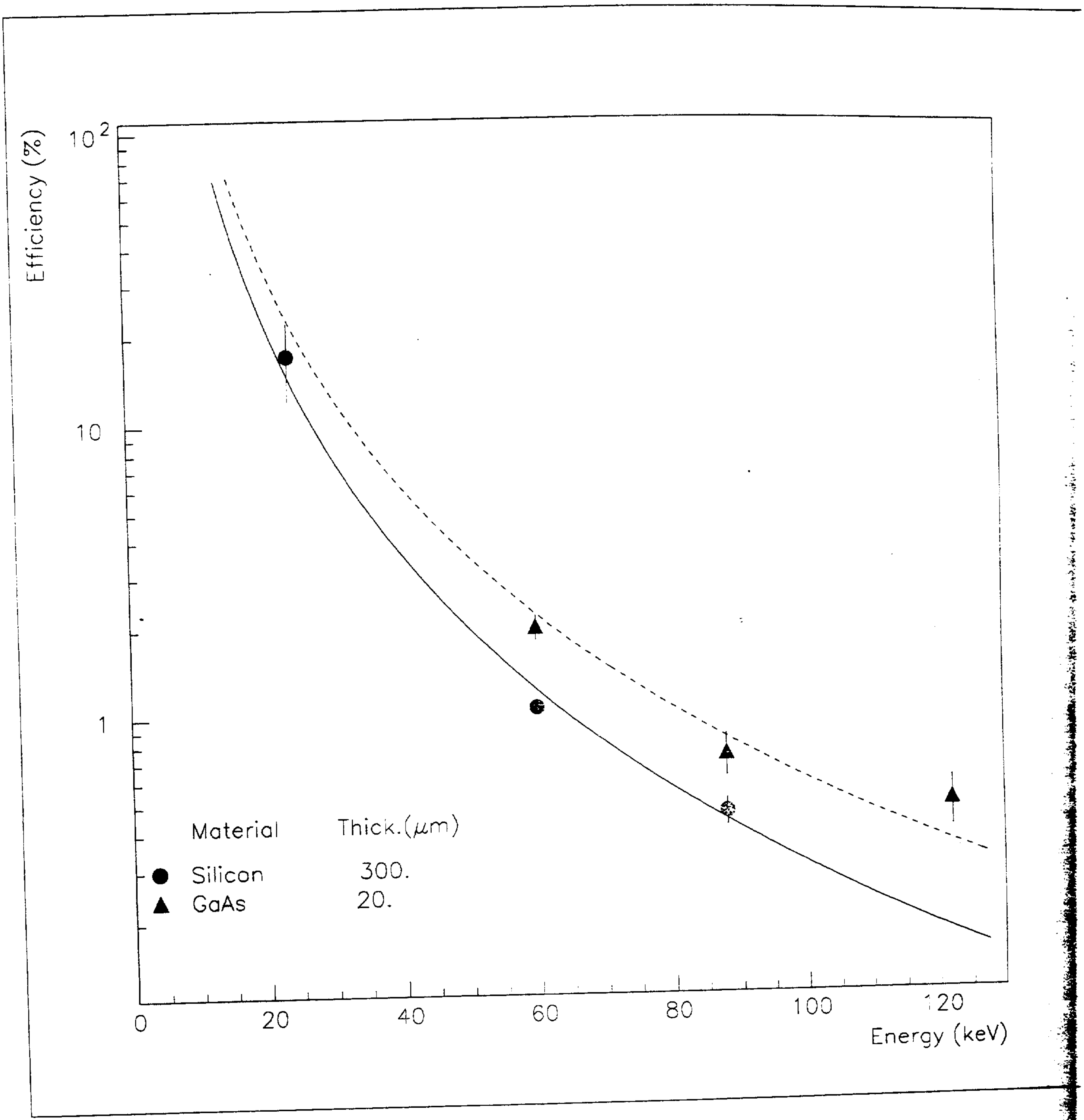

Efficiency (%)
10^2
10
1
Energy (keV)
0
20
40
60
80
100
120
Material
Thick.(μm)
Silicon
300.
GaAs
20.

▲ W. [illegible]

from Bencivelli et al, Nucl. Instr. Meth. A 346 (1994) 372.

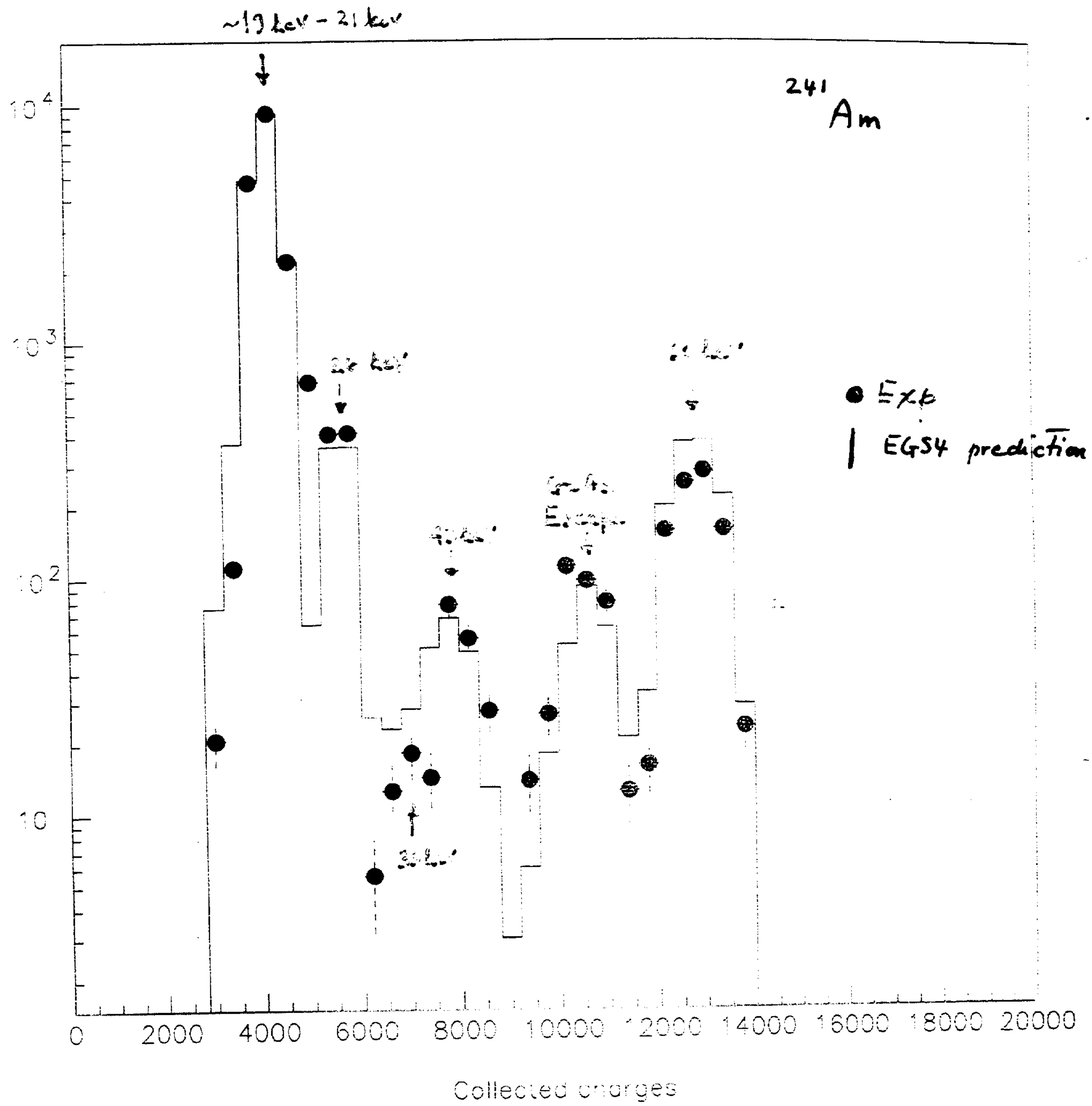

ANSTO detector
↓
LPE (liquid Phase Epitaxy)

Detector #	Material firm	Contacts firm	Thickness (μm)	Pixel diameter (mm)
1	AXT	ALENIA	350	2
2	MCP	Un. Glasgow	80	1
3	MCP	Un. Glasgow	630	2
4	SUMITOMO	ALENIA+	200	3
5	SUMITOMO	ALENIA	200	3
6	NIPPON M.	Un. Lecce	400	1
7	NIPPON M.	Un. Lecce	70	0.2++

Fabrication and geometrical characteristics of the LEC detectors.

+ The rear surface has been polished.

++ Side length of the square pixel.

#	V_{bias} (V)	cce (%)	σ/E (%)	J (Acm^{-2})	C (Fcm^{-2})	C_g(Fcm^{-2})
1	350	43.7±8.8	20.2±4.1	$(1.9\pm0.2)10^{-6}$	$(8.0\pm0.8)10^{-10}$	$3.3\ 10^{-11}$
2	80	81.9±6.1	7.5±0.6	$(2.2\pm0.2)10^{-6}$	$(1.5\pm0.2)10^{-10}$	$1.4\ 10^{-10}$
3	450	36.4±11.5	32.7±10.7	$(1.1\pm0.1)10^{-6}$	$(1.6\pm0.2)10^{-11}$	$1.9\ 10^{-11}$
4	160	60.5±15.0	24.8±6.1	$(2.8\pm0.3)10^{-6}$	$(6.2\pm0.6)10^{-11}$	$5.7\ 10^{-11}$
5	160	63.1±14.7	23.4±5.4	$(3.0\pm0.3)10^{-6}$	$(6.4\pm0.6)10^{-11}$	$5.7\ 10^{-11}$
6	700	39.1±14.9	38.0±10.9	$(3.6\pm0.4)10^{-6}$	$(1.3\pm0.1)10^{-11}$	$2.9\ 10^{-11}$
7	80	87.6±4.8	5.5±0.3	$(7.9\pm0.8)10^{-6}$	(a)	$1.6\ 10^{-10}$

Charge collection efficiency (cce) and energy resolution (σ/E) at 60 keV photon energy, measured density current (J), measured density capacitance (C) and geometrical density capacitance (C_g) for all detectors at the maximum bias voltage. (a): The value of the capacitance (F) is lower than the sensitivity of the capacitance meter, due to the pixel dimensions.

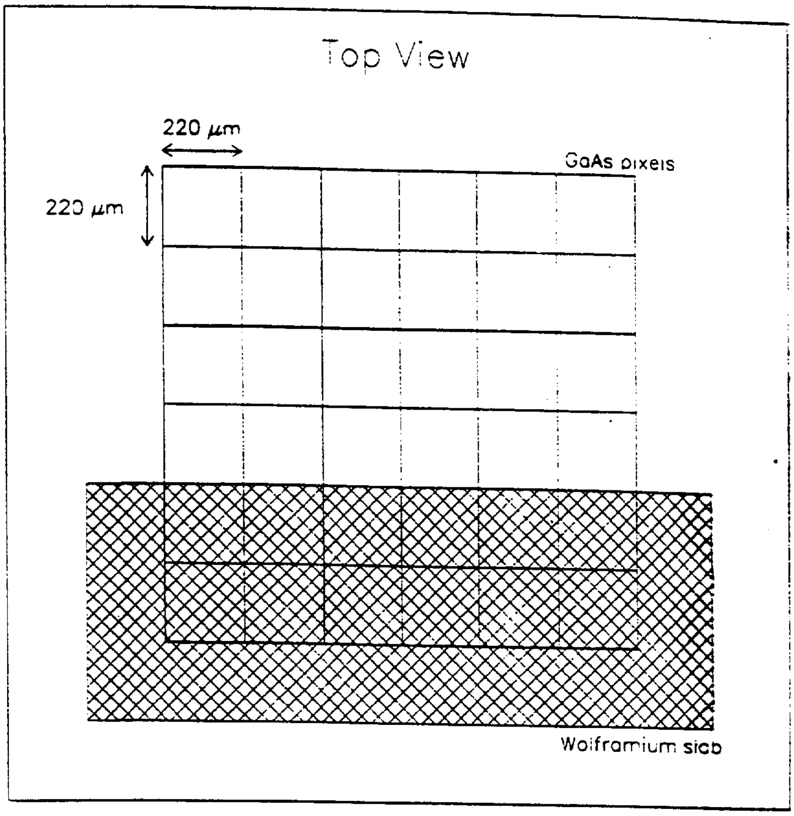
Top View
220 μm
220 μm
GaAs pixels
Wolframium slab

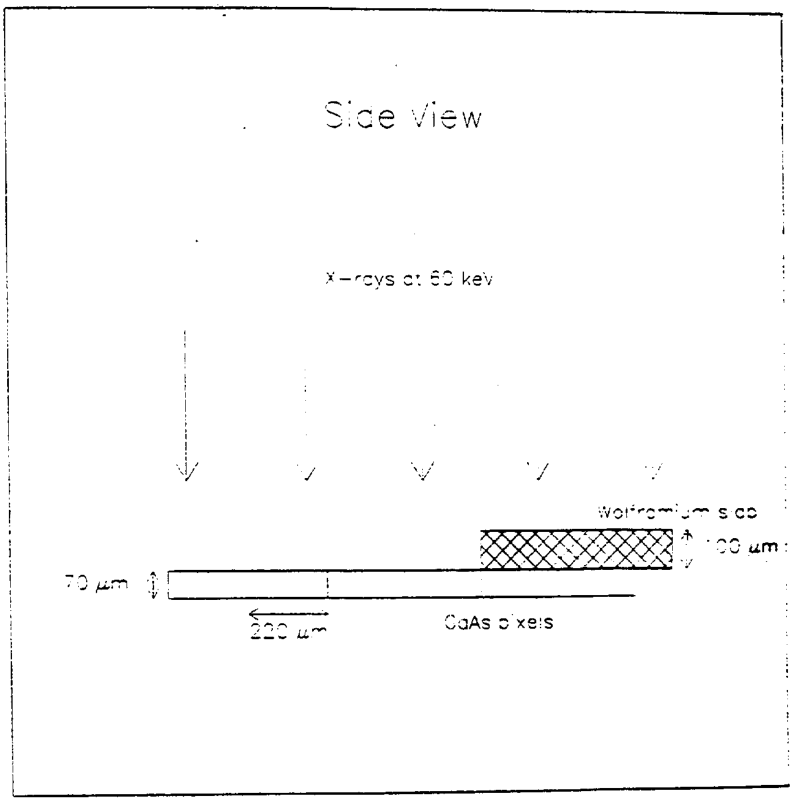
Side View
X−rays at 60 keV
70 μm
220 μm
GaAs pixels

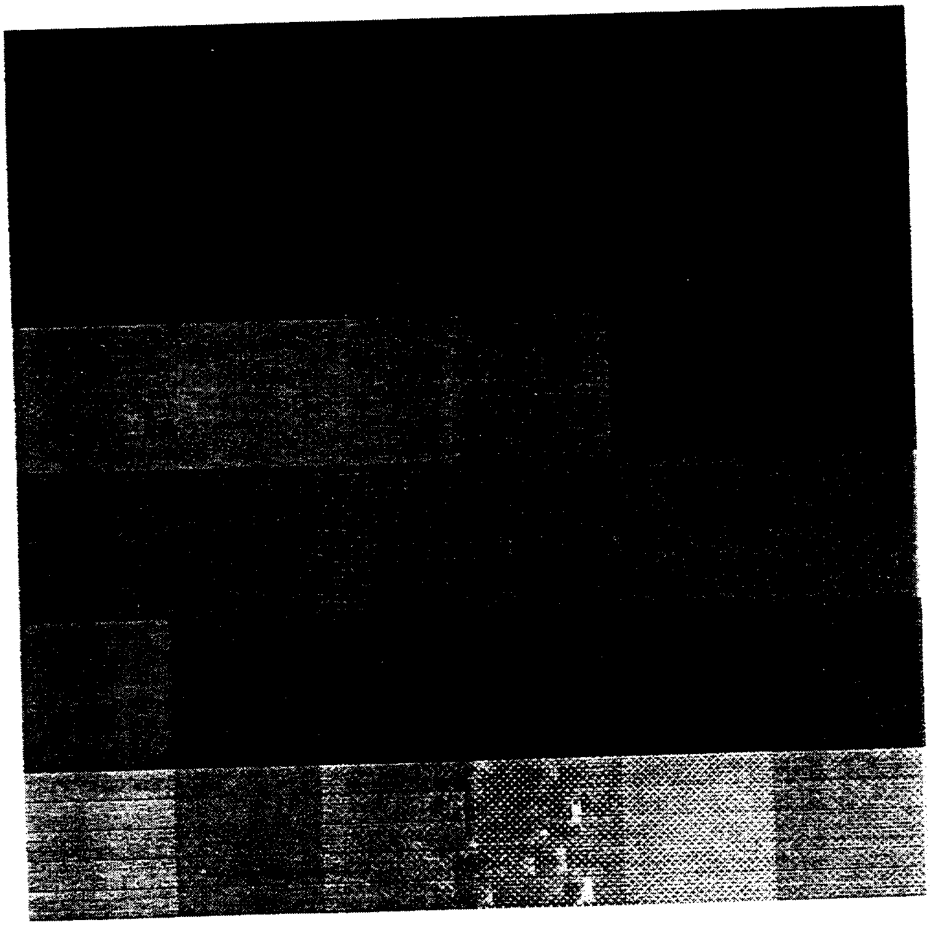

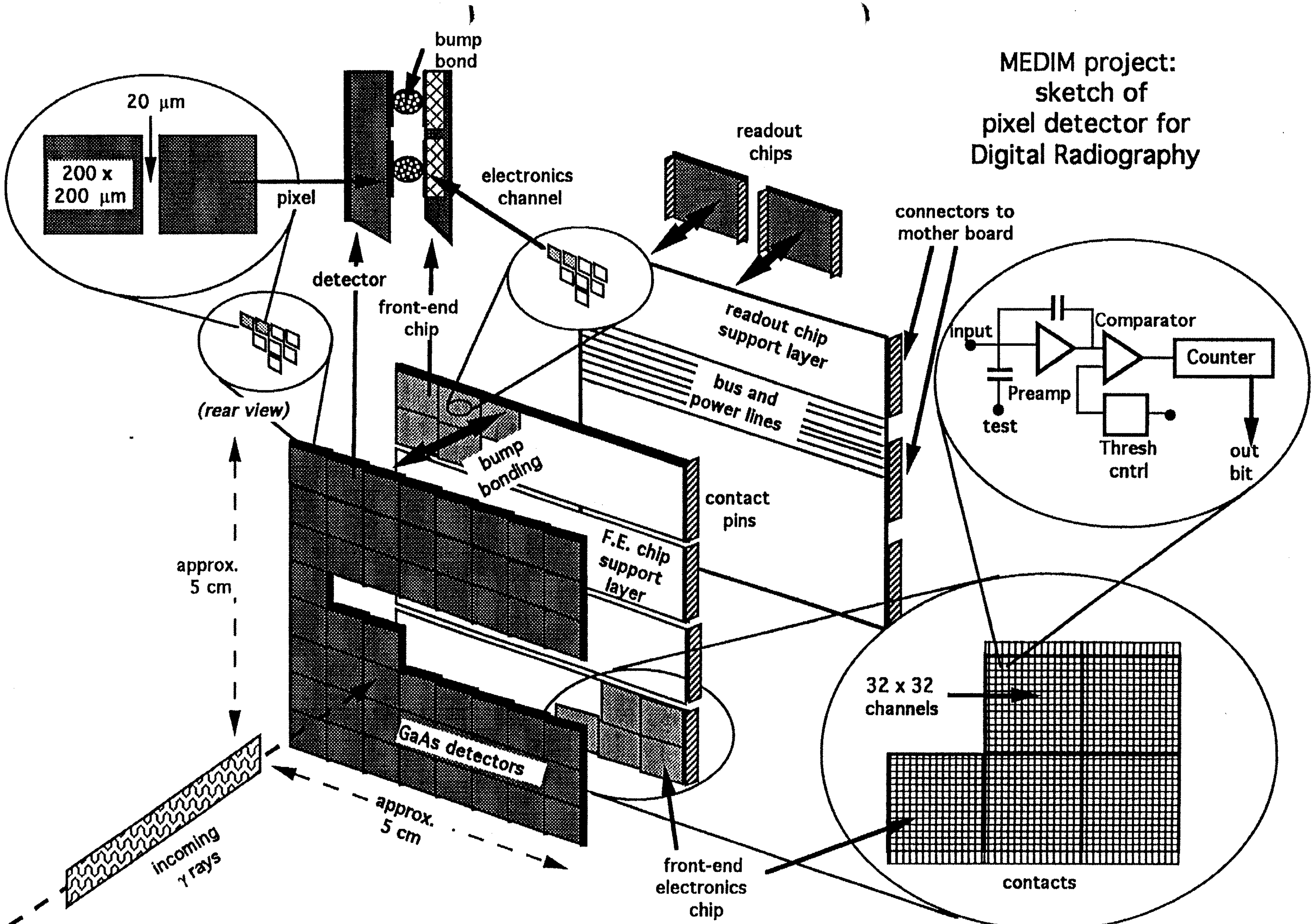

MEDIM project:
sketch of
pixel detector for
Digital Radiography
20 μm
200 x 200 μm
pixel
bump bond
electronics channel
readout chips
connectors to mother board
detector
front-end chip
(rear view)
readout chip support layer
bus and power lines
Input
Comparator
Counter
Preamp
test
Thresh cntrl
out bit
bump bonding
contact pins
F.E. chip support layer
approx. 5 cm
32 x 32 channels
GaAs detectors
approx. 5 cm
incoming γ rays
front-end electronics chip
contacts
SRA 940101

from Jennings et al. Medical Physics 8 (1981) 629

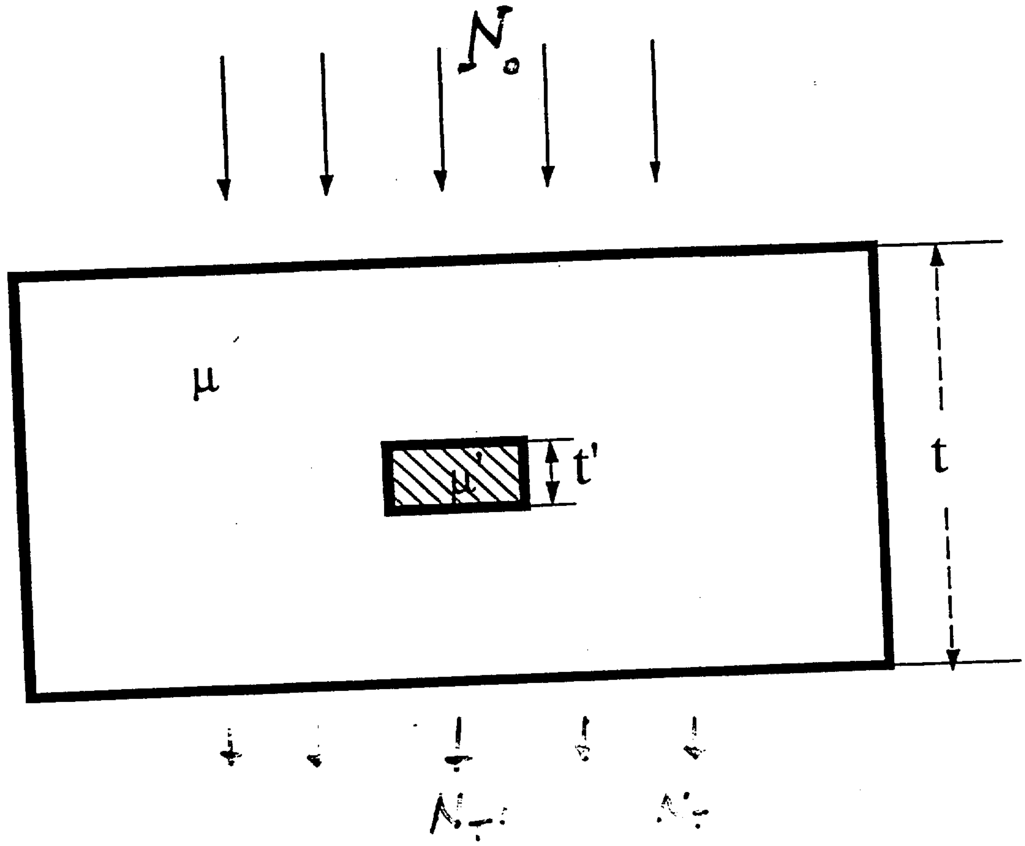

$$n = N_T A = N_0 A e^{-\mu t}$$

$$n' = N_T' A = N_0 e^{-\mu(t-t')} e^{-\mu' t'}$$

$$C = \frac{|n-n'|}{n+n'} = \frac{|N_0 A e^{-\mu t} - N_0 A e^{-\mu(t-t')} e^{-\mu' t'}|}{N_0 A e^{-\mu t} + N_0 A e^{-\mu(t-t')} e^{-\mu' t'}}$$

for $n \sim n'$ $\Rightarrow$ [illegible] $\simeq \frac{|\mu' - \mu| t'}{2}$

$$C_{noise} = \delta\left\{\frac{|n-n'|}{n+n'}\right\} \text{ for } n \sim n' = \frac{\sqrt{n}}{n} = \frac{1}{\sqrt{n}}$$ [illegible]

$$= \frac{1}{\sqrt{\eta n}} = \left(\eta N_0 A e^{-\mu t}\right)^{-1/2}$$

$$SNR = \frac{|n-n'|}{\sqrt{n+n'}} \text{ for } n \sim n' = C \times \sqrt{2} \times \sqrt{n} = \sqrt{2}\, C / C)_{noise}$$

$$\boxed{SNR^2 = 2\left[C/C_{noise}\right]^2 = \frac{1}{2}(\mu' - \mu)^2 t'^2 \eta N_0 A e^{-\mu t}}$$

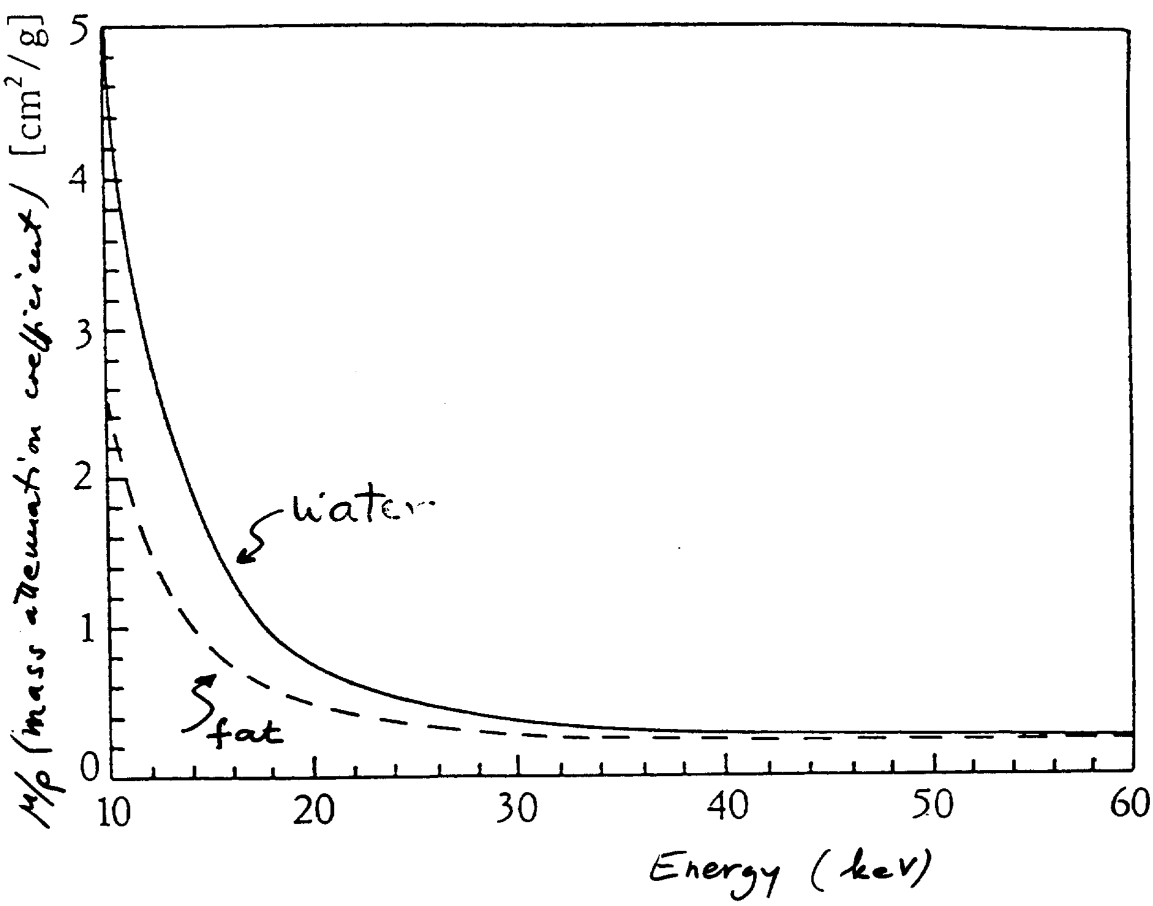

Breast tissue : 50% water + 50% fat
Tumor 100% water

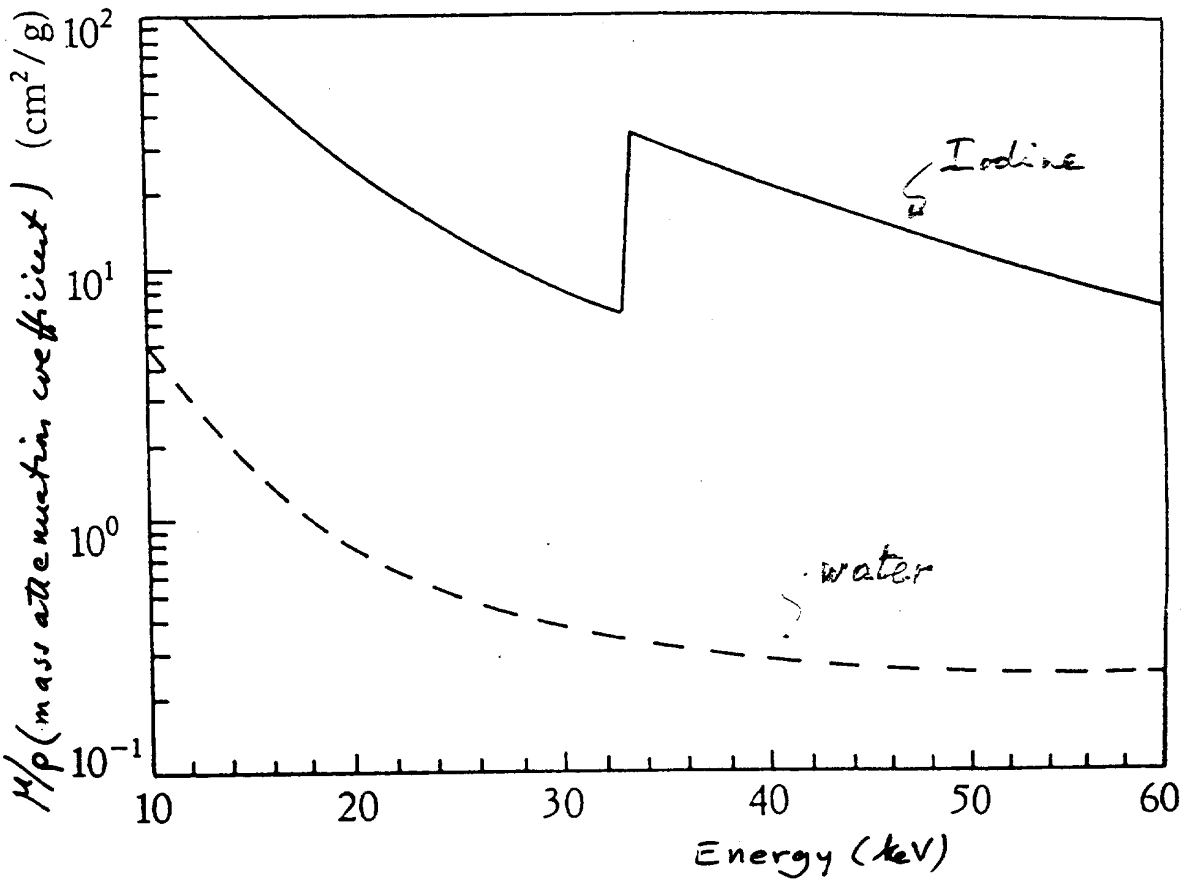
10^2
10^1
10^0
10^{-1}
10
20
30
40
50
60
μ/ρ (mass attenuation coefficient) (cm^2/g)
Energy (keV)
Iodine
water

CONVENTIONAL MAMMOGRAPHY

X-ray tube generally used in mammography:

anode	molybdenum
window	beryllum
added filtration	molybdenum 0.030 mm

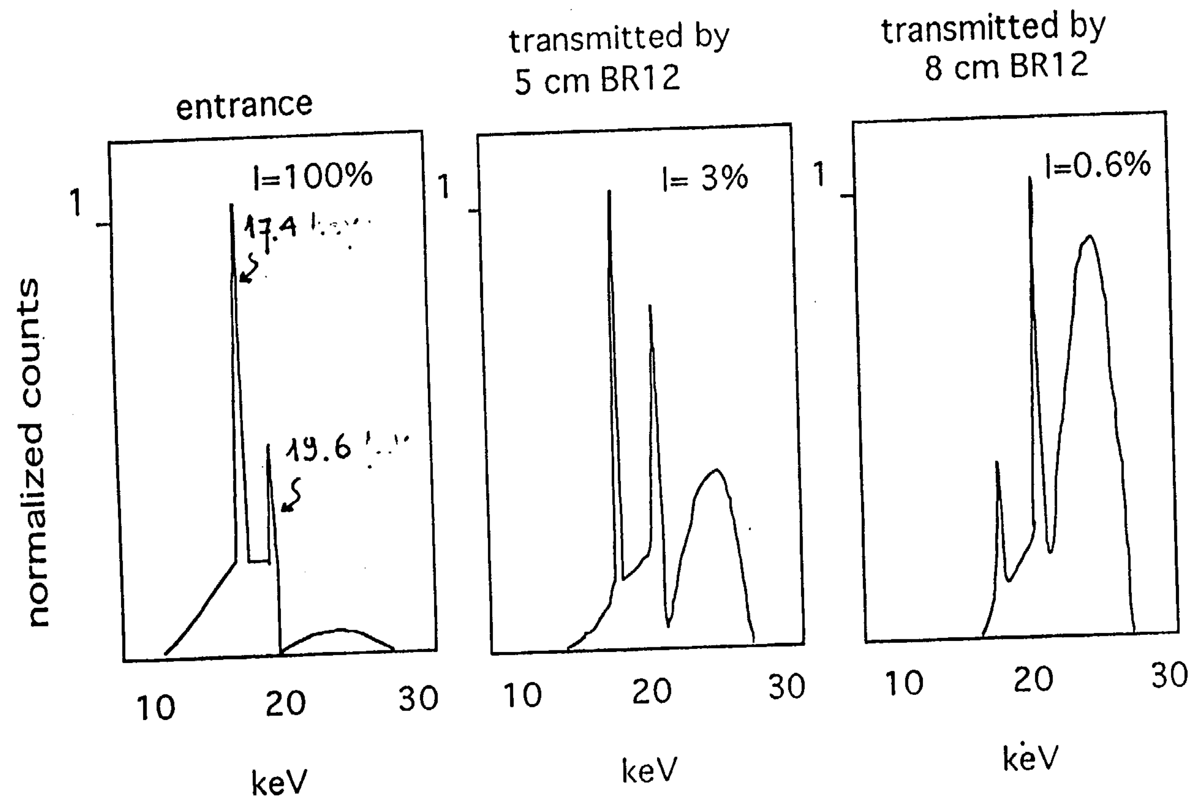

SYNCHROTRON RADIATION MAMMOGRAPHY

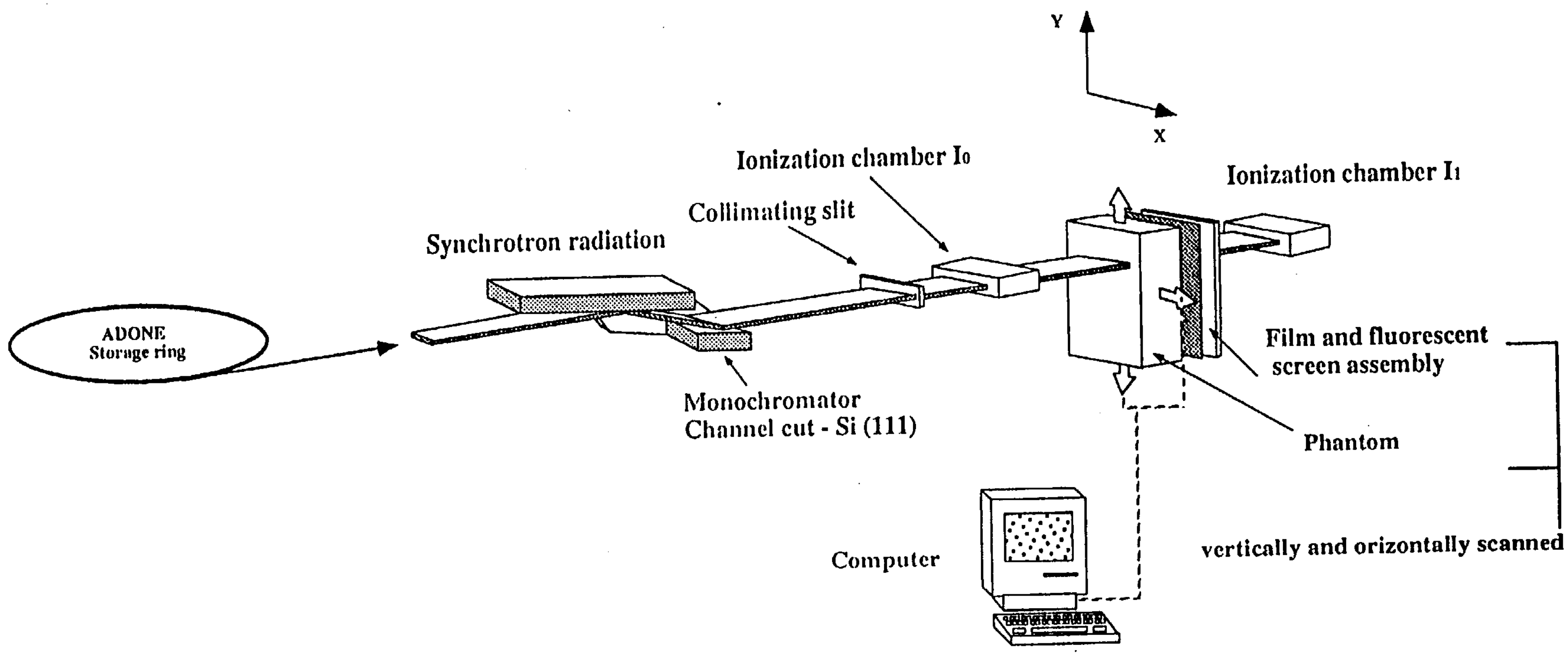

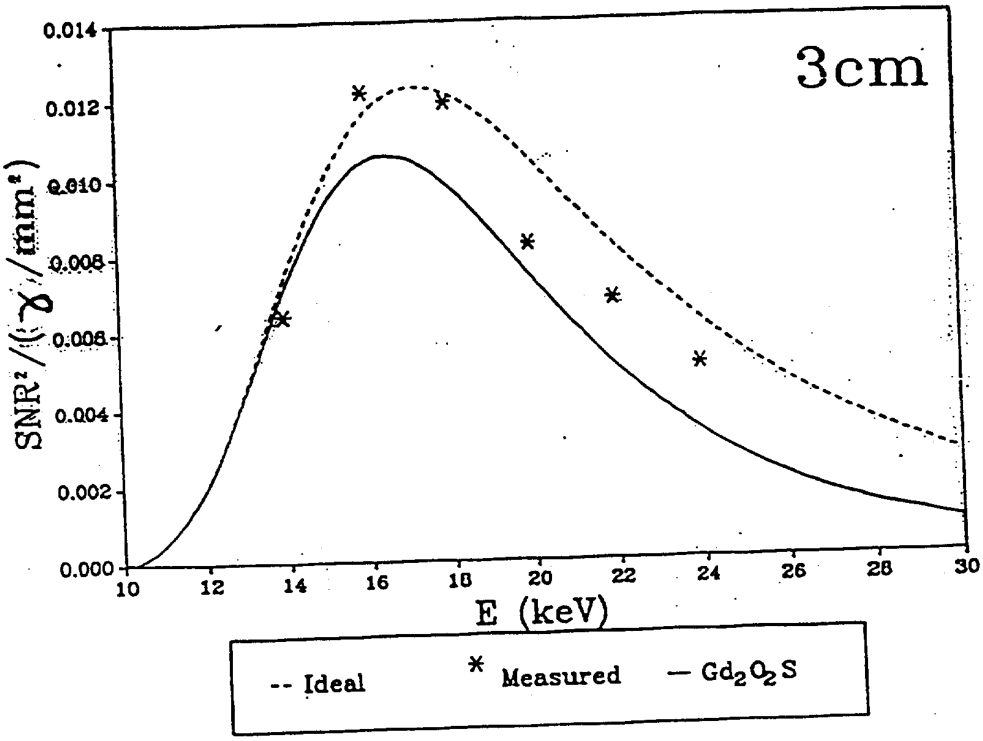

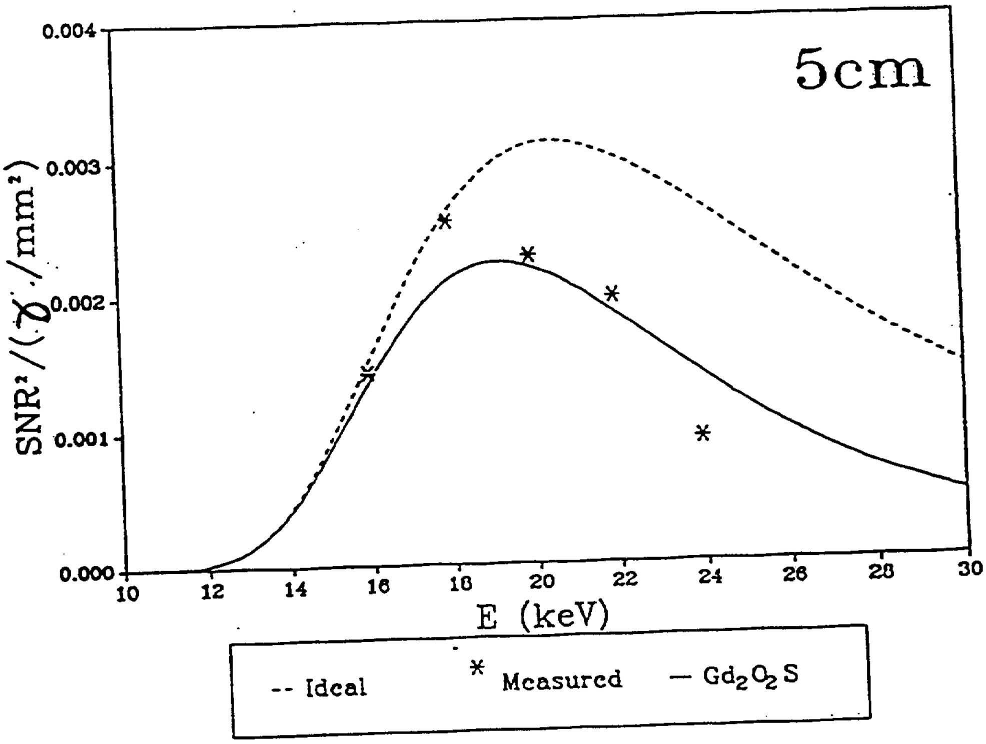

from Burattini et al, Physica Medica, VI (1990) 299

Table. 3. Entrance exposure (with backscatter), BR12 entrance dose and mean dose to a BR12 phantom 5 cm thick delivered by synchrotron radiation and conventional mammography.

IMAGING SOURCE	entrance exposure X_e	entrance dose D_e	mean dose D
Synchrotron radiation 17 keV	887 mR 2.29 10^{-4} C/kg	585 mrad 5.85 mGy	155 mrad 1.55 mGy
Synchrotron radiation 18 keV	406 mR 1.05 10^{-4} C/kg	268 mrad 2.68 mGy	80.2 mrad 0.802 mGy
Conventional 26 kV no grid	508 mR 1.31 10^{-4} C/kg	335 mrad 3.35 mGy	74.2 mrad 0.742 mGy
Conventional 28 kV grid	1055 mR 2.72 10^{-4} C/kg	696 mrad 6.96 mGy	151 mrad 1.51 mGy

E. Burattini et al., Eur. Radiol 4 (1994) 464

102

Bragg law $\Rightarrow$ $2d \operatorname{sen} \vartheta = \lambda$

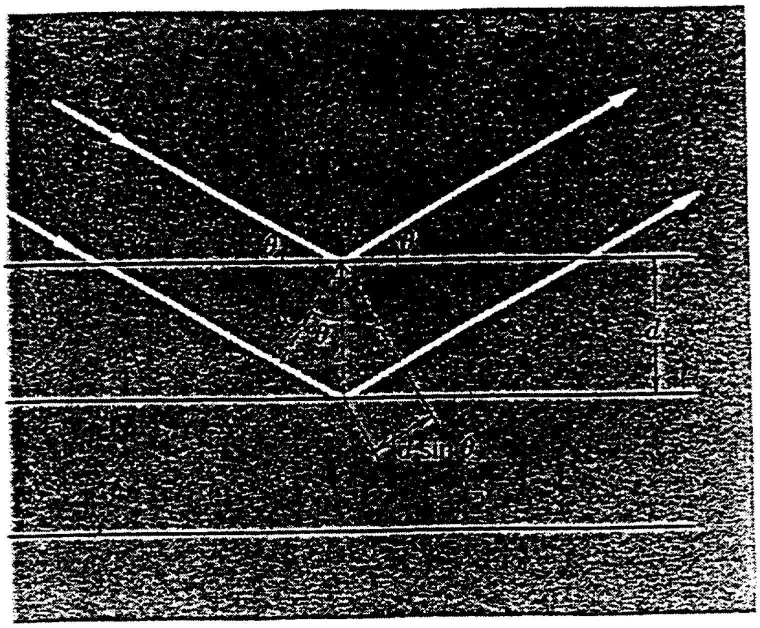

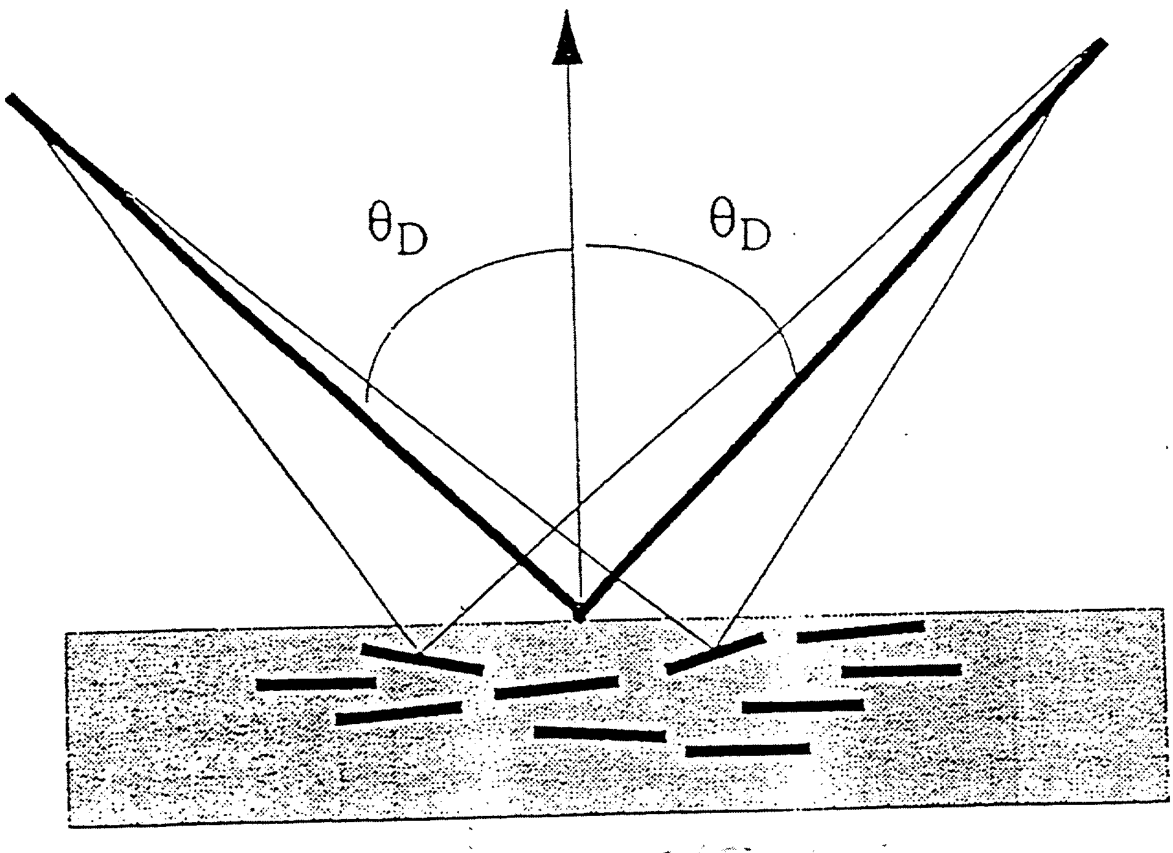

Mosaic spread $\sim 0.2°$ (FWHM)

from: F. Frontera et al, SPIE vol 1549, "X-ray, and γ-ray..." pg 113

spectrometric assembly

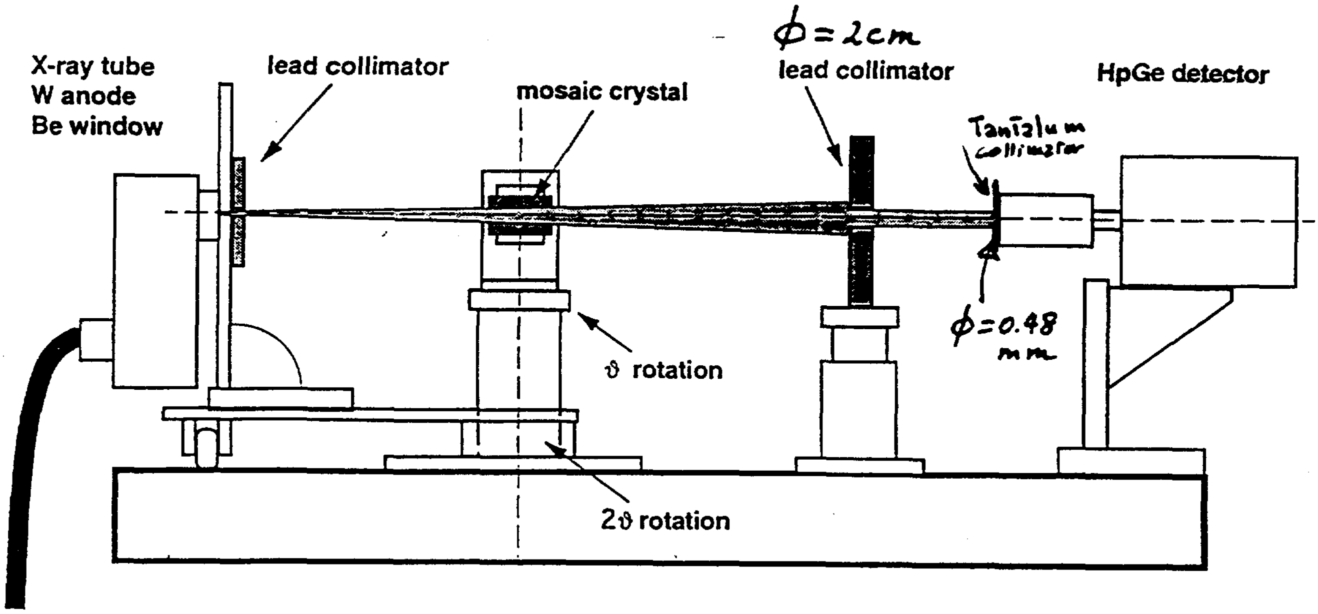

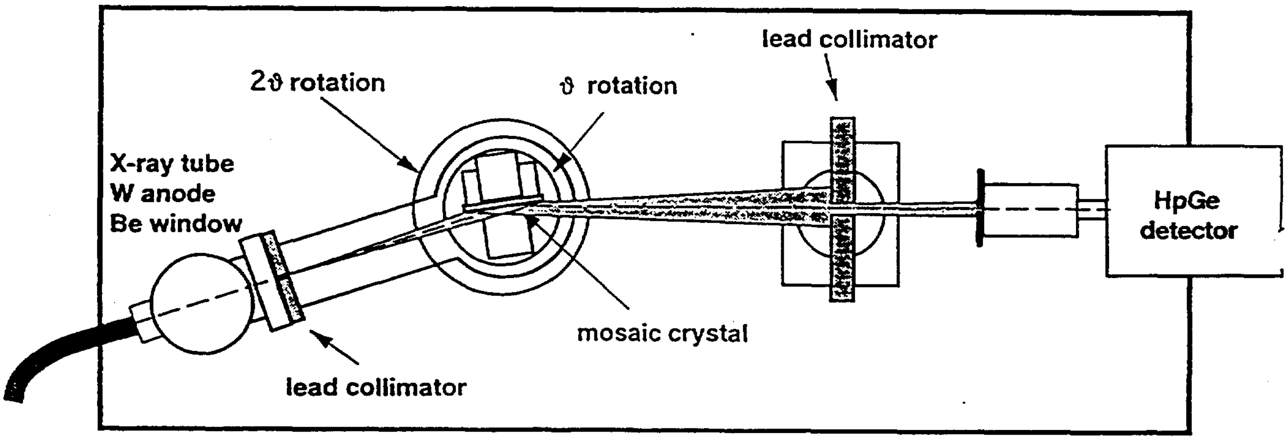

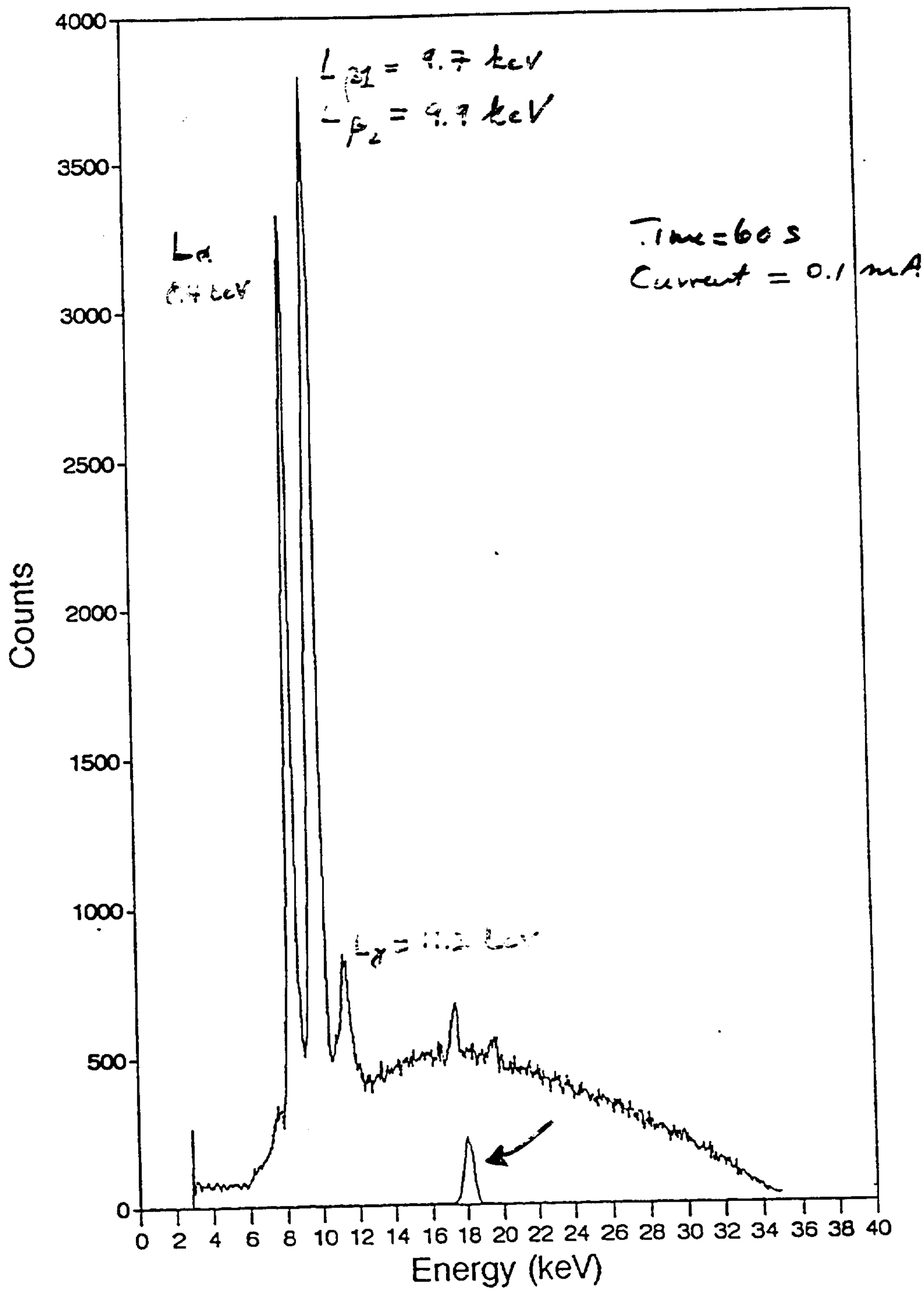

4000
3500
3000
2500
2000
1500
1000
500
0
Counts
0 2 4 6 8 10 12 14 16 18 20 22 24 26 28 30 32 34 36 38 40
Energy (keV)
$L_{\beta 1}$ = 9.7 keV
$L_{\beta 2}$ = 9.9 keV
L_α
8.4 keV
Time = 60 s
Current = 0.1 mA
L_γ = 11.2 keV

$E_p = 30\ kV_p$

Energy (keV)	photon flux (photons $mA^{-1}\ s^{-1}\ mm^{-2}$)	FWHM (keV)	Energy Resolution (%)
16	1.16×10^4	0.67	4.1
18	1.60×10^4	0.83	4.5
20	1.90×10^4	0.94	4.7
22	2.14×10^4	1.06	4.8

16 - 22 kv

(4-5%)

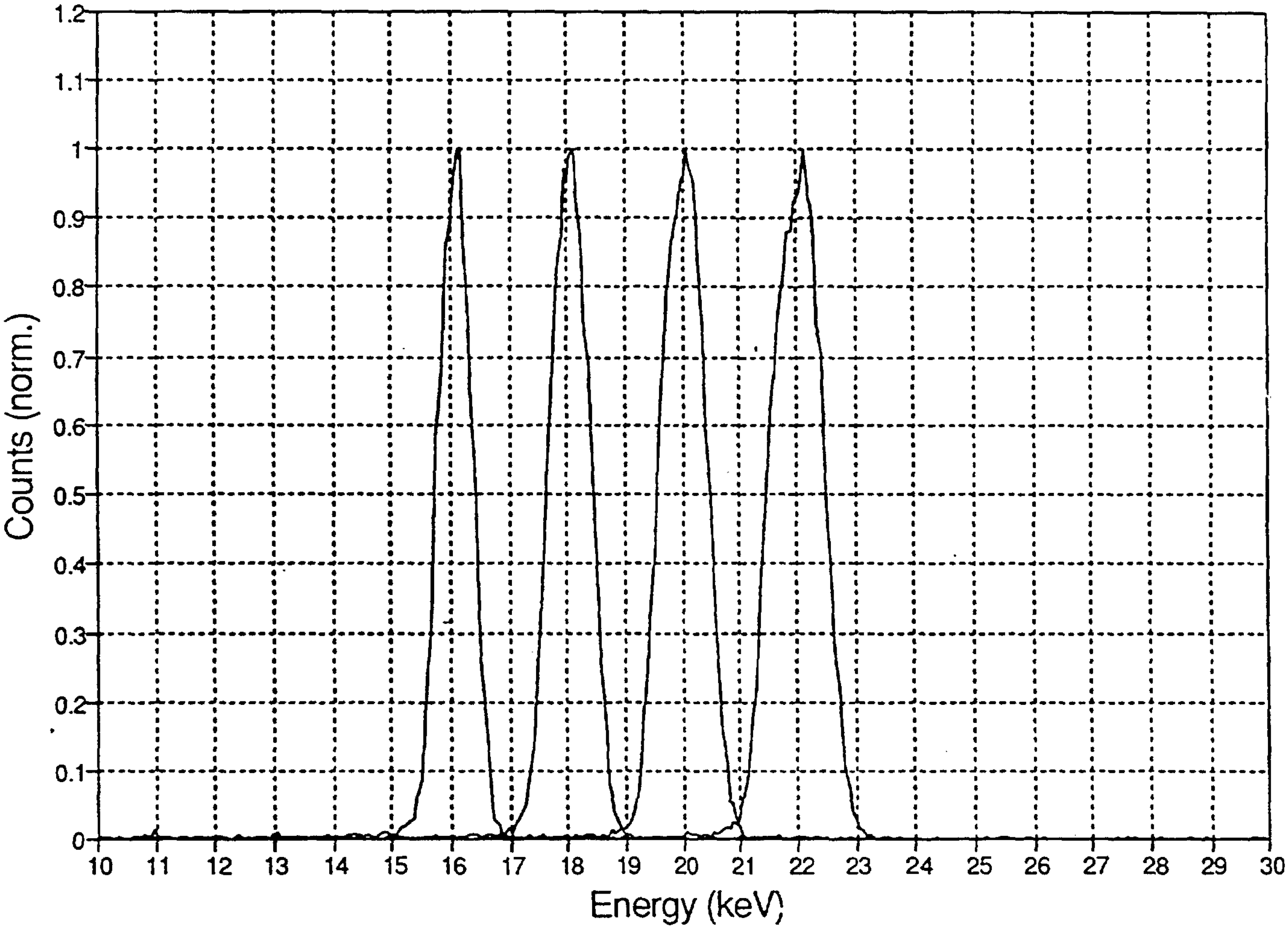

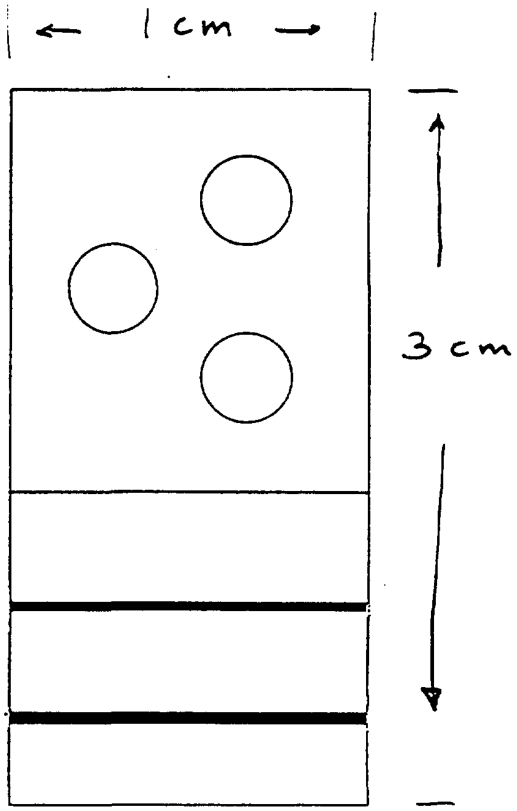

	Thickness (mm)		
Aluminium disks (Ø=3 mm)	0.5	0.25	0.125
Aluminium wires	0.5	0.25	0.125
Contrast	0.6	0.3	0.15

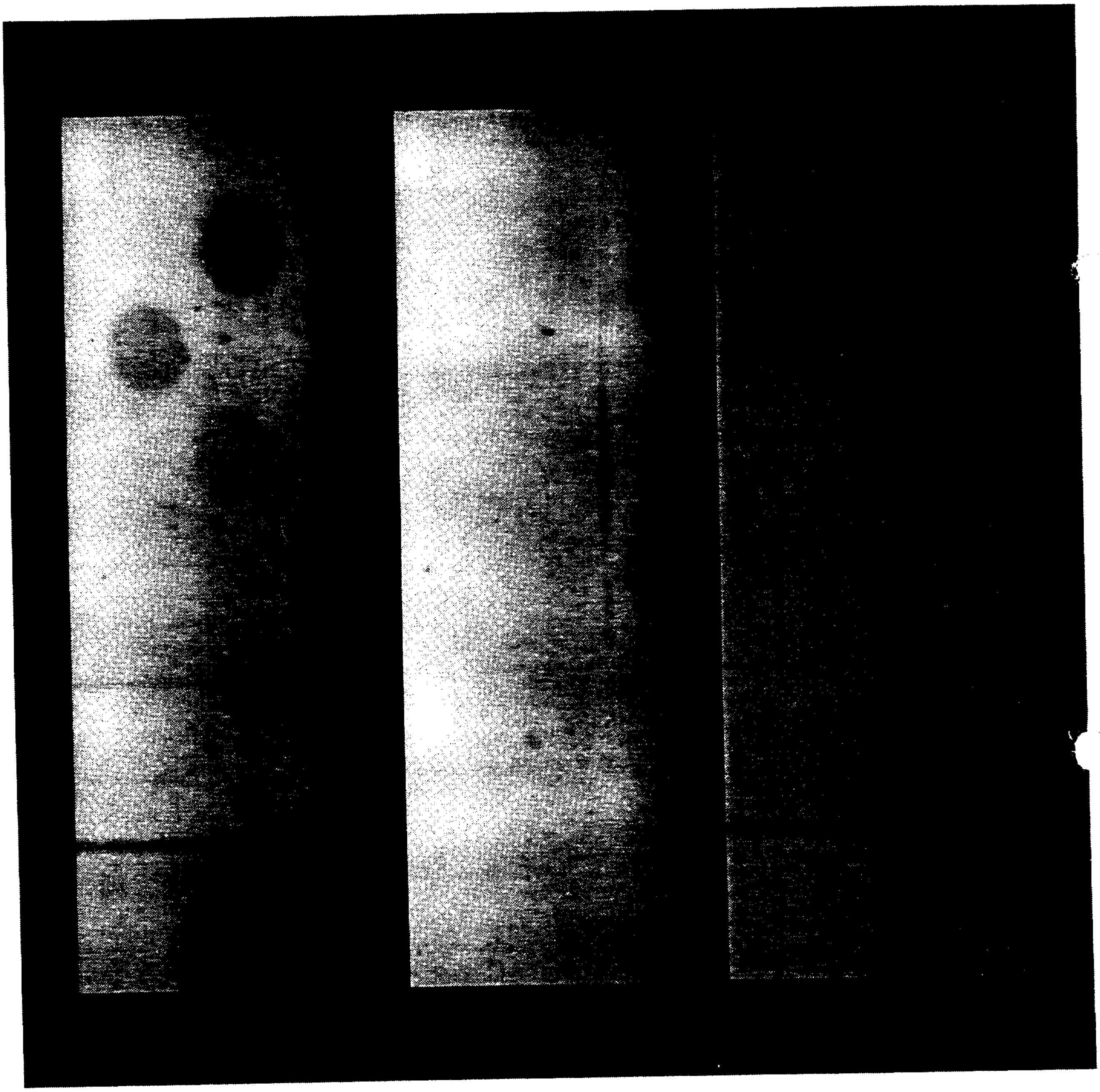

ORIGINAL

Background
(flood field)

CORRECTED

Physica Medica - Vol. IX, N. 2-3, April-September 1993

A Position Sensitive Multi Channel Ion Chamber (MCIC) for Non Invasive Coronary Angiography with Synchrotron Radiation

H. J. Besch[1], W. R. Dix[2], U. Großmann[1], J. Heuer[2], R. Langer[1], M. Lohmann[2], R. H. Menk[2], H. W. Schenk[1], U. Tafelmeier[2], M. Wagener[1], A. H. Walenta[1], H. C. Xu[1]

1. *Universität-Gesamthochschule-Siegen, Fachbereich Physik, Siegen (Germany)*
2. *Hasylab at DESY, Hamburg (Germany)*

Abstract

A position sensitive 1-dimensional x-ray detector with high dynamic range (> 20000:1) for a high photon flux (> 10^9 photons/mm$^2\cdot$ s) with fast image recording sequence (in principle up to 1 MHz) has been developed for medical applications. A detective quantum efficiency DQE of at least 55% could be achieved for 33 keV photons. The position resolution is 450 μm (fwhm) for this energy.

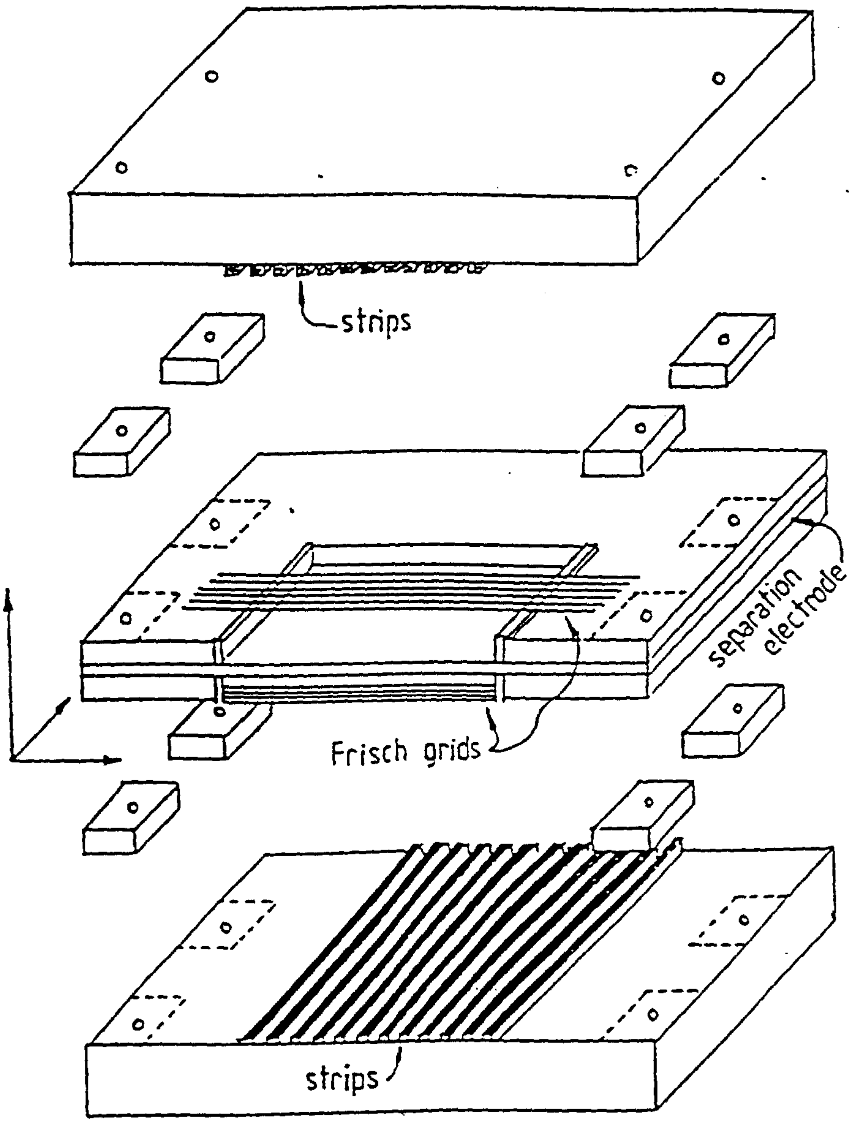

Fig. 3 – Exploded view of the multi-channel ion chamber pair.

DIGITAL SUBTRACTION CORONARY ANJOGRAPHY

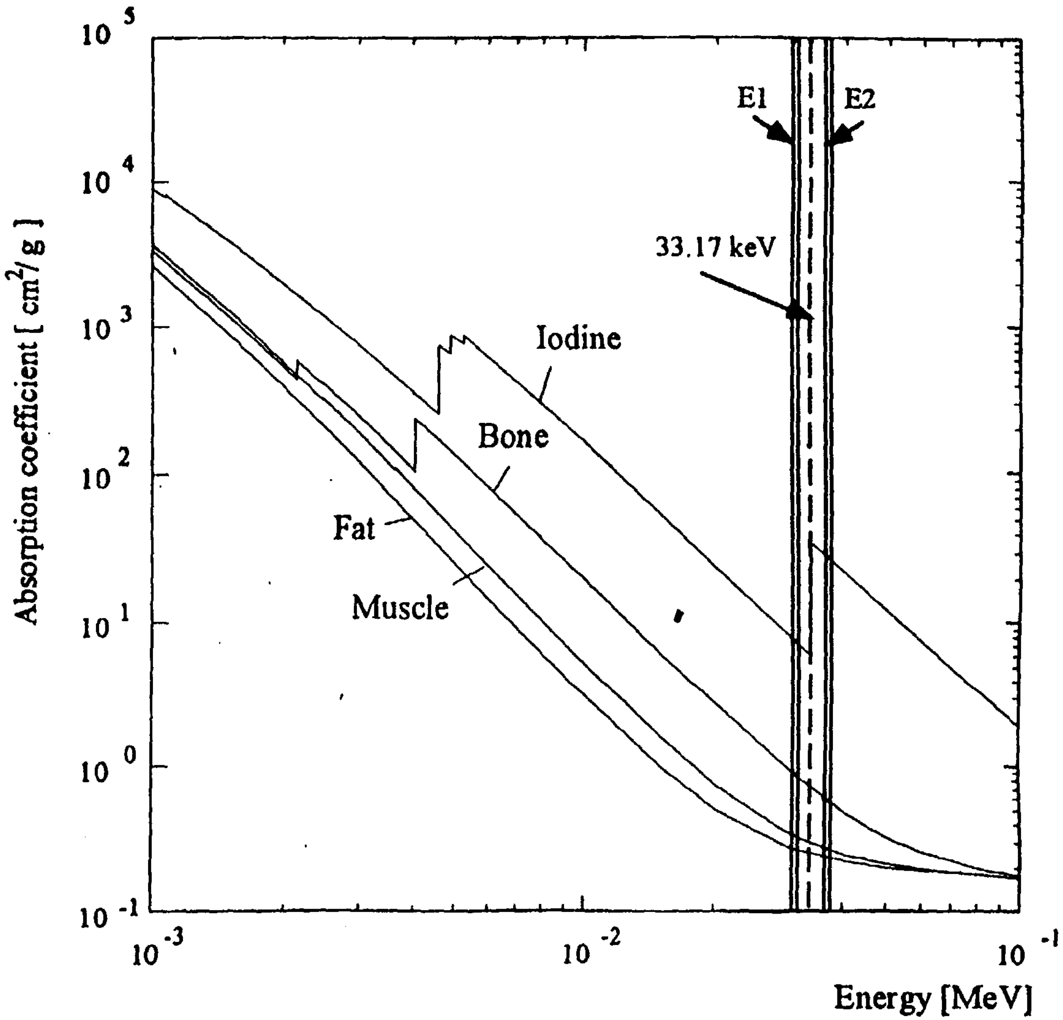

110

NON-INVASIVE CORONARY ANGIOGRAPHY WITH SYNCHROTRON RADIATION

DESY (Hamburg)

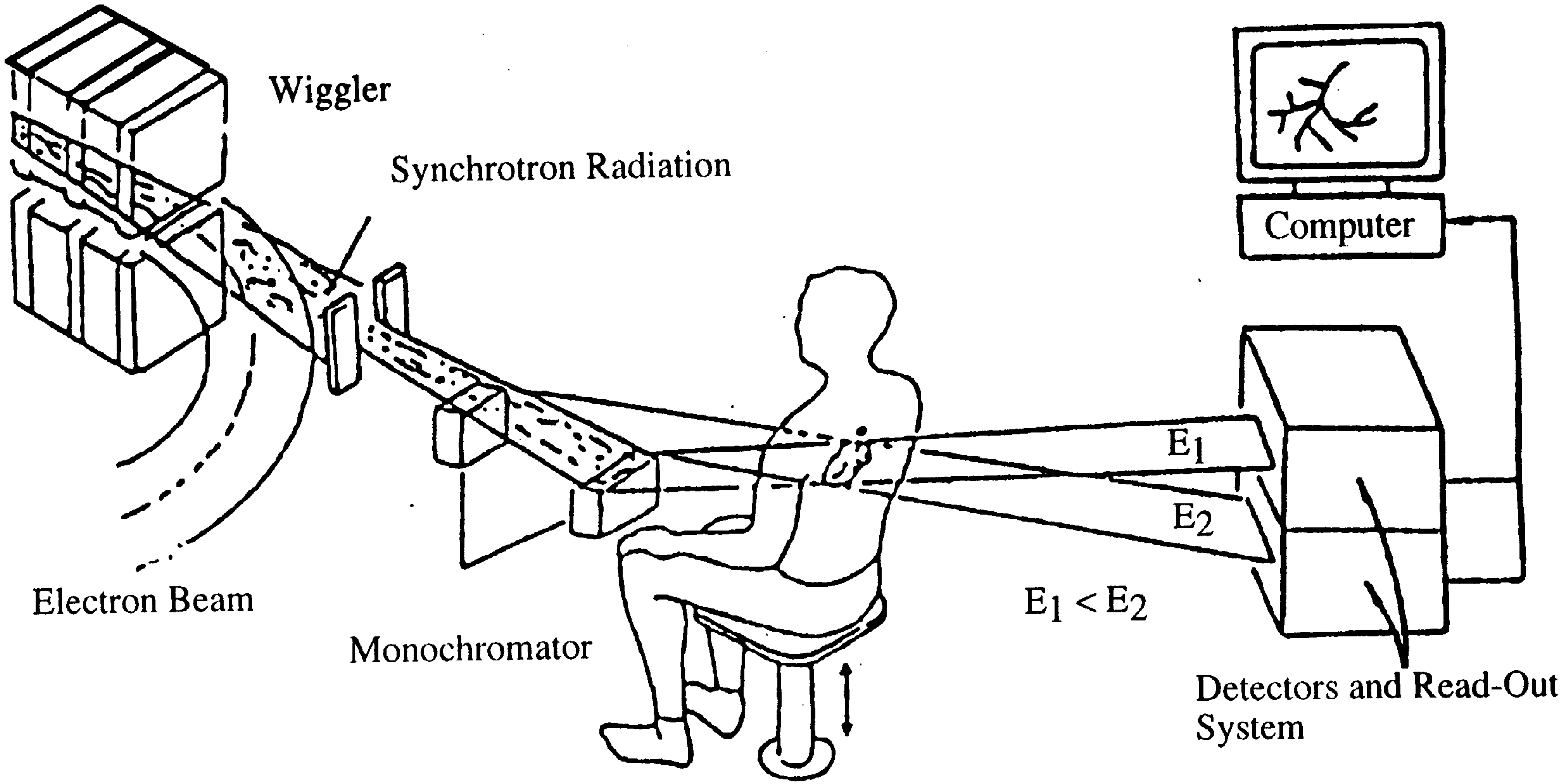

H.J. Besh et al, Phys. Medica IX (1993) 171
W.-R. Dix et al, DESY SR 94-01

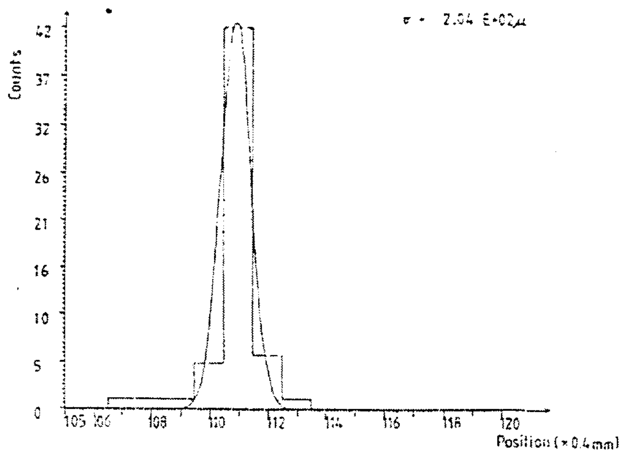

Fig. 5 – Resolution Curve of the Detector.

Fig. 6 – Radiography of the Heart of a Pig.

112

A. Thompson et al
"A 1200 Element Si(Li) Detector for Synchrotron-Based Coronary Angiography", Physica Medica IX (1993) 165-

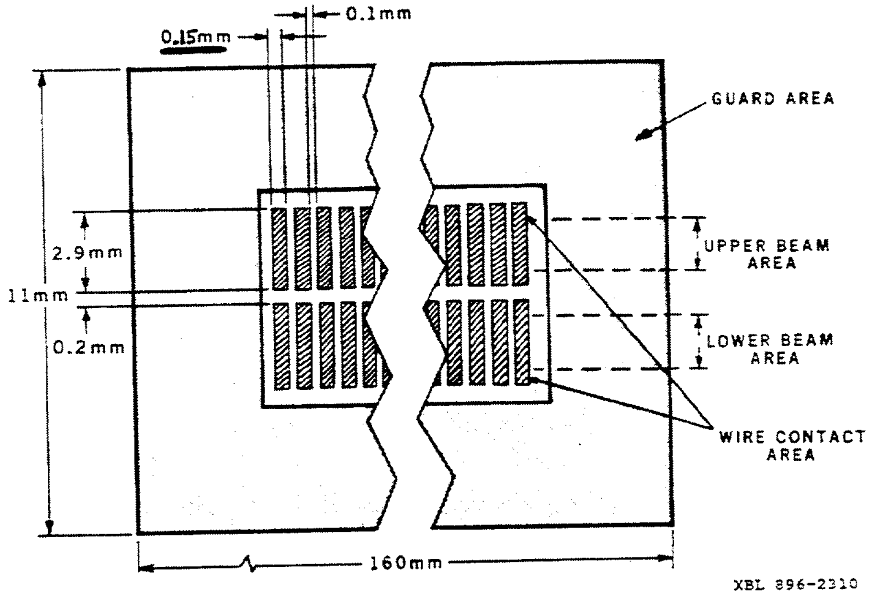

Fig. 2 – Geometry of multi-element detector.

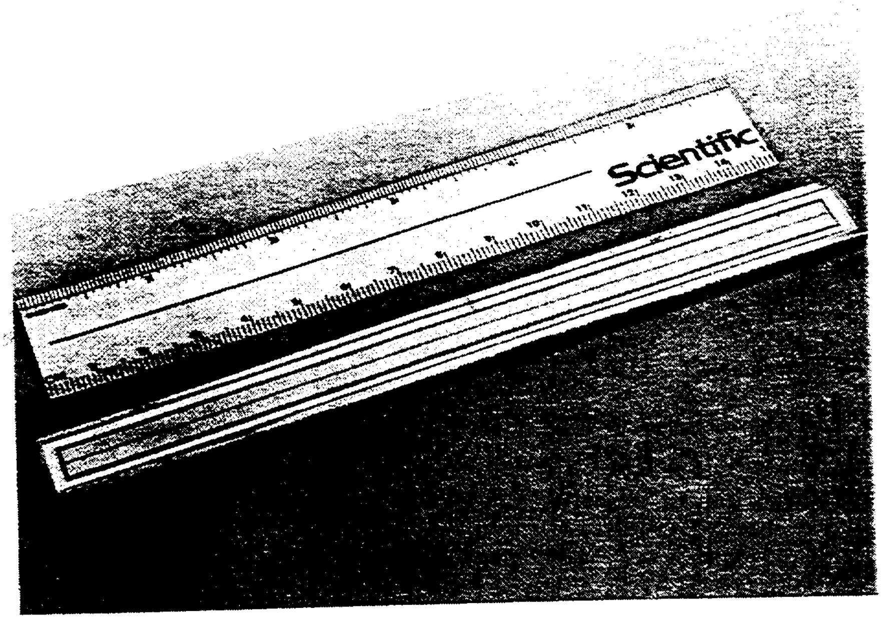

Fig. 3 – Photograph of 1200 element detector before installation in the cryostat.

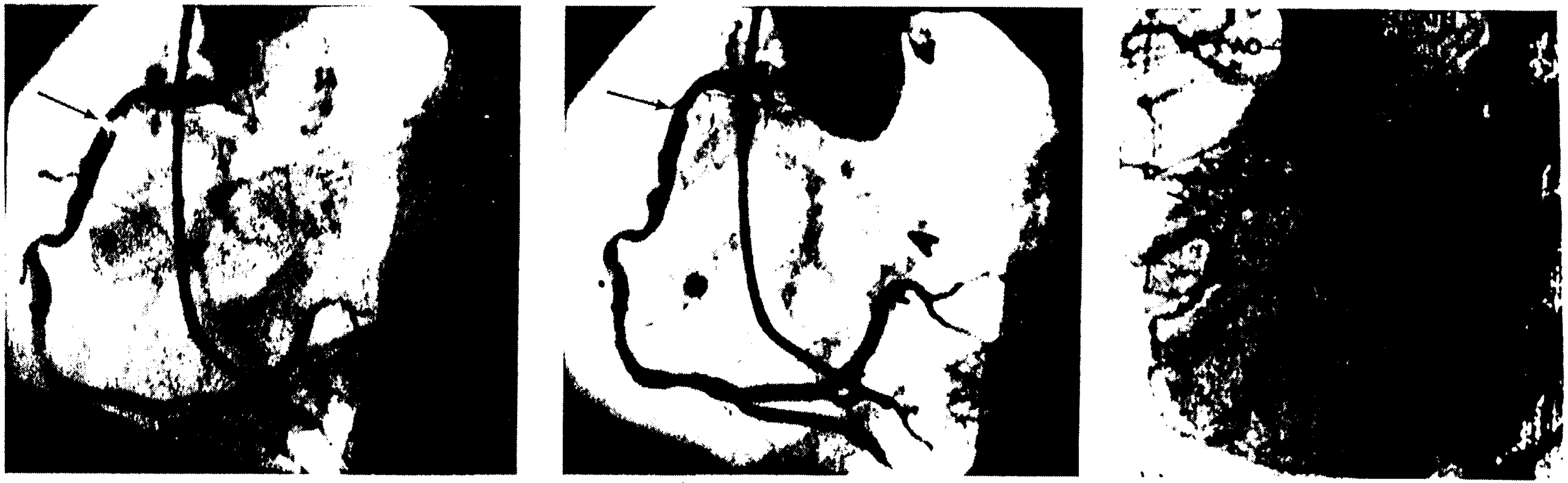

Fig. 7 – Image of patient taken with the 600 element detector system.

114

SILICON X-RAY DETECTOR FOR DIGITAL RADIOGRAPHY:

SYRMEP

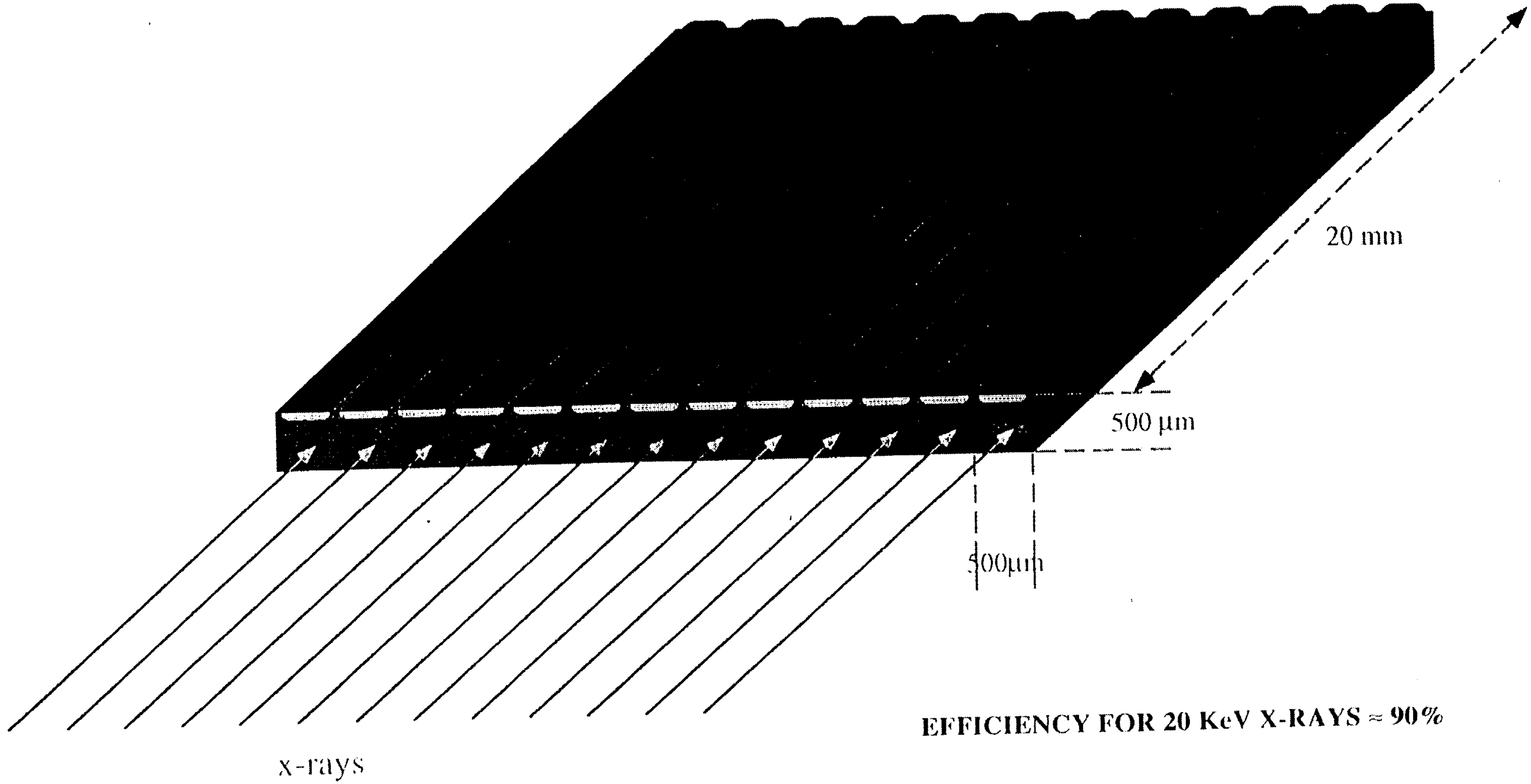

EFFICIENCY FOR 20 KeV X-RAYS ≈ 90%

F. Arfelli et at, INFN/TC-94/09
Synchrotron Radiation Facility (ELETTRA), Trieste, Italy

DIGITAL RADIOGRAPHY OF STANDARD MAMMOGRAPHY PHANTOM

6 mm Ø. 75 μm thick aluminum disk emedded in 16 mm thick plastic

Fluence (photons/mm^2)

6.9×10^3

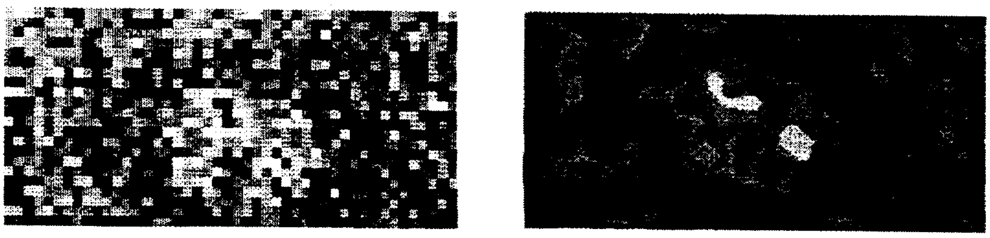

2.2×10^4

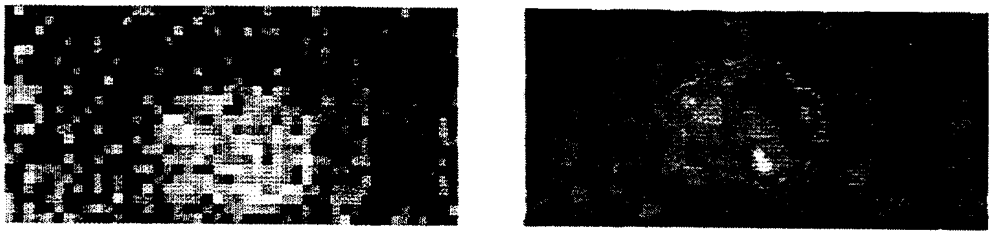

3.8×10^4

7.5×10^4

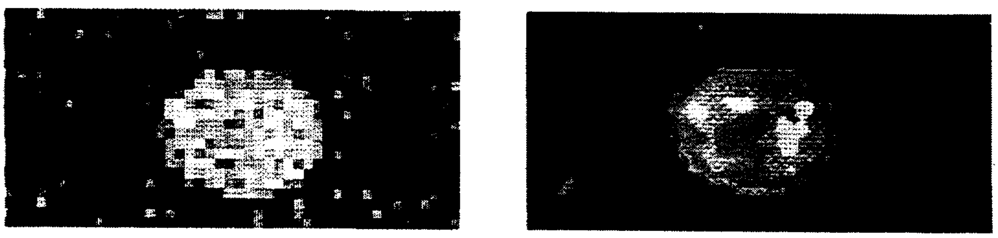

F. Arfelli et at. INFN/TC-94/09